

# A Survey of Reynolds Number and Wing Geometry Effects on Lift Characteristics in the Low Speed Stall Region

---

*Edward C. Polhamus, Consultant • Newport News, Virginia*

Printed copies available from the following:

NASA Center for AeroSpace Information  
800 Elkridge Landing Road  
Linthicum Heights, MD 21090-2934  
(301) 621-0390

National Technical Information Service (NTIS)  
5285 Port Royal Road  
Springfield, VA 22161-2171  
(703) 487-4650

## TABLE OF CONTENTS

SUMMARY	2
INTRODUCTION	3
1. LEADING EDGE SEPARATION ON AIRFOILS	5
1.1 Early Research	5
1.2 Classification of Stall Types	5
1.3 Experimental Results Related to Stall	7
1.3.1 Effects of profile on separation and stall	7
1.3.2 Influence of Reynolds number on stall	11
1.4 Stall Boundaries	12
1.5 Airfoil Maximum Lift Coefficients	14
2. EDGE SEPARATIONS ON RECTANGULAR WINGS	16
2.1 Sources of Edge Separation	16
2.2 Prediction Methods	17
2.2.1 Some early studies	18
2.2.2 Development of an approximate method	18
2.3 Comparison of Predictions and Experiments	22
2.3.1 Effect of aspect ratio on root stall	22
2.3.2 Effect of aspect ratio on overall wing stall	26
2.3.3 Reynolds number influence on wing stall	30
3. SWEPTBACK WINGS	32
3.1 Some Early Research	32
3.2 Some Types of Flow	34
3.2.1 Tip stall	34
3.2.2 Leading-edge separation bubble	35
3.2.3 Leading-edge vortex lift	35
3.3 General Effects of Sweep and Reynolds Number	36
3.3.1 Predictions of turbulent reattachment	37
3.3.2 Overall lift characteristics	40
3.3.3 Summary of maximum lift	43
3.4 Influence of Reynolds Number on Local Flow	46
3.4.1 Prediction of turbulent reattachment	46
4. SLENDER DELTA WINGS	49
4.1 Analysis Methods	49
4.1.1 Induced camber distributions	49
4.1.2 Vortex-flow theories	51
4.2 Sharp Leading-Edge Delta Wing Reynolds Number Studies	54
4.2.1 Overall lift characteristics	54
4.2.2 Secondary - vortex flow	56
4.2.3 Maximum lift coefficient	58
4.3 Round Leading-Edge Delta Wings	60
4.3.1 Effect of profile	60
5. CONCLUDING REMARKS	62
6. APPENDIX	64
7. SYMBOLS	66
8. REFERENCES	68
9. ACKNOWLEDGEMENT	75

## SUMMARY

This paper presents a survey of the effects of Reynolds number on the low-speed lift characteristics of wings encountering separated flows at their leading and side edges, with emphasis on the region near the stall. The influence of leading-edge profile and Reynolds number on the stall characteristics of two-dimensional airfoils are reviewed first to provide a basis for evaluating three-dimensional effects associated with various wing planforms. This is followed by examples of the effects of Reynolds number and geometry on the lift characteristics near the stall for a series of three-dimensional wings typical of those suitable for high-speed aircraft and missiles. Included are examples of the effects of wing geometry on the onset and spanwise progression of turbulent reattachment near the leading edge and illustrations of the degree to which simplified theoretical approaches can be useful in defining the influence of the various geometric parameters.

Also illustrated is the manner in which the Reynolds number and wing geometry parameters influence whether the turbulent reattachment near the leading edge results in a sudden loss of lift, as in the two-dimensional case, or the formation of a leading-edge vortex with its increase in lift followed by a gentle stall as in the highly swept wing case. Particular emphasis is placed on the strong influence of "induced camber" on the development of turbulent reattachment.

It is believed that the examples selected for this report may be useful in evaluating viscous flow solutions by the new computational methods based on the Navier-Stokes equations as well as defining fruitful research areas for the high-Reynolds-number wind tunnels.

## INTRODUCTION

While the geometric characteristics of wings for high-speed aircraft and missiles are widely varied, they tend to have a common susceptibility to leading-edge and side-edge separations which can play an important role with regard to their low speed lift in the stall region. Because of their speed requirements they often utilize thin wings having relatively sharp leading and side edges which, of course, tend to promote Reynolds number dependent boundary-layer separations in the vicinity of these edges. These edge separations are also influenced by planform through the aerodynamic induction effects on the pressure gradients in the edge regions. The planforms used for high speed applications include, for example, the low-aspect-ratio rectangular planforms often used for missiles, the moderately sweptback moderate-aspect-ratio wings of transonic aircraft, and the higher swept slender delta type often applied to supersonic and hypersonic vehicles. These planform variations contribute a variety of influences on the boundary-layer characteristics leading to separation as well as influencing the type of overall wingflow produced by the separation. Thus, the effects of Reynolds number, of primary interest in this paper, are greatly influenced by these geometric parameters. For example, not only is the onset and spanwise progression of turbulent reattachment aft of the leading-edge transitional bubble dependent on these factors, but whether this separation results in a sudden loss of lift or in the formation of a separation induced edge vortex with its resulting increase in lift also depends on these factors.

Although the various types of edge separations are well documented in the literature it is felt that a survey paper tying together the relation between two dimensional and various three dimensional effects might be found useful. The purpose of this paper is therefore to review examples from selected experimental studies that provide parametric illustrations of the interacting effects of wing geometry and Reynolds number on the lift characteristics in the low speed stall region for wings

encountering the above types of edge separations. Such a review should provide some assistance in selecting critical viscous flow cases for use in evaluating new design and analysis methods such as those based on the Navier-Stokes equations as well as indicating areas needing additional research utilizing the relatively new high Reynolds number wind tunnels. The experimental data selected and the simplified prediction methods utilized provide a viscous flow analysis capability sometimes not easily extracted from available experimental data or from a particular computational code.

To accomplish the above purpose the paper is divided into sections dealing with four classes of wing planform. First, a review of the influences of geometry and Reynolds number on the types of separations encountered in the leading-edge region and their influence on stalling for a parametric series of two-dimensional airfoils will be made. This will be followed by two sections illustrating the influences of three-dimensional effects associated with finite span and leading-edge sweep on turbulent reattachment in the leading-edge region as well as examples of leading-edge and side-edge vortex lift. In addition to experimental examples relatively simple theoretical approaches are used to illustrate the influence of wing planform on induced camber and its effect on turbulent reattachment and stall.

The final section deals primarily with slender delta planforms having vortex flow originating at sharp leading-edges. In addition to parametric experimental results several vortex-flow theories are utilized as a means of isolating various influences such as the leading-edge vortex trajectory and breakdown on the stall.

It should be noted that the examples used are limited to planar wings and no discussion of warped wings or flow control devices is included. Throughout the text, brief mention is made of some of the early research in various areas which might be of historical interest.

## 1. LEADING-EDGE SEPARATION ON AIRFOILS

### 1.1 Early Research

Lanchester (1907) discussed the probability of a small pocket of "dead water" associated with a leading-edge separation on thin airfoils accompanying a small increase in angle of attack beyond the design condition and a completely separated region at some higher angle. However, it was not until the early 1930's that research such as that by Jacobs (1931), Millikan and Klein (1933), and Jones (1933, 1934) began to clearly identify the role of the boundary layer and Reynolds number on airfoil stall characteristics. As a result of his research, Jones identified a trailing-edge stall and two types of leading-edge stall - one associated with a round leading edge and the other associated with a sharp leading edge.

Research on leading-edge separation began to accelerate in the late 1930's (see Jacobs and Sherman (1937) for example) due to the interest in thin wings to alleviate compressibility effects. Probably the earliest proposal of a mechanism for the formation of a laminar separation bubble was that of von Doenhoff (1938). Systematic experimental studies of leading-edge separation on airfoils began following World War II with those of Loftin and Bursnall (1948) and McCullough and Gault (1951) providing much of the basis for stall classification and a review of this research has been made by Tani (1964).

### 1.2 Classification of Stall Types

The types of leading-edge separation to be described here will, in general, be identified by their influence on the airfoil stalling characteristics as classified by McCullough and Gault (1951) and Gault (1957), but will be limited to symmetrical airfoils to be consistent with the subsequent review of three-dimensional wing stalling characteristics.

The three types of leading-edge separations are those leading to (a) thin-airfoil stall, (b) leading-edge stall, and (c) combined trailing-edge and leading-edge stall,

and are illustrated in figure 1.1. In the upper portion of the figure sketches of the various boundary layer separation characteristics (not to scale) are presented for the three stall classifications and the corresponding lift and stall characteristics are shown in the lower part. Few details will be included here but will be discussed in connection with subsequent detailed figures.

The thin-airfoil type of stall is illustrated in part (a) by a thin airfoil having a sharp leading edge for which laminar separation occurs at the leading edge followed by turbulent reattachment forming a separation bubble. The separation occurs as soon as the angle of attack departs from zero and the reattachment point moves rearward with increasing angle of attack. This expanding "long-type" bubble results in a rather gentle stall as the reattachment point reaches the trailing-edge region. This type of stall also occurs on round edge airfoils for certain combinations of leading-edge radius and Reynolds number.

Part (b) of figure 1.1 illustrates the stall classified as a leading-edge stall which is characterized by an abrupt loss of a large amount of lift occurring when an expanding long bubble occurs at a relative high angle-of-attack such that its initial length is very long. The long bubble is formed after a considerable contraction of the transitional (short) bubble and in this paper its origin will be termed as the turbulent reattachment point. Two mechanisms for this type of separation have been established. One is a bursting of the transitional (short) bubble, for example, by Owen and Klanfer (1953), Crabtree (1957), Gaster (1966), and Ingen (1975). The other is a turbulent separation aft of the transitional (short) bubble attachment line, sometimes referred to as "turbulent reattachment," with research by Wallis (1954), Hurley (1955), Evans and Mort (1959), and Berg (1981) identifying this type as did studies on three-dimensional wings by Poll (1983, 1986). Inasmuch as both of the above proposed mechanisms involves the sudden formation of a long bubble subsequent to the turbulent attachment

forming the short (transitional) bubble, the term "turbulent reattachment" will be used herein in relation to this type of long bubble.

The third classification of stall type, illustrated in part (c) of figure 1.1, is the combined trailing-edge/leading-edge encountered as the leading-edge radius or Reynolds number increases. This is a result of the leading-edge separation being delayed until some angle-of-attack higher than that at which trailing-edge separation has begun. As the trailing-edge separation moves forward with angle of attack, there is a gradual reduction in the rate of lift growth. With further increases in angle of attack, the pressure gradient in the leading region becomes sufficient to cause the turbulent reattachment with its sudden stall.

It should be noted there that a fourth type of stall classified as a trailing-edge stall which involves essentially no pronounced separation the leading-edge region will receive no detailed analysis in this paper except to define the upper Reynolds number limits of the other stalls. The trailing-edge stall is a gradual stall associated with the forward movement of trailing-edge separation.

### 1.3 Experimental Results Related to Stall

The purpose of this section is to describe in more detail the primary flow mechanisms contributing to the various type of airfoil stall illustrated in figure 1.1 by the use of some selected results of two-dimensional wind tunnel studies of boundary-layer separation and lift characteristics in the stall region. The first subsection deals with some effects of airfoils profile while the second presents two examples of Reynolds number effect.

#### 1.3.1 Effects of profile on separation and stall

Summarized here are some results of an extensive and systematic series of wind tunnel studies of the boundary-layer separation and stall characteristics for a series of airfoils tested in the same facility at a Reynolds number of  $5.8 \times 10^6$  and a Mach Number of 0.167 with free transition. This research covered a wide angle-of-attack

range and provided complete chordwise measurements of surface pressures and boundary-layer velocity profiles in regions of the separation bubbles identified by the liquid-film technique. The airfoils consisted of a sharp edge airfoil (double wedge) with the data being published by Rose and Altman (1950) and three NACA 6-series airfoils (64A006, 63-009, and 63<sub>1</sub>-012) published by McCollough and Gault (1948, 1949) and by Gault (1949).

Using the data from the above studies figure 1.2 has been prepared to illustrate the effect of angle of attack on the transitional (short) bubble turbulent reattachment location, the angle of attack and chordwise location for turbulent reattachment, and the variation with angle of attack of the location of the long-bubble reattachment. To illustrate the influence of these effects on airfoil lift and stall characteristics figure, 1.3 presents the lift versus angle-of-attack data for the same airfoils obtained from the above references. These two figures will be used together to describe the effects of profile on separation and stall.

Turning to figure 1.2 the turbulent reattachment point, measured from leading edge and normalized by the airfoil chord is shown in the bottom part of the figure at an expanded scale to accurately cover the forward 2-percent of the airfoil chord and provide details of the forward movement of transitional-bubble reattachment point with increasing angle of attack. The vertical lines of arrows illustrate the rather sudden transition from the contracted transitional bubble to the long bubble associated with turbulent reattachment shown in the upper part of the figure. The upper part of the figure covers the complete chord (note scale change) to allow total coverage of the rearward travel of the subsequent long-bubble reattachment point with angle of attack.

Regarding the data for the double wedge (4.26-percent thick) it should be noted that at angles of attack of 1° and 2° a separated flow region was observed, but no accurate determination of its extent could be made. Beyond 3°, the long-bubble reattachment point was reasonably well defined by boundary-layer profiles and

surface flow studies indicating a rather rapidly expanding long bubble with the reattachment point reaching the trailing edge at about  $7.5^\circ$  angle of attack. Beyond this angle of attack a thin-airfoil (long-bubble) type of stall occurs and a maximum lift coefficient of about 0.83 is reached as seen in figure 1.3.

Since the upper surface velocity gradients in the leading-edge region have a strong influence on the transitional (short) bubble development and the subsequent turbulent reattachment the airfoil contour in that region is important. With their effects generally occurring close to the leading-edge the leading-edge radius is often used as a convenient and fairly successful parameter for correlating leading-edge contour effects. Therefore, the leading-edge radius will be identified with the airfoils being discussed and used later as a parameter for a summary correlation.

The data for the round leading-edge NACA 64A006 and 63-009 airfoils, which have leading-edge radii of 0.26 and 0.63-percent chord respectively, provide excellent examples of the transition from the short (transitional) bubble at low angles of attack to the long bubble at higher angles of attack. This is followed by a sudden turbulent reattachment and conversion to a long bubble with the reattachment point moving aft with further increases in angle of attack at a rate somewhat similar to that observed for the sharp-edge airfoil. The bubbles are located very near the leading edge and have negligible effect on the airfoil characteristics.

For the 64A006 the turbulent reattachment onset occurs at a sufficiently low angle of attack that the initial length of the resulting long-type bubble is relatively short, and only a very slight "jog" in the lift curve occurs at an angle of attack of  $5^\circ$ . As seen in figure 1.3 this is not sufficient to cause stalling and is followed by an expanding long bubble and a thin-airfoil type of stall similar to that for the double-wedge airfoil but generating a slightly higher maximum lift coefficient of about 0.90. More information on the slight "jog" that can precede the thin-airfoil type of stall and the leading-edge type of stall can be found in the paper by McCullough (1955) dealing with a series of

symmetrical NACA 4-digit airfoils. The airfoils were relatively thin having thickness ratios of 6 percent, 7 percent, 7.5 percent, and 8 percent and the angles-of-attack were varied in small increments in the region of the jog and the stall. Briefly, the results illustrate that as the thickness ratio and leading-edge radius increases the jog, or discontinuity associated with turbulent reattachment, occurs at increasing lift coefficient and becomes more pronounced until it produces a leading-edge type of stall as illustrated by the NACA 63-009 airfoil in figure 1.3.

Returning to figure 1.3 it is seen that for the 63-009 airfoil the larger leading-edge radius relative to the 64A006 airfoil reduces the adverse pressure gradient and turbulent reattachment is delayed to about  $8.5^\circ$  resulting in a higher maximum lift coefficient of about 1.15. However, the delay in turbulent reattachment results in a more aft turbulent reattachment with the longer bubble resulting in a sudden stall of the leading-edge type followed by some lift recovery.

The data for the 63-012 airfoil, with its large leading-edge radius of 1.09 illustrates a case where turbulent reattachment is delayed to about  $13^\circ$  resulting in an even higher maximum lift coefficient of 1.5, but the resulting long bubble does not reattach and a very large and sudden loss of lift occurs as seen in figure 1.3. Careful inspection of the lift indicated some trailing-edge separation just prior to the sudden leading-edge stall, thus placing the stall in the combined trailing-edge/leading-edge category of figure 1.1.

It should be mentioned here that for this moderate Reynolds number of  $5.8 \times 10^6$  the transition from a combined trailing-edge/leading-edge type of stall to a pure trailing-edge type does not occur until thickness ratios well beyond those of interest to this paper are reached. However, as will be shown in the following sections this situation changes at higher Reynolds numbers.

### 1.3.2. Influence of Reynolds number on stall

The above results, illustrating the transition of stall types from thin airfoil to leading edge to the combined trailing edge/leading edge as the airfoil thickness and leading-edge radius increases, were for a constant Reynolds of  $5.8 \times 10^6$ . Similar transitions can also occur with increasing Reynolds number for a given airfoil and examples are presented in figure 1.4. Since there appears to be no data available for a single 6-series airfoil that includes all of the types of stall two 9-percent thick 6-series airfoils which differ only slightly in leading-edge radius will be used. These are the 66-009 having a leading-edge radius of 0.53-percent chord and the 64-009 having radius of 0.58-percent from the studies by Abbott et. al., (1945) and Loftin and Bursnall (1948) respectively.

The data for the 66-009 airfoil is shown in part (a) and clearly illustrates the change from a thin-airfoil type of stall at a Reynolds number of  $3 \times 10^6$  to a leading-edge type of stall for the Reynolds numbers of  $6 \times 10^6$ . Between the Reynolds number of  $3 \times 10^6$  and  $6 \times 10^6$ , the transition to turbulent flow apparently moves forward sufficiently to induce turbulent reattachment close to the leading edge resulting in a short bubble followed, at an angle of attack of  $10^\circ$ , by a turbulent reattachment. Since the separation occurs at a relative high angle of attack, the bubble reattachment is sufficiently far aft to cause a sudden leading-edge type of stall. Although not shown, the resulting leading-edge stall is still evident at the highest test Reynolds number of  $9 \times 10^6$  (see Abbott et. al., 1945). It should be noted that for these relatively sharp edged airfoils any combined trailing-edge/leading-edge stall is probably confined to a rather short range of Reynolds number if it occurs at all.

The high Reynolds number data in figure 1.4 (b) obtained with the NACA 64-009 airfoil which has a leading-edge radius,  $r/c$ , of 0.58-percent illustrates the transition from a leading-edge to a trailing-edge type of stall. For a Reynolds number of  $9 \times 10^6$ , the stall is of the leading-edge type as for the NACA 66-009. At some Reynolds

number between  $9 \times 10^6$  and  $15 \times 10^6$ , transition apparently occurs ahead of the theoretical laminar separation point, thereby suppressing leading-edge separation, and the stall becomes of the trailing-edge type.

For both of these airfoils, there is some evidence of a possible combined trailing and leading-edge stall. However, for these relatively thin airfoils, trailing-edge separation of sufficient chord extent to effect the lift does not occur until the angle of attack has almost reached the condition for leading-edge stall. In this regard, evidence will be seen in the next section that for the airfoils with larger values of leading-edge radius the stall appears to shift directly from the thin-airfoil type to the combined trailing-edge/leading-edge type. This appears to be associated with the forward movement of the transition to turbulent flow to the region ahead of the theoretical laminar separation point, thereby delaying leading-edge separation until trailing-edge separation has begun.

#### 1.4 Stall Boundaries

As a convenient way to summarize the influence of Reynolds number and airfoil leading-edge contour on the type of stall experienced by a large number of symmetrical NACA 6-series airfoils, a set of stall boundaries has been developed and is presented in figure 1.5. This set of stall boundaries is similar to that developed earlier by Gault (1957) for a large number of symmetrical and cambered airfoils covering a wide range of thickness ratios. In an attempt to include thickness distribution and camber into one velocity gradient parameter Gault selected, by trial correlations, an upper surface ordinate (measured from the chord line) near the leading-edge. Although the resulting correlation was fairly successful he pointed out that the parameter has no apparent physical significance and that the correlation seemed fortuitous. Due to this and the fact that the present study is limited to uncambered airfoils the more physically significant, and often used, leading-edge radius, which defines the surface curvature and therefore, is related to the upper

surface velocity gradients is used in the present set of stall boundaries. Since, as shown in figure 1.2, the turbulent reattachment generally occurs ahead of the one-half percent chord station for the types of airfoils of interest here, the leading-edge radius appears particularly suitable.

Turning now to the stall boundaries of figure 1.5 it is seen that the data used to establish the boundaries is limited to numerous symmetrical airfoils of the NACA 6 series tested over a wide range of Reynolds numbers in the Langley two-dimensional Low-Turbulence Pressure Tunnel. The results are for the transition free condition and based on data in the stall region reported by Abbott et. al. (1945), Loftin (1947), Loftin and Bursnall (1948), and Loftin and Smith (1949). The correlation covers a chord Reynolds number range of  $7 \times 10^5$  to  $3 \times 10^7$  and a leading edge radius,  $r/c$ , range from 0.24-percent to 1.56-percent.

The combinations of Reynolds numbers and leading-edge radii that define the approximate boundaries (cross hatched bands) between the various types of stall have been established from the above data references using symbol types to identify the type of stall for each test Reynolds number. Also shown by the dashed lines are the vertical cut and the two horizontal cuts through the boundaries that are related to figures 1.3 and 1.4. The boundaries appear to be reasonably well established but it must be recognized that boundaries for other airfoil series will probably vary somewhat, in particular the one defining the onset of trailing-edge stall due to the influence of trailing-edge closure angle. However, for the lower thickness range of interest in this paper it may not be too significant.

Finally, the correlation illustrates that in the high Reynolds number range the boundaries are converging rather rapidly indicating the possibility that at some Reynolds number above  $20 \times 10^7$  there may only be two types of stall; the thin-airfoil type and the trailing-edge type. Both, of course, produce a gradual variation of lift in the stall region, the first produced by the gradual aft expansion of the long bubble and

the second associated with a gradual forward expansion of the trailing edge separation.

### 1.5 Airfoil Maximum Lift Coefficients

The variation of the maximum lift coefficient of selected 6-series airfoils with Reynolds number is summarized in figure 1.6. Again the data are limited to NACA 6-series airfoils tested in the Langley two-dimensional Low-Turbulence Pressure Tunnel and the maximum lift coefficients, for free transition are plotted against the chord Reynolds number covering a range from  $0.7 \times 10^6$  to  $3 \times 10^7$  at Mach numbers no greater than 0.15. Shown for reference are the thin-airfoil and the trailing-edge stall regions taken from the stall boundaries of figure 1.5. For the purpose of this section the leading-edge stall region and the trailing-edge/leading-edge stall region shown in figure 1.5 are combined in figure 1.6 and fall, of course, between the two boundaries shown.

As discussed earlier both the thin-airfoil type stall and the trailing-edge type stall are similar in that the stall is rather gradual with the former associated with the gradual downstream growth of the separation region and the latter with the gradual upstream growth. However, there are several well-known differences in the magnitude of the maximum lift coefficient in these two regions. In the thin-airfoil stall region where the long separation bubble originates at a rather low angle of attack, the maximum lift coefficients for this round-edge airfoil series are confined to a rather narrow range from about 0.8 to about 1.0. In the trailing-edge stall region, which occurs in the high Reynolds number range, the well known benefit of increasing leading-edge radius on the maximum lift coefficient is observed. In this high Reynolds Number region separation near the leading-edge is, of course, suppressed and as the leading-edge radius increases the adverse pressure gradients decrease and reduce the turbulent boundary-layer growth and the trailing-edge separation. The other characteristic of interest is the lack of any appreciable increase in maximum lift with increasing

Reynolds number in this stall region. In this regard the reader is referred to Loftin and Bursnall (1948) who discuss a possible regenerative process, involving the mutual influence of trailing edge separation and leading-edge separation.

It should be pointed out that in the high Reynolds number range where the two boundaries appear to converge it is possible that the 64-006 airfoil may have transitioned from a thin-airfoil stall to a trailing-edge stall. However, with both types experiencing a gradual stall and in the absence of pressure and moment data in the high Reynolds number range, no attempt at clarification will be made.

Turning to the region between the above two stall-type boundaries it is seen that in this region the maximum lift coefficient is a strong function of both Reynolds number and airfoil contour with, for this series, the leading-edge radius being the dominant contour parameter. As mentioned above, this region contains both the pure leading-edge stall type and the combined trailing-edge/leading-edge stall type. However, since both types encounter the sudden stall associated with turbulent reattachment (aft of the transitioned bubble) which is of major importance in the following sections on three-dimensional wings, the two regions are combined in figure 1.6. It is in this region that both increasing Reynolds number and increasing leading-edge radius delay the turbulent reattachment and the accompanying sudden stall to higher angles of attack thereby increasing the maximum lift coefficient.

Much of the remainder of this paper deals with the manner in which various three-dimensional induced effects associated with aspect ratio and sweep angle influence the onset of turbulent reattachment and control the type of wing flow and stalling that results. However, in general, these studies deal with wings which utilize airfoils other than the NACA 6-series. Therefore, figures 1.7 and 1.8 present the maximum lift coefficient variation with Reynolds number for the NACA 0012 and the ONERA "D" airfoils respectively to provide the two-dimensional baseline data for use in illustrating

some of the three-dimensional effects involving Reynolds number variations to be discussed later.

The NACA 0012 data in the low Reynolds number range was obtained in Langley Two-Dimensional Low-Turbulence Tunnel and published by Loftin and Smith (1949) while that above a Reynolds number of  $2.0 \times 10^6$  is from tests in the Langley Low Turbulence Pressure Tunnel published by Ladson (1988). The Mach number effects are shown only as an aid in extrapolating the ONERA "D" data as will be discussed below. The NACA 0012 airfoil, which has a leading-edge radius of 1.58-percent chord, has a trend with Reynolds number consistent with the 12-percent thick 6-series airfoils of figure 1.6.

The ONERA "D"  $r/c = 10.5\%$  airfoil data shown in figure 1.8, published by Erlich (1969), was obtained by variations in free stream Mach number rather than tunnel pressure and therefore encounters "shock stall" between a free stream Mach number of 0.12 and 0.18 which is similar to the constant tunnel pressure (dashed) lines drawn through the NACA 0012 data of figure 1.7. Based on the NACA 0012 shock free data the ONERA "D" data is extrapolated (dashed line) to cover the shock free range of the subsequent three-dimensional data. Although somewhat conjectural, this small extrapolation it is believed to be sufficiently accurate for the purpose of this paper.

It should be noted here that for both of the above airfoils the type of stall was independent of Mach number and remained of the trailing-edge/leading-edge type since the shock occurred in the leading-edge region.

## 2. EDGE SEPARATIONS ON RECTANGULAR WINGS

### 2.1 Sources of Edge Separation

Two sources of edge separation flows encountered on rectangular wings that influence their lift and stall characteristics are illustrated in figure 2.1. Part (a) illustrates, for the attached flow case, the type of change in chordwise pressure

distribution that results from the chordwise variation of normal velocities induced on the wing by the vortex wake associated with the three-dimensional flow. The resulting changes are illustrated by comparing a typical upper surface pressure distribution at the root section of a low aspect-ratio rectangular wing with that for a two dimensional airfoil at the same section lift coefficient,  $c_l$ . Of particular interest for this paper is the increase in the adverse pressure gradient near the leading edge for the low aspect-ratio wing, resulting from the fact that the downwash induced along the chord increases in the downstream direction producing an effect analogous to "streamline curvature" or "induced camber." This increase in the adverse pressure gradient causes the three-dimensional wing to encounter leading-edge separation in the root section at a lower section lift coefficient than in two dimensional flow. This effect of induced camber increases with decreasing aspect ratio and is related to the well known forward movement of the wing center-of-pressure which approaches the leading-edge as the aspect ratio approaches zero.

Part (b) illustrates both the leading-edge separation bubble discussed above and the side-edge separation which occurs for various combination of side-edge profile, Reynolds number and lift coefficient. Associated with this side-edge separation is the well known side-edge vortex flow and the resulting vortex-lift increment in the tip region. The case illustrated is for the tip of revolution where the side-edge separation origin is aft of the maximum span. The spanwise distribution of lifting pressure at an  $x/c = 0.8$  shown in the lower sketch is representative of the vortex lift effect.

## 2.2 Prediction Methods

The primary purpose of this section is to develop approximate methods of including the induced camber and vortex lift effects on the stall characteristics of rectangular wings. In addition, comparisons with experimental results will be made for a range of aspect ratio and Reynolds number. Because of the interest in this paper on Reynolds number effects, only round leading-edge wings will be discussed in this section.

### 2.2.1 Some early studies

Until the mid 1930's "lifting-line theory," which ignored the influence of induced camber, was the primary wing design method. This was satisfactory, in general, for the moderate to high aspect ratio wings of that period and avoided the time consuming effort required at that time to perform completely three-dimensional solutions.

Possibly the earliest detailed theoretical studies of the effect of induced camber on the pressure distributions of low aspect-ratio rectangular wings with attached flow were the approximate calculations of Fuchs (1939) and Wieghardt (1939). These studies and others such as those performed by Lawrence (1951), and Lomax and Sluder (1952), illustrated the increased pressure gradient at the leading edge, associated with induced camber, for the attached, inviscid flow condition. The early researchers, however, were primarily interested in the effect induced camber played in the overall wing aerodynamic center variation with regard to aircraft stability since the relatively thick, moderate-to-high aspect ratio, wings of the period usually encountered trailing-edge, rather than leading-edge separation. Later, with the advent of supersonic aircraft with thinner wings of low aspect-ratio, the effect of induced camber on leading-edge separation began to play a more prominent role.

### 2.2.2 Development of an Approximate Method

One of the purposes of this paper is to develop an approximate method of combining experimental two-dimensional airfoil data, such as that reviewed in section 1, with an induced camber method to predict the turbulent reattachment characteristics of three-dimensional wings. The method developed in this section utilized an approach similar to one developed by Polhamus (1955) for predicting the approximate effect of induced camber on the overall lift-dependent profile drag for low aspect ratio rectangular wings. Basically, this concept utilized the effect of induced camber on the adverse upper surface pressure gradient in the leading-edge region of the three-dimensional wings to establish an "effective" two-dimensional airfoil lift coefficient

having essentially this same adverse pressure gradient. The present method allows this "effective" two-dimensional lift coefficient,  $c_{l,cot}$ , to be established at any spanwise station desired, by utilizing lifting-surface theoretical solutions.

While any accurate lifting-surface solution could be used in the proposed method by use of appropriate pressure gradient extraction techniques, the theory developed by Multhopp (1950) uses an approach that is convenient for the present application. The method developed herein can be described with the aid of figures 2.2 and 2.3.

Basically, the Multhopp method utilizes a series of continuous chordwise distributions of circulation at discrete spanwise stations to satisfy the boundary conditions. As shown in figure 2.2, these distributions include the so-called "cotangent" loading that represents the pure angle-of-attack type (two-dimensional) distribution and a series of "sine" loadings which represent various induced camber distributions. The primary advantage of the Multhopp method lies in its use of the "cotangent" loading term. However the same general approach could be applied to other lifting surface methods.

As will be shown below, the pressure gradient associated with the cotangent loading predominates in the leading-edge region where the turbulent reattachment, of interest here, occurs. Therefore, it would be expected that the onset of turbulent reattachment in the three-dimensional case would occur at the spanwise location where the value of  $c_{l,cot}$  reaches the value of the two-dimensional airfoil lift coefficient corresponding to turbulent reattachment.

One of the simplifying assumptions in the method to be developed is that the influence of induced camber on the upper surface adverse pressure gradient can be approximated to sufficient accuracy by ignoring the effect of thickness. These "flat plate" solutions for  $c_{l,cot}$  will then be utilized in conjunction with the experimental data, obtained with the appropriate airfoil section, at the desired Reynolds number, to estimate the lift coefficient for the onset of turbulent reattachment in the three-

dimensional case. This use of the experimental data provides the major effect of thickness.

The concept will be illustrated in figures 2.2 and 2.3 by use of the resulting  $\Delta C_p$  distributions contributed by the "cotangent" and various "sine" loadings calculated by the Lan and Lamar (1977) version of the Multhopp (1950) approach. For the readers convenience, the relationships between the chord-loading series of Multhopp (1950) and those of Lan and Lamar (1977), used herein are presented in the appendix. The  $\Delta C_p$  distribution was selected because of its more direct relationship to lift coefficient. For these "flat plate" solutions, a match of the  $\Delta C_p$  gradients also signifies a match of the upper surface adverse pressure gradients. The expression for  $\Delta C_p$  is given by:

$$\Delta C_p(\phi, \eta) = \frac{2}{\pi} \left[ \frac{q_0(\eta)}{c(\eta)} \cot\left(\frac{\phi}{2}\right) + \sum_{n=1}^{\infty} \frac{q_n(\eta)}{c(\eta)} \sin(n\phi) \right]$$

where the q's are coefficients of the various chordwise loadings which are determined by satisfying appropriate boundary conditions over the wing surface. The chordwise station,  $x/c$ , is related to the angle  $\phi$ , as indicated in figure 2.2(a).

As an illustration of the types of chordwise loadings that are involved, figure 2.2(b) presents the results obtained for a rectangular wing of aspect ratio 0.5. These results are for the wing centerline at a section lift coefficient of 1.0. This very low aspect ratio wing was selected because its large induced camber provides a clearer illustration of the concept. The centerline location is chosen since that is where the turbulent reattachment begins for rectangular wings.

For the solution shown in figure 2.2(b), four chordwise loading distributions were utilized; the "cot  $\phi/2$ " loading which represents the pure angle-of-attack loading, and the first three "sine" loadings representing various induced camber loadings. It will be noted that the cot  $\phi/2$  and the sin  $\phi$  loadings are, by far, the most prominent contributors to the chordwise pressure distribution. The sin  $\phi$  induced camber term produces a large negative lift, due to the increasing downwash in the downstream direction, which must be offset by an increase in the cot  $\phi/2$  loading in order to

maintain the section lift coefficient,  $c_l$ , of 1.0. For the case shown, the  $c_{l, \cot}$  term associated with the  $\cot \phi/2$  loading term is equal to 1.62 which represents a 62-percent increase over the total section lift coefficient of 1.0. Thus, for this low aspect ratio wing, turbulent reattachment near the leading edge would be expected to occur at a much lower section lift coefficient than for the two-dimensional case.

The above effects are illustrated further in figure 2.3(a) where, for the total section lift coefficient of 1.0, the summation of the four chordwise loading terms of figure 2.2(b), labeled "total," is compared with the  $\cot \phi/2$  term. Also shown is the distribution of the lifting pressure term of the two-dimensional case for a section lift coefficient of 1.0, to illustrate the greater adverse pressure gradient near the leading-edge for the low aspect ratio wing.

The total adverse pressure gradient near the leading edge can be accurately represented by the  $\cot \phi/2$  term, as illustrated in figure 2.3(b), for the forward 2-percent of the wing chord. The accuracy appears sufficient for the purpose of this paper and is best defined by the ratio  $K$  in the upper part of the figure. This parameter indicated less than 1-percent difference between the two loadings for a typical region of turbulent reattachment taken from figure 1.2.

The variation of  $c_{l, \cot}$  across the span of the  $A = 0.5$  wing is shown in figure 2.4(a). It should be noted that both the local values of  $c_{l, \cot}$  and  $c_l$  are normalized by the overall wing lift coefficient,  $C_L$ . The results illustrate that the magnitude of  $c_{l, \cot}$  is considerably greater than the corresponding total sectional lift coefficient,  $c_l$  at all spanwise stations; and at the mid semi-span station,  $c_{l, \cot}$  is approximately 60-percent to 65-percent greater than the corresponding total section lift coefficient,  $c_l$ . The reader is reminded that the actual span load distribution across the wing is represented by the usual  $c_l/C_L$  distribution and that the  $c_{l, \cot}/C_L$  distribution represents an equivalent section lift coefficient having the same adverse chordwise gradient in the leading-edge region as in the real three-dimensional flow.

The formation of the transitional separation bubble and the subsequent turbulent reattachment are, for a given Reynolds number, primarily dependent on the magnitude of the adverse pressure gradient close to the leading-edge which is dominated by the cotangent loading. As mentioned above, leading-edge stall, resulting from turbulent reattachment, would be expected to occur when  $c_{l,cot}$  rather than  $c_l$  reaches a value approximately equal to the two-dimensional airfoil lift coefficient corresponding to stall. Thus, for the  $A = 0.5$  wing example shown, leading-edge stall would begin at the root station for a total section lift coefficient,  $c_l$ , that is only about 62-percent of the two-dimensional airfoil lift coefficient corresponding to stall in the two-dimensional case.

Since, for rectangular untwisted wings, leading-edge separation occurs first at the root station ( $\eta = 0$ ) the variation of  $(c_{l,cot}/c_l)_{\eta=0}$ , with wing aspect-ratio is presented on figure 2.4(b). The results illustrate the large increase in  $(c_{l,cot}/c_l)_{\eta=0}$ , with decreasing aspect ratio. This theoretical variation of  $c_{l,cot}/c_l$   $\eta = 0$  will be used in the following analysis of experimental data related to the leading-edge separation characteristics of low aspect-ratio rectangular wings to illustrate the magnitude of induced camber effects on root section stall.

### 2.3 Comparison of Predictions and Experiments

This section will be devoted to predicted and experimental examples of the influence of aspect ratio on root stall, on total wing stall, and some interacting effects of aspect ratio and Reynolds number on overall wing stall.

#### 2.3.1 Effect of aspect ratio on root stall

Inasmuch as the stall of uncambered and untwisted rectangular wings is initiated at the wing root the induced camber effect at that station is of particular importance. To illustrate its effect the experimental study by Brebner et. al. (1965) of five rectangular wings having RAE 101 (10-percent) symmetrical airfoil sections and tips of revolution will be used. The wings covered an aspect ratio range from 4.0 to 0.5 and the data to be used here which, except for one case, reached the stall, was obtained at a chord

Reynolds number of  $1.6 \times 10^6$ , and a Mach number of 0.11. The experimental two-dimensional data for the RAE 101 (10-percent) airfoil, required for application of the prediction method is obtained from Brebner and Bagley (1952). It was tested in the same wind tunnel as the three dimensional wings at a Reynolds number of  $1.7 \times 10^6$  and a Mach number of 0.09. For the convenience of the reader the theoretical values of the induce camber parameter  $(c_{l,cot}/c_{l})_{\eta=0}$  from figure 2.4(b) are listed here for the five wings of the experimental series with the induced camber parameter in parenthesis following each aspect ratio: 4(1.03), 2.5(1.08), 1.4(1.23), 1.0(1.36) and 0.5(1.62). Figure 2.5 presents some selected pressure data while figure 2.6 summarizes the lift data.

Figure 2.5 is presented to illustrate, with experimental upper surface pressure data, the influence of induced camber on the pressure distribution in the leading-edge region of the wing root section. The aspect ratio 1.4 and 1.0 wings were selected because their high level of induced camber allows for a more critical evaluation of the prediction method. The root section of the lowest aspect ratio wing (0.5) encounters some strong effects induced by the separation - induced tip vortex flow which will be discussed later. The tabular pressure data for the two wings were not included in the paper by Brebner et. al. (1965) but were obtained from those authors. Inasmuch as turbulent reattachment probably occurs forward of the one-percent chord station (see figure 1.2) the data is limited to the forward 2-percent of the chord to allow for an expanded scale.

Turning first to the wing of aspect ratio 1.4 it will be noted that three conditions are presented. One is for the three dimensional wing at the root station for a section lift coefficient of 0.78 which is slightly below the stall. The other two conditions are from the two-dimensional airfoil data ( $A = \infty$ ) of Brebner and Bagley (1952) at two lift coefficients, one being the same as that selected for the three-dimensional wing (0.78) and the other for a cotangent lift coefficient of 0.96 obtained by applying the induced

camber factor of 1.23. It should be noted here that only slight interpolations were required to obtain the two-dimensional pressure distributions for the required lift coefficients. Although the orifice locations for the three-dimensional wing are rather sparse the orifice at the  $x/c$  of 0.005 is expected to be near the turbulent reattachment point.

Regarding the results for the wing of aspect ratio 1.4 it will be noted first that the suction pressures and adverse pressure gradients are much greater than for the two-dimensional airfoil at the same lift coefficient (0.78) as would be expected due to the induced camber effect. Secondly, it is seen that the two-dimensional airfoil pressures for the lift coefficient of 0.96 that was obtained by applying the induced camber factor are in much better agreement with the wing of aspect ratio 1.4. Despite the few pressure orifices for the aspect ratio 1.4 wing the results appear to at least qualitatively confirm the accuracy of the prediction method.

The result for the wing of aspect ratio 1.0 which, of course, encounters an even greater induced camber effect also appears to confirm the prediction method. The wing of aspect ratio 0.5 has been omitted in figure 2.5 because strong effects of the separation-induced side-edge (tip) vortex illustrated in figure 2.1(b) extend inward to the wing root. This effect will be discussed subsequently.

Turning now to the lift and stall characteristics at the root section for the complete aspect ratio series figure 2.6 presents the sectional lift coefficient,  $(c_l)_{\eta=0}$ , obtained by Brebner et. al. (1965) through integration of surface pressure measurements, as a function of the wing angle of attack,  $\alpha$ , for a chord Reynolds number of  $1.6 \times 10^6$ . Also shown is the two-dimensional data on the same airfoil section as obtained at a Reynolds number of  $1.7 \times 10^6$  from the paper by Brebner and Bagley (1952). It should be noted that the two-dimensional data indicates a sudden stall of the leading-edge type resulting from turbulent reattachment and a  $c_{l,max}$  of 1.068. It is of interest that the Reynolds number of  $1.7 \times 10^6$  and the leading-edge radius of 0.76-percent of the

chord places this airfoil about on the boundary between thin-airfoil and leading-edge stall for the NACA 6-series airfoils of figure 1.5. The centerline lift data for the finite-span wings also indicates a leading-edge type of stall and a pronounced reduction in the centerline maximum lift coefficient with decreasing aspect ratio caused by the influence of induced camber on the upper surface pressure gradient discussed above.

Regarding the maximum lift coefficient, it should be noted that experimental results for inverted model test conditions is also presented in the stall region. Although the two model conditions were used by Brebner et. al. (1965) to correct the angle-of-attack for tunnel flow angularity, the differences in maximum lift coefficients indicate some measurable flow curvature effects in the tunnel stream producing an effective camber. In such a case, opposite, effects on  $c_{l,max}$  would be expected, with the true value lying between the two results.

To illustrate the degree to which the induced camber concept predicts this reduction in centerline maximum lift, predicted values of  $c_l$  corresponding to the onset of turbulent reattachment have been made by the method of this paper. For the leading-edge type of stall, the prediction also corresponds to the maximum lift coefficient. Using the theoretical ratio of cotangent lift to total lift,  $(c_{l,cot}/c_l)_{\eta = 0}$ , from figure 2.4(b), the value of total  $c_l$  required to provide a  $c_{l,cot}$  equal to the measured two-dimensional  $c_{l,max}$  of 1.068 was determined for each of the aspect ratios. The predicted values of the root-section lift coefficients for which turbulent reattachment onset and the accompanying leading-edge stall, occurs is indicated by the horizontal arrows for each aspect ratio except for the 0.5. The predicted values define rather accurately the reduction of the root-section maximum lift coefficient with decreasing aspect ratio. Since, as mentioned earlier, the stall of the complete wing is initiated at the root section the prediction of root section stall is, of course, an important ingredient in the complete wing stall.

Returning for a moment to the wing of aspect ratio 0.5 it seems apparent from the increasing slope of the lift versus angle-of-attack that a strong influence of the separation induced side-edge (tip) vortex extends to the root section contributing directly to the maximum lift and modifying the pressure gradients. Thus the prediction method developed for the root section does not apply for this very low aspect ratio wing and the resulting calculation which provides a fairly accurate but fortuitous value is not shown. This very low aspect ratio is of little practical importance and does not represent a serious shortcoming of the method.

### 2.3.2. Effect of aspect ratio on overall wing stall

This section describes the additional consideration required to predict the overall wing stall and makes comparisons with experimental results on rectangular wings including both aspect ratio and Reynolds number effects.

As in the previous section on root stall this section deals with wings encountering turbulent reattachment in the leading-edge region. The prediction of the overall stall for the complete wing involves the prediction of the root section stall as in the previous section except that the induced camber term must now be related to the total wing lift coefficient,  $C_L$ . The variation of this parameter,  $(c_i, cot)_{\eta=0} / C_L$ , with aspect ratio has been calculated by the Lan and Lamar (1977) method described earlier and is presented in figure 2.7(a). Also shown is the variation of the total root section lift coefficient parameter as an aid in establishing the magnitude of the induced camber effect. The reader is reminded that the  $(c_i, cot)_{\eta=0} / C_L$  term does not imply that the induced camber increases the root section lift coefficient. It only indicates the value of an equivalent two-dimensional airfoil lift coefficient that has a comparable upper surface pressure gradient in the leading-edge region, where turbulent reattachment occurs, as does the three-dimensional wing with its induced camber.

The overall wing stall is influenced not only by the turbulent reattachment in the root region but by the vortex lift produced by side-edge (tip) separation. This non-linear lift

becomes rather large in the low aspect ratio range and was observed rather early by several researchers such as, for example, Knight and Loeser (1927), Zimmerman (1932) and Winter (1936) and became the subject of continuing experimental research as the interest in moderate to low aspect ratio wings increased. Chosen here to predict this side-edge vortex lift is the side-edge suction analogy method developed by Lamar (1974) as an extension of the leading-edge suction analogy developed earlier for the vortex lift of slender delta wings. Lamar's method has proven to give accurate predictions of the vortex lift for the case of sharp side edges where all of the inviscid side-edge suction is converted to vortex normal force from which the lift can be calculated. The resulting vortex lift represents the "upper bound" associated with complete side-edge separation. Values of the constant of proportionality,  $K_{v,se}$ , in the vortex lift equation, to be discussed subsequently, have been taken from Lamar (1974) and are presented in figure 2.7(b) as a function of aspect ratio. Also shown is the variation of  $K_p$ , the theoretical inviscid lift curve slope to be used later.

Turning now to some experimental data, the effect of aspect ratio on the total lift and stall characteristics is illustrated in figure 2.8 for a series of rectangular wings having NACA 0012 airfoil sections and no tip fairings. Also presented is the data for the two dimensional 0012 airfoil obtained from the study by Loftin et. al. (1949). The data for the wing of aspect ratio 6 is from Muse (1943) and that for the wings of aspect ratio 3 and 2 from Jones (1952). All the tests were for Mach numbers less than 0.10 and a chord Reynolds number of  $3.0 \times 10^6$  with all but the wing of aspect ratio 6 being tested in the Langley two-dimensional low-turbulence pressure tunnel. In addition to the experimental data two theoretical variations are shown for the finite aspect ratio wings; the inviscid attached flow theory given by  $K_p \sin \alpha$ , the full side-edge vortex lift theory given by adding the vortex lift increment  $K_{v,se} \sin^2 \alpha \cos \alpha$  to the attached flow theory. The values of  $K_p$  and  $K_{v,se}$  were obtained from figure 2.7(b).

From figure 2.8 it is seen that for these square-edge wings prior to the stall the experimental lift (shown by the data points) is in good agreement with the solid line which represents the sum of the theoretical inviscid lift and the theoretical side-edge vortex-lift theory. Also the large increase in the vortex lift as aspect ratio is reduced is clearly evident. It should be pointed out, however, that for wings with the usual tips-of-revolution complete separation would not be expected and less side-edge vortex-lift would be produced.

With regard to the total wing stall characteristics it is seen that while there is a 16-percent reduction in maximum lift coefficient between the two-dimensional case and the aspect ratio 3.0 case there is a recovery of some of that loss by the wing of aspect ratio 2.0. This of course is due to the increase in vortex lift which counteracts a considerable portion of the loss of maximum lift coefficient associated with the influence of induced camber on the turbulent reattachment at the root section. To further illustrate these influences, predictions of these effects using the two-dimensional airfoil maximum lift coefficient corrected for induced camber and adding the theoretical vortex lift increment are made in the following section.

The two-dimensional NACA 0012 airfoil with its rather large leading-edge radius (1.58-percent  $c$ ) experiences the combined trailing-edge/leading-edge type of stall illustrated in figure 1.1(c) in which some trailing-edge separation occurs prior to the sudden leading-edge stall. For the total wing lift of the three-dimensional wings the combination of non-linear side-edge vortex-lift and delay in trailing-edge separation on their outer portions tend to offset the influence of the trailing-edge separation in their root regions. However, with the sudden stall of the three-dimensional wings being initiated in the root region it is assumed that the two-dimensional data can be used in predicting the three-dimensional total wing maximum lift-coefficient in a manner similar to that used in section 2.3.1 for the root section. The vortex lift must, of course, be

included and these two primary influences are combined in the following equation with the assumption that, for the purpose of this paper, their interactions can be ignored in the aspect ratio range considered. This results in:

$$C_{L,max} = \left[ C_{i,max} / \frac{(C_{i,cot})_{\eta=0}}{C_L} \right] + [K_{v,SE} \sin^2 \alpha_{crit} \cos \alpha_{crit}] \quad (2.1)$$

The calculation performed in the first set of brackets establishes the contributions of the root section stall to the total wing maximum lift coefficient by dividing the experimental two-dimensional  $C_{i,max}$  by the theoretical induced camber term at  $\eta = 0$  which as noted earlier is normalized by the total wing lift coefficient, neglecting the vortex lift, and is obtained from figure 2.7(a). This component of the total maximum lift coefficient corresponds to the onset of turbulent reattachment and decreases with decreasing aspect ratio similar to the decrease shown in figure 2.6 for the root section of the RAE 101 (10 percent) wings.

The calculation performed within the second set of brackets in the above equation predicts the magnitude of the side-edge vortex lift at the angle of attack,  $\alpha_{crit}$ , for which the predicted sudden root-stall associated with turbulent reattachment onset occurs. The variation of  $K_{v,se}$  with aspect ratio, obtained by the side-edge suction analogy method of Lamar (1974), is presented in figure 2.7(b) for rectangular wings. The values of  $\alpha_{crit}$  are obtained from:

$$\alpha_{crit} = \arcsin \left[ C_{i,max} / \frac{(C_{i,cot})_{\eta=0}}{C_L} \right] \frac{1}{K_p}$$

where  $K_p$  is the theoretical inviscid three-dimensional lift curve slope, obtained from figure 2.7(b).

The results of the application of the above prediction method are indicated in figure 2.8. The three predicted parameters are defined for the wing of aspect ratio 2.0. The

horizontal arrow labeled "turbulent reattachment onset" defines the total wing inviscid lift coefficient corresponding to leading-edge stall at the root as calculated by the first bracketed term in equation (2.1) and also defines " $\alpha_{crit}$ " which is used in the second bracketed term in equation (2.1) to predict the vortex-lift contribution to the total wing maximum lift coefficient. The sum of the predicted lift coefficient corresponding to leading-edge stall at the root and the predicted vortex-lift increment at  $\alpha_{crit}$  represents the predicted total wing maximum lift coefficient and is shown by the solid horizontal arrow labeled " $C_{Lmax}$ ".

The above labeling of the predicted parameters is used for all three of the finite span wings and it is seen that the methods used result in reasonably good agreement with the experimental results. From these comparisons it is seen that the effect of induced camber on the root stall contribution to the total wing maximum lift-coefficient results in a rather large decrease with decreasing aspect ratio. This decrease amounts to 29-percent for the aspect ratio 2.0 wing relative to the two-dimensional airfoils and for a wing with no side-edge (tip) separation it would represent the reduction in the total wing maximum lift coefficient. However, for these wings with complete side-edge separation the increase in vortex-lift contribution with decreasing aspect ratio offsets a sizable portion of the induced camber effect.

### 2.3.3. Reynolds number influence on wing stall

Turning now to the influence of Reynolds number, the prediction method developed above for combining the leading-edge stall and side-edge vortex lift will be used as an analysis aid. Although the primary effect of Reynolds number on  $C_{Lmax}$  is expected to be similar to that encountered in two-dimensional flow, as discussed in section 1.5, the above method indicated several three-dimensional effects that can alter the magnitude of the Reynolds number effects encountered by low aspect-ratio rectangular wings. For example, the increase in  $\alpha_{crit}$  with increasing Reynolds

number, due to the delay in leading-edge root stall, results in an increase in the magnitude of the side-edge vortex lift. Inasmuch as the vortex-lift effect increases with decreasing aspect ratio, it would be expected that the influence of Reynolds number would be dependent on the aspect ratio.

The most extensive experimental data base available for evaluating the effects of Reynolds number over a range of aspect ratios appears to be that associated with investigations utilizing the NACA 0012 airfoil section on rectangular wings having square side edges used in the previous section and reported by Muse (1943) and Jones (1952). The data was obtained in tunnels having relatively low turbulence levels, and the models were tested in the "free transition" condition. For the data presented here the Mach number was no greater than 0.13.

Evaluating first the aspect-ratio 6 case, figure 2.9 presents  $C_{L,max}$  as a function of Reynolds number as predicted by the present method and as obtained from the experimental study by Muse (1943). Shown for comparison are the two-dimensional results from figure 1.7. The two predicted curves were determined with the present three-dimensional prediction methods. The dashed line represents the prediction neglecting the side-edge vortex lift and the difference between it and the two-dimensional results represents the influence of the three-dimensional effects on the turbulent reattachment in the leading-edge region. The solid line represents the predicted total  $C_{L,max}$  resulting from the inclusion of the side-edge vortex lift. It will be noted that the increment associated with the side-edge vortex lift increases slightly with increasing Reynolds number. The results indicate the prediction method to be reasonably accurate.

Figures 2.10 and 2.11 present the same type of comparisons as in figure 2.9 but extends them to the low aspect ratio range with the aid of the experimental data for aspect ratios of 3 and 2 from the study by Jones (1952). In both cases, there is good agreement between the experimental results and the present prediction method.

There are several items of interest illustrated by figures 2.9 through 2.11. First, it is noted that as the aspect ratio is reduced, the vortex lift contributed by the side-edge vortex flow increases; in addition, this vortex lift increment increases as Reynolds number is increased. This increase in the vortex lift results from the increase with Reynolds number of the angle of attack,  $\alpha_{crit}$ , at which the leading-edge stall (turbulent reattachment) at the root occurs, thereby resulting in a stronger side-edge separation vortex. A second item of interest is seen by comparing figures 2.10 and 2.11. This comparison indicates that due to the compensating effects of induced camber and side-edge vortex-lift illustrated in figure 2.8, the values of  $C_{L,max}$  are essentially equal for the wings of aspect ratio 3 and 2 over the Reynolds number range studied. However for lower aspect ratios the vortex flow would be expected to dominate and an increase in  $C_{L,max}$  would occur. However, as mentioned earlier, it should be stated that for the more usual practice of utilizing a tip of revolution some reduction in the vortex lift occurs which will modify the above trade-off.

In concluding this section it should be pointed out that for wing-fuselage combinations the additional influence of the fuselage-induced upwash over the inboard portion of the wing must be considered with regard to root stall. Also, of course, the use of wing warp to optimize various design requirements will modify the above results as well as those in the following sections, but are beyond the scope this paper.

### 3. SWEPTBACK WINGS

#### 3.1 Some Early Research

By the mid-1940's a great deal of interest in sweptback wings for high speed aircraft was developing because of their advantage in delaying the onset of adverse compressibility effects. This interest was generated first in Germany where it can be traced to the supersonic sweptback wing theory of Buseman (1935), and later in the United States as a result of the independent development of the theory by Jones

(1945) who, in addition, extended the supersonic theory to include the important subsonic edge case associated with highly swept wings. Both demonstrated that it was the component of Mach number normal to the isobars that was critical.

However, with regard to the effect of sweepback on the low speed lift and stalling characteristics, of interest in this paper, it appears that the first related work appeared much earlier in a paper published by Munk (1923). In connection with the effect of sweep on lateral stability, Munk stated that "in straight flight only the component of the velocity,  $V \cos \Lambda$ , is effective for the creation of the lift." Possibly the first published work directly related to the stalling of swept wings was that of Betz (1935) who, in discussing the stall of rectangular wings in oblique (yawed) flow stated that "the decrease in maximum lift for varying angles of approach (yaw) might be expected to be proportional to  $\cos^2\psi$ , but the assumption that the superposition of a transverse velocity does not materially affect the separation phenomena is somewhat uncertain....." Betz also pointed out that the meager data available at the time indicted the decrease in maximum lift to be somewhat less than suggested by the "cosine squared" rule. Since, in the mid-1930's, the interest in wing sweep was confined primarily to very modest degrees of sweepback, related primarily to the stability and controllability of tailless aircraft, little research was carried out on the effect of moderate and high sweep angles on wing stalling until, as mentioned earlier, the benefits to the high speed performance were recognized. With the interest turning to highly sweptback wings to provide efficient supersonic capability and with separation occurring at lower lift coefficients as predicted by the Betz cosine-squared rule, there was an acceleration of research related to the take-off and landing capabilities and the low speed stability and control characteristics.

## 3.2 Some Types of Flow

While it is beyond the scope of this paper to review in detail this early research, a brief mention of some of the primary flow phenomena which influence the separation and stalling of sweptback wings would be useful for the review of combined sweep and Reynolds number effects to follow. To this end figure 3.1 presents, in simplified form, three of the primary phenomena to be dealt with in this section.

### 3.2.1 Tip stall

The sketch in the upper left illustrates the type of change in the attached flow upper surface chordwise and spanwise pressure distribution across the span that occurs on unwarped sweptback wings. Early wind tunnel tests and "lifting line" theories demonstrated the occurrence of tip stall due to an increasing upwash angle induced towards the wing tip. Soon "lifting surface" theory and detailed pressure measurements demonstrated that, near the wing root, the chordwise distribution of induced angle (induced camber) is such as to reduce the adverse chordwise pressure gradient near the leading-edge while the opposite effect occurs in the tip region. Thus, only in the mid-semispan region of the wing does the simple infinite span oblique wing theory tend to apply. This is also seen from the fact that in the regions of the tip and root the streamlines, in plan view, cannot curve to satisfy the oblique wing theory but are forced to remain in the free-stream direction. This so-called "kink" effect requires that the isobars cross the plane of symmetry at a right angle as indicated in the sketch. A similar effect occurs at the wingtip. These effects shear the chordwise pressure distributions across the span such as to create the changes in induced camber and pressure gradients near the leading edge in the manner described above and illustrated in the upper left of figure 3.1 thereby creating tip stall. For a more detailed discussion of these effects the reader is referred to Kuchemann (1978).

### 3.2.2 Leading-edge separation bubble

The sketch in the upper right of figure 3.1 illustrates in simplified form the primary influence of the spanwise variation of the adverse chordwise pressure gradient in the leading edge region as it applies to this paper. In contrast to the rectangular wings of section 2, the turbulent reattachment and resulting expanding long bubble begins outboard on the wing and its rate of inboard progression with angle-of-attack reduces as sweepback increases.

The induced camber effects associated with sweepback, as discussed with the above two sketches, will subsequently be analyzed using the cotangent loading concept in a manner similar to that used for the rectangular wings of section 2.

### 3.2.3 Leading-edge vortex lift

Another phenomenon of interest in this section is illustrated, again in simplified form, in the lower sketch of figure 3.1. For wings of moderate-to-high sweepback the spanwise pressure gradients on the upper surface can induce spanwise velocities in the leading-edge region of sufficient magnitude to convert the expanding long bubble flow described above into the vortex flow illustrated in the sketch. This, of course, is the well known, highly stable, leading-edge separation induced vortex flow. This vortex flow entrains an additional mass of air and provides a downward deflection thereby producing an increase in lift above that expected from inviscid theory and referred to as "vortex lift." This appears to have first been demonstrated at Langley in 1946 and reported by Wilson and Lovell (1946) who demonstrated that the poor maximum lift of a highly swept delta wing was greatly improved when the round leading edge was made sharp thereby creating the now well-known leading-edge vortex. A "cross flow separation" model of the vortex flow was also proposed in this early paper. This research remained classified for 4 years but stimulated additional

studies in the United States. International interest in vortex lift appears to stem from its independent discovery in France during 1951 and 1952 as reviewed by Legendre (1981).

Also influenced by sweep is the spanwise flow of the boundary layer induced by spanwise pressure gradients. The resulting increase in boundary layer thickness in the aft outboard region can, for thick wings in particular, produce earlier trailing edge separation with the accompanying adverse effects on the stall characteristics including stability and controllability problems. However, for the thin wings with turbulent reattachment at the leading-edge of interest in this paper, this is not a major factor and will not be discussed.

By the late 1940's and early 1950's the major influences of the above phenomena were fairly widely recognized as demonstrated in review papers such as, for example, those published by Furlong and McHugh (1952) and by Kuchemann (1953). Much of the low speed, swept wing research that followed was directed towards the development of a data base covering effects of planform, airfoil section and Reynolds number as well as the development of warped wings and passive and adjustable devices to provide some control of the separation. However, consistent with the previous parts of this paper, the following discussion will deal only with the influence of wing geometry and Reynolds number on leading-edge separation and its influence on the stalling of unwarped wings without flow control devices.

### 3.3 General Effects of Sweep and Reynolds Number

This section will review some of the general effects of sweepback and Reynolds number on the overall lift and stalling characteristics. To provide continuity with the prior section on rectangular wings, experimental results for constant-chord-length wings will be used as illustrations. The influence of taper will however be discussed in later sections of the paper.

### 3.3.1 Prediction of turbulent reattachment

Many studies of the flow about sweptback wings, dating back to the late 1940's have indicated that, for symmetrical airfoil sections in the thickness range of interest for high speed aircraft, the most prevalent type of separation affecting the lift is that which occurs near the leading edge. Also studies such as those by Poll (1983, 1986), for example, demonstrated that in general the leading-edge flow on sweptback wings often was quite similar to that on upswept wings in that a transitional bubble near the leading edge occurs first followed by a turbulent reattachment. However depending on the sweepback angle and Reynolds number this can result in a leading-edge vortex flow.

In view of the above, an attempt to relate the effect of Reynolds number on the onset of turbulent reattachment for sweptback wings to those observed on two-dimensional airfoils in section 1.3.2 will be made by use of a simple extension of the method developed for rectangular wings in section 2.2.1.

To extend the method developed in section 2.2.1, the following modifications are made:

1. The effect of sweep is, of course, included in the calculation of the variation of the inviscid values of the flat plate cotangent lift coefficients across the span, and
2. the maximum value of the section cotangent lift coefficient across the span is equated to an appropriate value of the two-dimensional lift coefficient at the onset of turbulent reattachment corrected to an infinite span swept wing by the Betz cosine squared rule. It must be remembered that the section cotangent lift coefficient is an equivalent flat plate section lift coefficient that provides the same pressure gradient at the leading edge as occurs on the wing due to the three-dimensional induced angle of attack and induced camber.

With regard to item (1), the major influences of sweepback on the induced camber effects are illustrated in figure 3.2, which presents spanwise distribution of the total

section lift coefficient,  $c_l$ , and the cotangent type section lift coefficient,  $c_{l,cot}$  (both normalized by the total wing lift coefficient,  $C_L$ ). These constant-chord wings are of aspect ratio 3 and have sweepback angles of  $0^\circ$ ,  $30^\circ$ , and  $55^\circ$ , and the solutions used the first three chordwise pressure modes (see section 2.2.1).

For the unswept wing, the lift loss associated with the negative induced camber must be offset by an increase in angle of attack which causes an increase in the adverse pressure gradient in the leading-edge region. This is indicated by the fact that the angle-of-attack type chord load, as measured by  $c_{l,cot}$ , is greater than the total chord load as measured by  $c_l$ . Although it causes an earlier stall, as discussed in section 2.1, the stall originates at the root and, based on the spanwise distributions, the induced camber would be expected to have a relatively small influence on the stall progression towards the tip.

For the  $30^\circ$  sweptback wing, however, the induced camber is positive in the root region, thereby reducing the adverse pressure gradient at the leading edge for the inboard region as indicated by the reduced level of the  $c_{l,cot}$  term. Through its effect in delaying the onset of turbulent reattachment for wings with airfoil sections exhibiting "thin airfoil" or "leading edge" classes of separation (see section 1.2), the induced camber is the primary contributor to the delayed stall of the root region. Over the outboard region the induced camber is negative, thereby increasing the adverse pressure gradient and causing the turbulent reattachment to begin in the mid-semispan region rather than the root region that might be expected if only the total section lift coefficient,  $c_l$ , distribution is considered. For wings in this range a leading-edge sweepback, the turbulent reattachment combined with the spanwise flow can cause partial span leading-edge separation-induced vortex flow depending on the leading-edge radius and Reynolds number. An example of a flow study illustrating this dependency is that made by Poll (1983 and 1986).

Turning to the  $55^\circ$  sweptback wing example, it is seen that the general effects of induced camber on the distribution of the angle-of-attack type chordwise loading parameter,  $c_{l,\text{cot}}/C_L$ , are similar to those for the  $30^\circ$  sweptback wing. However, the peak value is shifted much closer to the wing tip and the reduction in the root region is greater. This implies, of course, that the onset of turbulent reattachment will occur much closer to the tip than implied by the total section lift coefficient and the inboard progression will be slower than for the  $30^\circ$  sweptback wing, thereby further delaying the root stall.

Regarding item (2) above the following assumptions are made relative to the 2-dimensional data selection. First, the airfoil section in the plane normal to the leading edge (plane of maximum adverse pressure gradient) will be used in accordance with the Betz (1935) theory applicable to the inviscid pressure for an infinite span oblique wing. The most serious problem is the selection of a Reynolds number which in the 2-dimensional airfoil flow at the equivalent lift coefficient,  $c_l \cos^2 \Lambda$ , will at least approximately correspond to the condition of the onset of turbulent reattachment in the swept case.

For a pure laminar boundary-layer case the "independence principle" of Jones (1947) would apply for the infinite span oblique wing and the Reynolds number normal to the leading-edge would be appropriate. However, as suspected by Betz (1935), it was determined in the 1950's that the development of the transitional and turbulent boundary-layer is influenced by both the flow normal and the flow parallel to the leading-edge. Of particular importance is the influence of crossflow (spanwise) instability which produces attachment line transition. For two of the more recent summaries of the various effects, the reader is referred to Kuchemann (1978) and Amal (1987). Since the "independence principle" cannot be applied in the selection of an equivalent Reynolds number for application of the 2-dimensional data to turbulent-reattachment the streamwise Reynolds number for sweptback wing in question will be

used herein. While this is arbitrary, there appears to be no practical alternative to this approach for the present purpose. Some related experimental justification can be found in the studies of yawed circular cylinders, such as that by Bursnall and Loftin (1951). The reader must keep in mind, however, that this approach is only an attempt to relate the general trends with regard to the effects of Reynolds number on the turbulent reattachment between the 2-dimensional and 3-dimensional flows. This represents one of the areas where turbulent-flow Navier-Stokes theoretical studies should be very helpful.

### 3.3.2 Overall lift characteristics

An illustration of some experimentally determined effects of wing sweepback angle and Reynolds number on the overall lift characteristics is presented in figure 3.3. The sweptback wings had ONERA "D" airfoil sections placed perpendicular to the leading edge and two-dimensional unswept airfoil data for this section are presented on the left for reference.

The airfoil data is from Erlich (1969) and section lift results for root chord Reynolds numbers of 0.8 and 2.1 million are presented as a function of angle of attack. The ONERA "D" airfoil, a symmetrical "peaky" type, has a thickness ratio of 10.5-percent and a leading-edge radius of 1.4-percent chord. For the lower Reynolds number a gradual stall of the "thin-airfoil" type occurs, while at the higher Reynolds number the "trailing-edge followed by leading-edge" type of stall occurs. This trend with Reynolds number is consistent with the stall boundaries of figure 1.5 for the NACA 6-series airfoils. For the variation of  $c_{l,max}$  with Reynolds number the reader is referred to figure 1.8.

The two sweptback wing cases are taken from a variable-sweep study carried out in several ONERA wind tunnels. This experimental study was selected because of its systematic coverage of both sweepback angle and Reynolds number, and the use of

raked tips which tend to confine the separation-induced vortex flow to the wing leading edge.

For the 30° sweep case, the  $R_{Cr} = 0.9 \times 10^6$  data was extracted from the data in figure 44 of Poisson-Quinton (1978) and the  $R_{Cr} = 2.2 \times 10^6$  data from the data in figure 9 of Manie, et. al. (1978). For this low sweep case, the effect of Reynolds number on the type of stall is quite similar to that observed for the two-dimensional airfoil. The most obvious effect is, of course, the well-known influence of the  $\cos^2 \Lambda$  rule in reducing the maximum lift coefficient with the three-dimensional effects being rather small for this relatively high aspect ratio of 6.86. However, it is of interest here to examine the degree to which the simplified approach of this paper predicts the effect of sweep and aspect ratio on the onset of turbulent reattachment.

Turning first to the high-Reynolds-number case and taking the airfoil maximum lift coefficient of 1.53 as the onset of turbulent reattachment for the two-dimensional case, converting to the two-dimensional oblique wing by the "cosine squared" rule and applying the correction for induced camber by the method of this paper results in a value of 1.02 for the three-dimensional lift coefficient corresponding to the onset of turbulent reattachment. This is shown in figure 3.3 by the horizontal arrow and is seen to closely predict the stall. This implies that for this relatively low sweep angle, the level of spanwise flow is insufficient to create a leading-edge vortex flow of sufficient strength to alter the type of stall. There may be at least a "part span" vortex influence beyond the stall as observed, for example, by the flow studies on a similar wing by Poll (1983, 1986).

For the low-Reynolds-number condition the predicted turbulent reattachment appears to be reasonable and there is evidence of some influence of vortex flow in providing a further softening of the stall relative to the two-dimensional case.

Results shown in figure 3.3 for the 50° sweptback wing are quite different. For this case, the predicted overall lift coefficient corresponding to the onset of turbulent

reseparation is 0.54. As shown by the horizontal arrow, this prediction corresponds closely to the measured onset of an increase in lift gradient with angle of attack rather than the loss of lift shown for the 30° wing. This, of course, is associated with the well-known vortex lift effect resulting from the combination of the turbulent reseparation and the strong spanwise flow present on this more highly sweptback wing.

As will be discussed subsequently, the vortex flow on this wing becomes the predominate factor in determining the high-lift characteristics with the inboard progression of the vortex origin and the vortex breakdown development establishing the type of stall. As can be seen, the stall associated with the vortex flow is rather gentle and is due to the inboard progression of the vortex breakdown with increasing angle-of-attack.

Some additional details of the effect of Reynolds number on the vortex lift characteristics of the 50° sweptback wing are given in figure 3.4. Where the total lift coefficient is presented as a function of angle of attack for chord Reynolds numbers, in millions, of 1.2, 2.3, and 3.0. Shown by the two dashed lines are the theoretical results for attached flow and for full vortex flow. The vortex flow theory is based on the leading-edge suction analogy of Polhamus (1966) for a sharp leading edge and therefore represents the probable "upper bound." Additional description of the analogy is presented in section 4.1.2. The experimental results illustrate the increase in the lift coefficient corresponding to the onset of vortex lift as the Reynolds number increases. The predicted lift coefficients for the onset of turbulent reseparation are indicated, as in the previous figure, by the horizontal arrows for the three Reynolds numbers (identified by the symbols) based on the maximum lift coefficients for the ONERA "D" airfoil presented in figure 1.8. The results indicate a reasonably good prediction of the delay in the onset of vortex flow as the Reynolds number is increased. However it should be noted that for the Reynolds number of  $3.0 \times 10^6$  the two-

dimensional data presented in figure 1.8 involved a small extrapolation to eliminate a shock effect as discussed in section 1.5.

Some pressure data for this same wing is presented in figure 3.5 where the effect of Reynolds number on the upper surface chordwise pressure distributions is shown, for the four spanwise stations (A through D) shown in the sketch, at an angle of attack of  $12^\circ$ . For the Reynolds number of  $3.0 \times 10^6$ , it is seen that the flow is essentially attached over the entire region of the wing shown while for the Reynolds number of  $2.0 \times 10^6$  vortex flow, resulting from turbulent reattachment, has been established over the entire region. The rearward movement of the vortex-induced reattachment point as the wing tip is approached is evident and illustrates the growth of the vortex.

### 3.3.3 Summary of maximum lift

The data for the variable-sweep wing series described in the previous section were obtained in the ONERA S1Ca and S2Ca low-speed atmospheric wind tunnels. To provide data over a wider range of Reynolds numbers, tests were later made in the relatively new ONERA F1 tunnel which operates up to 4 atmospheres pressure. A brief summary, without analysis, of the effect of Reynolds number on the maximum lift coefficient from these tests, at sweep angles ranging from  $0^\circ$  to  $50^\circ$ , has been published by Carrara and Masson (1980). No source for the basic data was cited. These data and that for the  $60^\circ$  wing from Manie (1978) and Brocard and Manie (1979) for the same wing series are summarized in figure 3.6 as a function of  $R_{cr}$ . To be consistent with this paper, the reference length, for Reynolds number has been converted to the streamwise chord. Shown for reference is a portion of the two-dimensional airfoil data for the ONERA "D" airfoil taken from figure 1.8.

While Carrara and Masson (1980) present the maximum lift coefficients, they do not present the lift versus angle of attack needed to definitely classify the type of stall. However, with the aid of the lift versus angle of attack data of Manie, et. al. (1978), some observations from figure 3.6 can be made. Regarding the  $30^\circ$  sweptback wing,

the strong increase of  $C_{L,max}$  with Reynolds number in figure 3.6 and the lift data of figure 3.3 indicate that for this modest sweep angle the stall characteristics with angle of attack and Reynolds number are similar to those observed in two-dimensional flow for the ONERA "D" airfoil (Erich 1969). This, of course, does not preclude some part-span vortex flow occurring beyond the stall or of insufficient vortex strength to change the type of stall. For the 50° sweptback wing, the data of figure 3.6 indicate that the strong vortex flow observed in figure 3.3 exists over the entire Reynolds number range tested and that the maximum lift developed decreases slightly with Reynolds number in this range transition from a trailing-edge/leading-edge stall to the vortex-flow stall. The results for the 40° and 60° wings will be discussed subsequently.

A somewhat more informative way of illustrating the combined effects of sweep angle and Reynolds number on the maximum lift coefficient is presented in figure 3.7 for three Reynolds numbers using the experimental data of figure 3.6. As an analysis aid, the predicted turbulent reattachment onset is shown by the dashed curves as obtained from the maximum lift coefficient data for the ONERA "D" airfoil presented in figure 1.8, corrected for the two-dimensional sweep effect and the three-dimensional induced angle of attack and camber effects according to the method presented herein. The results of these calculations illustrate the effect of sweep and Reynolds number on the maximum lift coefficient that would be expected due to turbulent reattachment if no vortex lift was encountered.

The experimental data for the 30° sweptback wing is in reasonably good agreement with the predicted values for all three Reynolds numbers, tending to confirm the previous conclusion that the maximum lift for this wing is associated with a sudden "trailing-edge/leading-edge" type stall with little vortex lift being developed (see fig. 3.3).

Between sweep angles of 30° and 40°, the vortex flow, resulting from the turbulent reattachment and the crossflow, begins to dominate the stall characteristics as

discussed above. The associated vortex lift provides increases in maximum lift coefficient above those predicted for turbulent reattachment without vortex development, as shown by the dashed lines. The increment in  $C_{L,max}$  associated with the vortex flow decreases with increasing Reynolds number, resulting in a convergence such that for the  $\Lambda = 50^\circ$  condition, maximum lift coefficient is relatively independent of Reynolds number over the range tested. Although only the  $3.5 \times 10^6$  Reynolds number of maximum lift coefficient data for the  $60^\circ$  wing is included in the above cited references, earlier data by Cahill and Gottlieb (1950) for a tapered wing in the same leading-edge sweep and leading-edge radius range indicated a relative insensitivity to Reynolds number. This insensitivity is associated with the fact that for the high sweep angles the flow at the higher angles of attack is dominated by the leading-edge vortex flow and maximum lift is controlled primarily by vortex breakdown as will be discussed in section 4.2.3.

Also shown in figure 3.7 (by the flagged symbols) are the measured values of the inflection lift coefficient,  $C_{L,inf}$ , for the  $50^\circ$  sweptback wing. The inflection lift coefficient is that at which a change in the lift and moment gradient with angle of attack occurs. It is associated with leading-edge turbulent reattachment and initiation of vortex lift, as was illustrated in figure 3.4. From this result, it appears that the inflection lift coefficients correspond reasonably close to the predicted onset of turbulent reattachment conditions. For the  $30^\circ$  sweptback wing, which exhibits a sudden leading-edge stall, the inflection lift coefficient corresponds to the maximum lift coefficient. Regarding the  $40^\circ$  sweptback wing, only the maximum lift coefficients were reported by Carrara and Masson (1980), but the indication from figure 3.7 is that the stall is influenced by vortex flow.

In summary, figure 3.7 illustrates the transition from the sudden leading-edge type of stall that occurs for sweep angles up to about  $30^\circ$  to the gentle stall at the higher sweep angles which, as a result of vortex flow, occurs well beyond the turbulent

resepation lift coefficient and tends to be dictated by the spanwise progression of vortex breakdown. It is of historical interest to note that these general trends had been observed by various researchers in the late 1940's and early 1950's and the reader is referred to the summary paper by Furlong and McHugh (1952) as an example.

### 3.4 Influence of Reynolds Number on Local Flow

In this section, some examples of the measured section lift characteristics at various spanwise stations on a tapered sweptback wing will be shown to illustrate some of the primary effects of Reynolds number and angle of attack on the local flow. An attempt will also be made to relate the local conditions to those encountered in two-dimensional flow as a means of illustrating various three-dimensional influences on a local stalling which may be of value in evaluating the ability of Navier-Stokes methods to predict local viscous effects.

The wing selected for this section is one for which Kolbe and Boltz (1951) performed detailed pressure and force tests over a Reynolds number range. The wing leading-edge sweep is  $49^\circ$ , the aspect ratio is 3.0, the taper ratio is 0.5, and the airfoil is a NACA 64A010 placed normal to the quarter-chord line.

#### 3.4.1 Prediction of turbulent reseparation

The same general approach as in section 3.2.1 will be used to predict the influence of the three-dimensional induced flow effects on turbulent reseparation. However, since these influences will be examined at local spanwise stations and related to two-dimensional flow, it is necessary to relate the section cotangent lift coefficient,  $c_{l,cot}$ , to the total section lift coefficient,  $c_l$ , as was done in the case of the rectangular unswept wings in section 2. Figure 3.8 presents the theoretical results for the various lift coefficient parameters as a function of spanwise location,  $\eta$ , for the above wing. As in figure 3.2 for constant chord sweptback wings, the left part of figure 3.8 presents the section lift parameters normalized by the total wing lift coefficient,  $C_L$ . Since the

analysis in this section also requires the  $c_{l,cot}$  parameter normalized by the local section lift coefficient,  $c_l$ , that parameter is presented on the right of figure 3.8.

As will be shown subsequently, this airfoil, in two-dimensional flow has a trailing-edge/leading-edge type of stall over the Reynolds number range of interest here. Therefore, the onset of turbulent reattachment corresponds to the maximum section lift coefficient. Thus, the predicted section lift coefficients corresponding to turbulent reattachment,  $c_{l,sep}$ , on the three-dimensional wing are determined at each span station as

$$c_{l,sep} = \frac{(c_{l,max})(\cos^2 \Lambda)}{(c_{l,cot} / c_l)}$$

where  $\Lambda$  corresponds to the sweep angle of the wing leading-edge (since it is a leading-edge separation condition),  $c_{l,max}$  is obtained by experimental two-dimensional airfoil data at a Reynolds number based on the local streamwise chord and the induced camber term,  $c_{l,cot}/c_l$  from figure 3.8.

### 3.3.2 Section normal-force characteristics

The section normal-force coefficient characteristics at the various span stations for  $R_{\bar{c}} = 4 \times 10^6$  are shown in figure 3.9 adapted from figure 7 of the paper by Kolbe and Boltz (1951). Also shown are the two-dimensional data for the NACA 64A010 airfoil from Loftin (1948) for chord Reynolds numbers of  $3 \times 10^6$ ,  $6 \times 10^6$ , and  $9 \times 10^6$ . The two-dimensional results indicate a combined trailing-edge/leading-edge type of stall consistent with the two-dimensional stall-type boundaries of figure 1.5 for this Reynolds number and leading-edge radius combination. The notable differences in the region of the local stall between the two-dimensional flow and the three-dimensional flow is readily apparent at all spanwise stations, consisting of a rapid increase in the slope of the  $c_n$  vs  $\alpha$  curves prior to the attainment of the maximum value. This increase occurs at all spanwise stations and is, of course, associated with leading-edge separation-induced vortex flow discussed earlier. The dashed lines are

extensions of the linear portion of the data to aid in illustrating the approximate vortex lift effect.

The predicted values of  $c_n$  for the onset of turbulent reattachment are shown by the horizontal arrows. Due to the fact that the wing is highly tapered, the local chord Reynolds numbers across the span were included in the predictions. The prediction of reattachment onset appears reasonably good at the wing tip where the separation originates and in the root region where the tip separation induced vortex flow produces little influence. However, in the mid semispan region where vortex flow interactions occur, that are not included in this simplified method, the agreement is not good.

It will be noted that the effect of induced camber in delaying the onset of turbulent reattachment is quite large in the inboard region. With regard to stall progression, it is assumed that the maximum local lift coefficient is established primarily by vortex breakdown. At present there appears to be no adequate method of predicting the influence of vortex breakdown on the local maximum lift of wings of this type having moderate sweep and a round leading edge. Some success has been obtained for the overall maximum lift for the special case of very slender delta wings having sharp leading-edges, and this will be discussed in section 4.2.3.

Turning now to the effect of Reynolds number on the section normal-force characteristics across the span, figure 3.10 compares the results from figure 3.9 with those obtained at the higher Reynolds number of  $8 \times 10^6$ . Again, the results are from the paper by Kolbe and Boltz (1951). The results illustrate a delay in turbulent reattachment and vortex formation in the outer region of the wing which results in higher local maximum normal forces. The results indicate the expected delay in the formation of vortex flow as the Reynolds number is increased and over the outboard half of the wing higher values of maximum normal force coefficient are developed. Over the inboard region of the wing, the maximum normal force coefficient was not

reached for either Reynolds number. Although these effects would lead to the expectation of an increase in the overall maximum lift coefficient for the wing, the results obtained by Kolbe and Boltz (1951) indicate only minor effects of Reynolds number (consistent with the  $50^\circ$  wing data of figure 3.6). Since the overall maximum lift coefficient occurs at an angle of attack of about  $25^\circ$ , it is possible that compensating effects over the inboard region might occur at angles of attack beyond those reached for the data of figure 3.10.

Before leaving this section, it should be mentioned that secondary and tertiary separations and accompanying vortex flow can be formed under the primary vortex and may have had some influence on the data presented. Studies of their effects will be discussed in the following section on delta wings.

#### 4. SLENDER DELTA WINGS

The stall of highly-swept (slender) delta wings, of interest for supersonic and hypersonic aircraft, are highly dependent on vortex lift and, as discussed in section 3.2.3, it was a 1946 study of a delta wing that uncovered and explained this phenomenon. This section will discuss some flow details in the stall region that were not covered in the section on swept-back wings such as, for example, the secondary separations induced by the flow beneath the primary (leading-edge) vortex, reversals in vortex paths, and prediction of vortex breakdown. In addition the suction analogy and free-vortex-sheet theories of leading-edge vortex flow will be described and applied.

##### 4.1 Analysis Methods

###### 4.1.1 Induced camber distributions

As in the previous sections the spanwise distributions of the cotangent chord-loading section lift parameter has been determined and is presented in figure 4.1 to illustrate the influence of induced camber on the leading-edge pressure gradient for

delta wings. All of the examples shown were obtained from calculations using the first three chordwise pressure modes described in section 2.1. For comparison purposes, the results from figure 3.2 for a  $55^\circ$  constant chord sweptback wing of aspect ratio 3.0 are shown on the left. Results for a  $55^\circ$  delta wing ( $A = 2.8$ ) are shown in the center section of figure 4.1. The most obvious difference between the swept wing and the delta wing is the well-known highly-loaded tip region on the delta wing, which occurs for both the total section lift parameter and the cotangent section lift parameter. Also apparent is the fact that for the delta wing the influence of induced camber in reducing the adverse pressure gradient at the leading-edge is extensive, covering essentially the complete semispan.

On the right of figure 4.1 the variation of the cotangent loading parameter is presented for a series of three delta wings covering the sweep range to be discussed in this section of the paper. The results indicate a reduction of the cotangent loading with increasing leading-edge sweep angle over the entire semispan.

For delta wings having round leading edges an indication of the influence of induced camber on the progression of turbulent reattachment aft of the transitional bubble can be extracted from the theoretical variation of the cotangent loading thus providing information regarding the origin of the vortex sheet. However, a major portion of the discussion of delta wings will deal with sharp leading-edge cases where separation occurs all along the edge at a very low angle-of-attack and, for the sweep angles involved, a resulting vortex sheet is attached to the sharp leading-edge. Since this type of flow is the dominant one for these wings the cotangent lift concept is not applicable to the prediction of the lift characteristic for the sharp edge case and vortex flow methods will be used. These methods are also useful in providing upper bounds of lift for the round edge cases to be discussed subsequently.

#### 4.1.2 Vortex-flow theories

Considerable progress is being made in the application of Navier-Stokes solutions to the viscous flow about slender delta wings having leading-edge vortex flow. However, parametric solutions covering the planforms and combined laminar and turbulent boundary-layer flows in the Reynolds number range of interest here do not appear to be available in the literature. Since the development of the specific solutions required to cover the Reynolds number range and wing geometries covered here is beyond the scope of this study, two existing vortex flow theories based on inviscid modeling will be used. These methods are often useful in establishing certain limits for the viscous flow and provide assistance in evaluating some of the vortex interactions. This approach is particularly applicable for the sharp leading-edge case, since the separation is fixed at the leading edge, and two theoretical methods have been chosen for use in this paper.

At subsonic speeds, the three-dimensional effects are significant and there is no region, even near the apex, that the flow is conical for either attached or vortex flow. For some discussion of this fact, the reader is referred, for example, to Thwaites (1960), and to Luckring (1985b). Therefore, completely three-dimensional theories will be used herein. However, conical flow solutions can be useful as a base for evaluating the magnitude of three-dimensional effects and for qualitative studies where their reduced computational requirements become attractive. The two non-conical flow theories selected for use in this paper are the leading-edge suction analogy and the free-vortex sheet method. These methods have been used extensively, particularly for delta wings, and contribute to the hierarchy of flow modeling that is useful in establishing the magnitude of some of the vortex flow effects.

The leading-edge suction analogy, developed by Polhamus (1966), is illustrated in part (a) of figure 4.2. This analogy equates the attached flow leading-edge suction force to the normal force produced by the separation-induced vortex flow, thereby

allowing linearized flow theory to be used for this nonlinear flow phenomenon. As a consequence, theoretical complexity and numerical run time, as well as cost, are greatly reduced and the limitations of slender-wing conical-flow theories are overcome. Briefly, this analogy assumes that the normal force associated with the vortex-induced reattachment of the flow is equal to the leading-edge suction force lost due to the separation. For detailed descriptions and evaluations of the method, the reader is referred to Polhamus (1969, 1986), and Lamar and Luckring (1979). This method provides accurate values of the overall forces and moments until vortex breakdown or strong interactions between the vortices are encountered.

The free-vortex-sheet theory (FVS) provides, in addition to overall forces and moments, detailed pressure distributions and accurately accounts for the vortex interactions. The wing and vortex sheets are modeled with biquadratically varying doublet panels; thickness effects can be represented with bilinear source panels. Salient features of this formulation are illustrated in part (b) of figure 4.2 and include: (1) the free-vortex-sheet which is locally force free and is a stream surface, (2) the fed sheet which approximates the physics of the vortex core region in a far field sense, (3) a higher-order near wake which accurately satisfies the trailing-edge Kutta condition by accounting for the effects of nonplanar vorticity, and (4) a trailing wake. Neither the shape of the three-dimensional vortex sheets nor the distribution of vorticity strength on them is known a priori, which results in a nonlinear problem requiring iteration schemes. The initial development work and some early applications are described by Gloss and Johnson (1976), and a current form of the computer program is documented by Johnson, et. al. (1980). Extensive validation and application studies have been carried out, and some are reviewed in the paper by Luckring, et. al. (1982). Additional improvements to the convergence properties of this method and listings of published solutions have been presented by Luckring, et. al. (1986).

Figure 4.3 compares both the suction analogy and free-vortex sheet theoretical results with the experimental lift of two highly swept delta wings having sharp leading-edges. The wings selected have leading-edge sweep angles of  $70^\circ$  and  $80^\circ$  and the experimental data are from Wentz and Kohlman (1971). For clarity the identification of the various calculated results is split between the two figures. The lift calculated by the suction analogy is believed to provide the "upper bound" of lift corresponding to an assumed condition where the cores of the vortices remain essentially along the wing-leading edges. In addition, the analogy does not account for vortex breakdown effects. The shaded region between the two theoretical results represents the loss of lift associated with the actual vortex core trajectories which are modeled in the free-vortex-sheet theory. There are two major features of these trajectories. First, and believed foremost, are the vortex-core trajectories in a cross flow plane which, with increasing angle of attack are in the upward and inward directions until their mutual interaction forces a spanwise reversal. This condition, defined as "diverging cores," is taken as a crude measure of the onset of strong vortex interactions or "crowding," which hinder flow reattachment to the wing surface thereby causing incomplete recovery of leading-edge suction as vortex-induced normal force in the context of the suction analogy. The lift coefficient for which the free-vortex-sheet theory predicts that the vortex cores begin to reverse their paths and move outboard with increasing angle of attack is indicated in figure 4.3 by the solid arrows. This "diverging cores" condition appears to reasonably predict the onset of incomplete suction recovery for both wings as illustrated in figure 4.3 by the cross-hatched regions representing the loss of lift relative to the suction analogy predictions.

The second trajectory feature modeled in the free-vortex-sheet theory is the upward curvature of the vortex cores as they approach the trailing edge. It is believed that its influence is primarily concentrated near the trailing edge and is secondary to the "diverging cores" effect. Shown on figure 4.3 by the half-solid arrows are the

theoretical values of lift coefficient for which vortex instability occurs as defined by the theory for the critical swirl condition developed by Luckring (1985). It is seen that for both wings this prediction, which relates to the onset of vortex breakdown, is in good agreement with the experimental maximum lift coefficient which was shown by Wentz and Kohlman (1971) to correspond to the condition where vortex breakdown in the wake has progressed forward to the trailing edge of the wing. With regard to the maximum lift, the free-vortex sheet theory results shown for the 80° delta indicate that little increase would be expected by eliminating vortex breakdown. However, for the 70° delta, which is of more practical interest for supersonic aircraft, the free-vortex sheet solutions indicate that sizable increases in maximum lift might be attainable by delaying vortex breakdown. A review of some effects of Reynolds number, sweep and profile on the lift characteristics of delta wings in the stall region will be presented in the following sections.

#### 4.2 Sharp Leading-Edge Delta Wing Reynolds Number Studies

Because of the interest in delta-type wings for supersonic cruise aircraft where wave drag tends to dictate relatively sharp wing leading-edges, the sharp leading-edge delta wing has been selected to be discussed first. In addition, both the experimental and theoretical results for the sharp edge cases provide informative "upper bounds" of vortex lift which will also be used in the analysis of the round leading edge cases in a subsequent section.

##### 4.2.1 Overall lift characteristics

For the sharp leading-edge case separation is, of course, fixed at the leading edge and little Reynolds number effect on the overall lift would be expected, except for possible effects of the secondary separation occurring in the outboard directed flow induced under the primary vortex. It was found in early studies of the vortex flow on slender, sharp-edge wings that the overall lift was, indeed, essentially independent of Reynolds number despite the existence of Reynolds number effects associated with

secondary separation on the surface pressure distributions. This Reynolds number independence for overall lift is illustrated in figure 4.4 for two leading-edge sweep angles. The data for the 70° wing was obtained from Gould and Cowdrey (1958), and for the 76° wing from Lemaire (1965). From these results, which were obtained with free transition, it is apparent that Reynolds number plays an insignificant role with regard to overall lift and stall, at least over the Reynolds number and wing sweep ranges investigated. Inasmuch as transition to turbulent flow along the primary reattachment line moves forward with both increasing angle of attack (see Hummel and Redeker (1972) for example), a rather wide variation in transition locations would be expected to be associated with these results. Pressure data at  $\alpha = 25^\circ$  for the 76° delta wing, to be discussed subsequently, illustrate these effects and the resulting sizable redistribution of pressures with Reynolds number in a manner that maintains essentially constant total lift. Additional total lift data illustrating the insensitivity of the overall lift to Reynolds number has been published by Peckham (1961).

Also shown in figure 4.4 are the theoretical calculations using the previously described suction analogy and free-vortex sheet methods. The comparisons of the two theories with the experimental results in figure 4.4 indicate that they are in excellent agreement and predict rather accurately the experimental results up to the lift coefficient corresponding to the theoretical critical swirl discussed above. The low values of lift predicted by attached flow theory provides a base for illustrating the well known large increase in lift associated with the vortex flow.

As the angle-of-attack increases beyond the lift coefficient for critical swirl the vortex breakdown point moves forward resulting in a gentle stall somewhat analogous to the trailing-edge class of stall which occurs on round edge airfoils as trailing-edge separation migrates forward from the trailing edge. However, the vortex breakdown type of stall is independent of Reynolds number over the range studied for these sharp leading-edge delta wings. As can be seen from figures 4.3 and 4.4 the leading-edge

vortex flow provides an increase in maximum lift relative to attached flow for these slender wings.

#### 4.2.2 Secondary-vortex flow

As discussed above, the overall lift of thin, sharp-edge delta wings is essentially invariant with Reynolds number. For these wings, where the primary separation is fixed at the sharp leading-edge, regardless of the state of the boundary layer approaching the sharp-edge from the stagnation line, this invariance is not totally unexpected. However, flow details associated with the state of the boundary layer on the wing upper surface can cause rather large variations in the pressure distributions through effects on the location and strength of secondary vortices and their subsequent influence on the primary vortices. These vortices occur when the flow under the primary vortex is swept toward the wing leading-edge by the action of the primary vortex encounters the adverse pressure gradient near the leading edge, then separates and rolls up into the so-called secondary vortex. This secondary vortex lies under, and outboard of the primary vortex core and has vorticity of the opposite sign relative to the primary vortex. This is illustrated in figure 4.5 by flow sketches and measured characteristics. The sketch on the left represents, generically, the vortex flow encountered on a slender sharp-edged delta wing. The primary and secondary vortices are illustrated on the right hand panel of the wing but are omitted on the left hand panel in order to facilitate the illustration of a typical transition of the secondary separation line from a laminar condition in the forward region of the wing to a turbulent condition (over the rear portion of the wing) which is further outboard. It should be noted that the size of the secondary vortex is exaggerated for illustrative purposes. The longitudinal location of this transition is, of course, a function of Reynolds number, angle of attack, and surface condition and will move forward as the Reynolds number or angle of attack is increased.

Shown on the right of figure 4.5 are the results of Lemaire (1965) illustrating the measured spanwise pressure distributions on the sharp edge  $76^\circ$  delta wing of figure 4.4. The wing has a 5-percent thick biconvex airfoil in the stream direction and the data was taken at an angle-of-attack of  $25^\circ$  which, as seen from figure 4.4, is well below the angle for critical swirl which defines the onset of vortex breakdown. For slender delta wings, spanwise distributions tend to be more informative than chordwise loadings and are used here. The upper surface pressures are plotted in the spanwise direction at the 25 percent root chord longitudinal location, as seen in the sketch, for the same Reynolds numbers as for the force data of figure 4.4. Also shown is the inviscid pressure distribution from the free-vortex-sheet method, described earlier, to illustrate the general character of the adverse pressure gradient encountered during the development of the secondary separation under the primary vortex.

It will be noted that for all the Reynolds numbers tested the deviations from the pressures calculated by the inviscid free-vortex-sheet theory, which includes only the primary vortex, indicate two pressure peaks; one inboard, which is under the primary vortex, and one outboard, under the secondary vortex.

It appears that the results for the Reynolds numbers (based on root chord) of  $1.6 \times 10^6$  and  $3.2 \times 10^6$  represent the laminar secondary separation condition with the suction peaks under both the primary and secondary vortices clearly evident and of similar magnitude. This is probably due to the fact that the laminar separation occurs in a high velocity region since it has difficulty penetrating the adverse gradient (represented by the FVS theory). Thus the secondary vortex strength is greater than it would be for turbulent separation.

The data for the Reynolds numbers of  $4.8 \times 10^6$  and  $6.4 \times 10^6$  illustrate that the transition to a turbulent secondary separation results in a reduced strength of the secondary vortex and a corresponding increased strength of the primary vortex. Thus

the pressure distribution approaches that of the inviscid free-vortex-sheet solution as Reynolds number increases. It is important to notice that while Reynolds number has a pronounced effect on the spanwise distribution of the upper surface pressures the change in lift under the two vortices is such as to maintain a relatively constant upper surface lift. This is consistent with the results of figure 4.4 which shows the total lift to be essentially independent of Reynolds number. Thus there seems to be a conservation of lift, possibly related to the suction analogy, that might be worth further study. From the lift data it appears that this conservation extends into the stall region.

In connection with the natural transition along the secondary separation line it is of interest that in a study on a similar delta wing Hummel (1965) concluded that transition from laminar to turbulent secondary separation, for  $\alpha = 25^\circ$  occurred at a constant local Reynolds number of about  $0.75 \times 10^6$  based on  $x$ . Converting to the model size in Lemaire's study a value of  $3.0 \times 10^6$  results which is in relatively good agreement with figure 4.5. Lemaire (1965) provided a considerable amount of additional data, which has been utilized by Polhamus (1986) to illustrate, at a more aft station, the non-conical flow effects, the conservation of lift, etc. Some Reynolds number studies have also been made by Carcaillet, et. al. (1986) on a  $75^\circ$  delta wing.

Finally, it should be mentioned that with regard to the strong effects of secondary separation on the surface pressure distributions, some evidence that the boundary layer displacement effects may be important has been generated in a study by Wai et. al. (1985).

#### 4.2.3 Maximum lift coefficient

This section presents a brief summary of the measured maximum lift coefficients of slender sharp-edged delta wings along with some of the related information that can be extracted from the suction analogy and the free-vortex-sheet theory. The results are presented in figure 4.6 as a function of leading-edge sweep angle.

Shown by the dashed line is a variation of the maximum lift coefficient as predicted by the suction analogy which is believed to represent the condition that would occur if the leading-edge vortex were to remain near the wing surface. Comparison with the free-vortex-sheet results (solid line) provides an indication of the loss in maximum lift coefficient, associated with the actual vortex trajectory that occurs above a sweep angle of about  $65^\circ$ .

The free-vortex-sheet solution for  $C_{L,max}$  represents the case where vortex interactions, with regard to vortex strength, size, and path, are included but where vortex breakdown and secondary separation is neglected. In order to provide a "bench mark" relative to vortex breakdown, the dash-dot curve represents the lift coefficient corresponding to the occurrence of the critical value of the swirl parameter at the trailing edge which precipitates vortex breakdown. This result was obtained by Luckring (1985) using the free-vortex-sheet theory and a concept of a critical swirl angle which defines the vortex instability condition. Above this critical swirl boundary, the forward migration of vortex breakdown causes reductions in the growth of lift with angle of attack to occur. It is of particular interest to note that above a leading-edge sweep angle of about  $75^\circ$  a rather narrow "corridor" is formed between the free-vortex-sheet solution for  $C_{L,max}$  and the critical swirl boundary. This implies that vortex breakdown will have a relatively small effect on  $C_{L,max}$  for these highly swept delta wings since it occurs very near to the theoretical value of  $C_{L,max}$  without breakdown.

The significance of the above observation can be seen from the experimental values of  $C_{L,max}$  obtained by Wentz (1968) for sharp edged delta wings as shown by the circular symbols. The experimental values fall within the narrow theoretical "corridor" in the high-sweep-angle range and the rapid loss of  $C_{L,max}$  with increasing sweep in this range can be well predicted with the combination of the two theories.

It appears that in this high sweep range, the presence of secondary separation has little effect on the maximum lift. In the lower sweep range, the increase in  $C_{L,max}$  with

increasing sweep reflects the similar trend in the theoretical values of the lift coefficient corresponding to the trailing-edge location of the critical swirl parameter. In this region of sweep angles, the theory indicates that large increases in  $C_{L,max}$  are available if design techniques for the delay in vortex breakdown can be developed.

It is important to keep in mind that while the overall lift for these sharp-edged wings are relatively insensitive to Reynolds number, the aerodynamic load distribution characteristics are sensitive to Reynolds number through the effects of secondary separation. Also, it should be pointed out that the secondary separation and resulting secondary vortex flow can have an influence when designing the planform and camber lines to optimize a particular aspect of the vortex flow. This, of course, applies to either fixed geometry wings or for devices such as "vortex flaps." It is important therefore, that theoretical methods be extended to include high Reynolds number secondary separation and that consideration be given to obtaining experimental data at higher Reynolds numbers.

#### 4.3 Round Leading-Edge Delta Wings

It appears that there is insufficient data in the literature to adequately illustrate the effects of Reynolds number on the lift characteristics in the stall region for delta wings having round leading-edge airfoil sections and the reader is referred to section 3.3.3 dealing with constant chord sweptback wings. However, data is available which allows a brief analysis of the effect of wing profile on the stall characteristics of slender delta wings which will be used to conclude this section on slender delta wings.

##### 4.3.1 Effect of profile

The effects of wing profile for a  $76^\circ$  delta planform are shown in figure 4.7. This figure is similar to one published much earlier by Weber (1955) but has been updated for the purposes of this paper by using the sharp edge data of Lemaire (1965) discussed earlier, and by using the suction analogy and free vortex sheet solutions for the vortex flow upper bound. Results for three profiles (parallel to the plane of

symmetry) are shown; the 5-percent thick biconvex from Lemaire (1965), and two round leading edge profiles, an FFA 104-5106 (10-percent thick) from Bemdt (1949), and an NACA 0012 from Lange/Wacke (1948). The leading-edge radius is indicated for each airfoil in percentage of the local streamwise chord. It should be noted that the results shown in figure 4.7 include some relatively small differences in Reynolds number with the biconvex data being obtained at a root-chord Reynolds number of  $1.6 \times 10^6$ , the FFA 104 at  $2.0 \times 10^6$ , and the 0012 at  $2.3 \times 10^6$ . However, since the sharp-edge case has been shown to be essentially insensitive to Reynolds number in this range (see figure 4.4) comparisons of the round-edge cases with the sharp-edge case represent the profile effect for the Reynolds number associated with the particular round-edge wing. The comparison of the two round edge wing cases, while containing some possible Reynolds number effects, at least qualitatively illustrate the type of effect on vortex lift associated with leading-edge radius.

The reduction in lift as the leading-edge radius is increases is due, of course, to the reduced magnitude of the adverse pressure gradient at the leading-edge which delays the turbulent reattachment near the leading-edge thereby delaying the formation of the leading-edge vortex. This results in a reduction of vortex lift in accordance with the "conservation of suction" concept discussed by Polhamus (1986).

During the early period of the development and application of the "suction analogy" to delta wings the possibility, for the round edge case, that the portion of the theoretical leading-edge suction lost would be recovered as vortex-induced normal force was explored. It was found that when the experimental values of the vortex-induced normal force and the remaining leading-edge suction were added, they were essentially equal to the full theoretical leading-edge suction. This provided an indication that the conservation of suction implied by the suction analogy for the sharp-edge wings also applied to the round-edge case. This initial study was not published at the time but was published several years later, with permission, by Kulfan (1979).

The first application of the concept to be published was that of Henderson (1976), who demonstrated experimentally that it applied to a variety of wing planforms.

From the distribution of the theoretical cotangent loading shown in figure 4.1 it is apparent that the onset of turbulent reattachment for these round edge delta wings and the resulting vortex expands inboard rather slowly with increasing angle-of-attack. This, of course, differs greatly from the sharp edge case, discussed earlier, where separation and loss of leading-edge suction, occurs all along the edge at a very low angle of attack. Any attempt to apply the various concepts noted in this section regarding the influence of turbulent reattachment or to extend the "critical swirl" theory of vortex breakdown to the round edge wings, etc., in order to predict the stall characteristics is beyond the scope of this paper. However, it should be noted that in contrast to the two-dimensional airfoil cases discussed in section 1.5 the maximum lift coefficient for these delta wings is reduced with increasing leading-edge radius due, of course, to the reduced magnitude of the vortex lift.

## 5. CONCLUDING REMARKS

This paper presented some selected examples of the effect of Reynolds number on the low-speed lift characteristics of wings encountering separated flows at their leading and side edges, with emphasis on the region near the stall. The influence of leading-edge profile and Reynolds number on the stall characteristics of two-dimensional airfoils was briefly reviewed, followed by examples of the effects of Reynolds number and geometry on the lift characteristics near the stall for a series of three-dimensional wings typical of those suitable for high-speed aircraft and missiles. Included were examples of the onset and spanwise progression of turbulent reattachment near the leading edge and illustrations of the degree to which simplified theoretical approaches are useful in defining the influence of the various geometric parameters.

The examples selected and methods of presentation are believed to provide a convenient source of information useful in the selection of fruitful test cases for the evaluation of the capabilities of theoretical viscous flow methods based on the Navier-Stokes equations. Of particular interest in this regard are the Reynolds number effects on leading-edge turbulent reattachment and the subsequent transition to vortex flow on swept back and delta planforms. The strong role played by induced camber was demonstrated and simplified prediction methods were developed which might be found useful in evaluating its influence on the lift and stall characteristics predicted by the developing Navier-Stokes type solutions. Finally it should be noted that the influences of Reynolds number shown may be helpful in designing research programs for the high Reynolds number wind tunnels.

## 6. APPENDIX

The functional representation of the chordwise loading used by Multhopp (1950) is given by

$$\Delta C_p(\phi, \eta) = \frac{2}{\pi} \left[ \frac{q_0(\eta)}{c(\eta)} \cot(\phi/2) + \sum_{n=1}^{\infty} \frac{q_n(\eta)}{c(\eta)} \sin(n\phi) \right]$$

with

$$\phi = \cos^{-1}(1-2\xi)$$

$$\xi = \frac{x - x_{le}(\eta)}{c(\eta)}$$

$$\eta = 2y/b$$

This functional form was utilized for the modified Multhopp method published by Lamar (1968). The nondimensional longitudinal gradient for this distribution is

$$\begin{aligned} \frac{d\Delta C_p(\phi, \eta)}{d(x/c)} &= \frac{d\Delta C_p(\phi, \eta)}{d\phi} \frac{d\phi}{d(x/c)} \\ &= \frac{4}{\pi \sin \phi} \left[ \frac{-q_0(\eta)}{c(\eta)(1-\cos \phi)} + \sum_{n=1}^{\infty} \frac{q_n(\eta)}{c(\eta)} n \cos(n\phi) \right] \end{aligned}$$

Near the leading edge, the dominant contribution to this gradient is due to the cotangent loading.

The chord-loading series implemented by Lan and Lamar (1977) in the method used for the present computations is

with

$$\Delta C_p(\phi, \eta) = \frac{2}{\pi} \sum_{n=0}^{\infty} \frac{p_n(\eta)}{c(\eta)} h_n \cos(n\phi)$$

$$h_n(\phi) = \frac{\cos(n\phi) + \cos((n+1)\phi)}{\sin \phi}$$

This representation is based upon Chebyshev polynomials as shown by

$$h_n(\xi) = \frac{1}{2} \sqrt{\frac{1-\xi}{\xi}} \left[ \frac{T_n(1-2\xi) + T_{n+1}(1-2\xi)}{1-\xi} \right]$$

where  $T_n$  denotes the  $n^{\text{th}}$  Chebyshev polynomial of the first kind with the argument  $1-2\xi$ . This formulation has been utilized by others and was selected by Lan and Lamar for certain advantages in resolving a logarithmic singularity correction over the conventional Muthopp series.

The cotangent loading coefficient,  $q_0$ , can be extracted from the present loading form by recognizing

$$\frac{\cos(n\phi) + \cos((n+1)\phi)}{\sin\phi} = \cot(\phi/2) - 2 \sum_{j=1}^n \sin(j\phi)$$

from which follows

$$q_0 = \sum_{n=0}^{\infty} p_n$$

$$q_n = \sum_{j=n}^{\infty} -2p_j; n \geq 1$$

The inverse relations are given by

$$p_0 = q_0 + (1/2)q_1$$

$$p_n = (1/2)(q_{n+1} - q_n); n \geq 1$$

## 7. SYMBOLS

$A$	wing aspect ratio, $b^2/s$
$b$	wing span
$c$	streamwise chord
$C_{dp,inf}$	inflection in profile drag versus $\alpha$
$c_r$	chord at wing root ( $\eta=0$ )
$\bar{c}$	average chord
$c_l$	section lift coefficient, lift/qc
$c_{l,cot}$	section lift coefficient produced by contangent type chord loading
$c_{l,max}$	maximum $c_l$
$C_L$	three-dimensional-wing lift coefficient, lift/qs
$C_{L,inf}$	$C_L$ for inflection from attached flow theory
$C_{L,max}$	maximum $C_L$
$C_{Lvse}$	side-edge vortex contribution to $C_L$
$\Delta C_{N,V}$	vortex-flow induced wing normal force coefficient
$C_S$	leading-edge suction coefficient
$(C_{P,U})_{min}$	minimum pressure coefficient on wing upper surface
FVS	free vortex sheet
$K_p$	factor in attached flow lift equation
$K_{v,le}$	factor in leading-edge vortex lift equation
$K_{v,se}$	factor in side-edge vortex lift equation
$r$	leading-edge radius
$R_{cr}$	Reynolds number based on root chord
$s$	wing semi-span
$t$	wing thickness
$x$	longitudinal distance from wing leading edge
$x_{le}$	leading-edge coordinate

$x_{r,l}$	distance from L.E. to long bubble reattachment
$x_{r,s}$	distance from L.E. to short bubble reattachment
$y$	lateral distance from wing centerline
$yc$	lateral distance from vortex core
$\alpha$	angle of attack
$\alpha_{crit}$	angle of attack for turbulent reattachment
$\Lambda$	leading-edge sweep angle
$\phi$	see figure 2.2(a)
$q_o$	cotangent chordwise loading coefficient
$q_n$	chord-loading coefficient
$z$	spanwise station
$C_p$	pressure coefficient, $(p-p_{oo})/q_{oo}$
$\Delta C_p$	lifting pressure coefficient, $C_{p, lower} - C_{p, upper}$

## 8. REFERENCES

- Abbott, Ira H., Von Doenhoff, Albert E., and Stivers, Louis S., Jr. (1945): Summary of Airfoil Data. NACA Rep. 824, 1945.
- Arnal, Daniel (1987): Three-Dimensional Boundary Layers: Laminar-Turbulent Transition. Paper No. 4 of AGARD Rept. No. 741, Feb. 1987.
- Berg, B. van den (1981): Role of Laminar Separation Bubbles in Airfoil Leading-Edge Stalls. AIAA Journal, Vol. 19, No. 5, May 1981.
- Berndt, S. B. (1949): Three component measurement and flow investigation of plane delta wings at low speeds and zero yaw. Swedish KTH Aero Tech. Note No. 4, 1949.
- Betz, A. (1935): Applied Aerofoil Theory. Unsymmetrical and Non-Steady Types of Motion. Vol. IV of Aerodynamic Theory, div. J, ch. IV, sec. 4, W. F. Durand, ed., Julius Springer (Berline), 1935, pp. 97-107.
- Brebner, G. G.; and Bagley, J. A. (1952): Pressure and Boundary Layer Measurements on a Two-Dimensional Wing at Low Speed. RAE Report Aero. 2455, Feb. 1952. (Also available as ARC R&M No. 2886, 1956)
- Brebner, G. G.; Wyatt, L. A.; and Illott, G. P. (1965): Low Speed Wind Tunnel Tests on a Series of Rectangular Wings of Varying Aspect Ratio and Aerofoil Section. RAE Technical Report No. 65236, Oct. 1965.
- Busemann, A. (1935): Aerodynamischer Auftrieb bei Uberschall geschwindigkeit. Luftfahrtforschung, Bd 12, No. 6, Oct. 3, 1935, pp. 210-220.
- Cahill, Jones F.; and Gottlieb, Stanley M. (1950): Low-Speed Aerodynamic Characteristics of a Series of Swept Wings Having NACA 65A006 Airfoil Sections. NACA RM L50F16, 1950.
- Carcaillet, R.; Manie, F.; and Pogan, D. (1986): Leading-Edge Vortex Flow over a 75° Swept Delta Wing: Experimental and Computational Results. ICAS, London, September 7-12, 1986.
- Carrarra, Jean-Marie; and Masson Alain (1980): Three Years of Operation of the ONERA Pressurized Subsonic Wind Tunnel. ICAS-80-23.1.
- Crabtree, L. F. (1957): Effects of leading-edge separation on thin wings in two-dimensional incompressible flow. J. Aero. Sci. 24, 597-604 (August 1957).
- Erich, Emile (1969): Exemples de Recherches sur les Profils Dans la Soufflerie S 10 DU C.E.A.T. A Toulouse. ONERA TP No. 766.
- Evans, T. E.; and Mort, K. W. (1959): Analysis of Computed Flow Parameters for a Set

of Sudden Stalls in Low-Speed Two-Dimensional Flow, NASA TN D-85, 1959.

Fuchs, R. (1939): Neue Behandlung der Tragflugeltheorie. Ing. Arc., Vol. 10, P. 48. 1939. and: Neue Berechnung des Abwinds am Flugel. FB.1035. 1939.

Furlong, G. Chester; and McHugh, James G. (1952): A Summary and Analysis of the Low-Speed Longitudinal Characteristics of Swept Wings at High Reynolds Number. NACA RM L52D16, 1952. (Also available as NASA TR 1339, 1952.)

Gaster, M. (1966): The Structure and Behavior of Laminar Separation Bubbles., NPL. Aero Rept. 1181, Aug. 1966, National Physical Lab, England.

Gault, Donald E. (1949): Boundary-Layer and Stalling Characteristics of the NACA 63-009 Airfoil Section. NACA TN 1894, 1949.

Gault, D. E. (1957): A Correlation of Low-Speed Airfoil Section Stalling Characteristics with Reynolds Number and Airfoil Geometry, NACA TN 3963, 1957.

Gloss, B. B.; and Johnson, F. T. (1976): Development of an Aerodynamic Theory Capable of Predicting Surface Loads on Slender Wings with Vortex Flow. Proceedings of the SCAR Conference. NASA CP-001, 1976, pp. 55-67.

Gould, R. W. F.; and Cowdrey, D. F. (1958): High Reynolds Number Tests on a 70° L.E. Sweptback Delta Wing and Body (HP 100) in the Compressed Air Tunnel. ARC CP No. 387, 1958.

Henderson, W. P. (1976): Effects of Wing Leading-Edge Radius and Reynolds Number of Longitudinal Aerodynamic Characteristics of Highly Swept Wing-Body Configurations at Subsonic Speeds. NASA TN D-8361, Dec. 1976.

Hummel, Deitrich (1965): Experimentelle Untersuchung der Stroemung aur der Saugseite eines schlanken Deltaflugels. Zietschrift fuer Flugwissenschaften, v. 13, July 1965, pp. 247-252. (English translation available as NASA TM-75897.)

Hummel, D; and Redeker, G. (1972): Experimentelle Bestimmung der gebundenen Wirbellinien sowie des Stromungsverlaufs in der Umgebung der Hinterkante eines schlanken Deltaflugels. Braunschweigische Wissenschaftliche Gesellschaft, Abhandlung, 1972, pp. 273-290. (English translation available as NASA TT F-15,012.)

Hurley, D. G. (1955): The Downstream Effect of a Local Thickening of the Laminar Boundary Layer, Aerodynamic Research Laboratires, Australia, Aero Not 146, 1955.

Ingen, J. L. van (1975): On the Calculation of Laminar Separation Bubbles in Two-Dimensional Incompressible Flow. AGARD Conference Proceedings 168, 1975.

Jacobs, Eastman N. (1931): The Aerodynamic Characteristics of Eight Very Thick A Airfoils from Tests in the Variable Density Wind Tunnel. NACA Rep. 391, 1931.

- Jacobs, Eastman N.; and Sherman, Albert (1937): Airfoil Section Characteristics as Affected by Variations of the Reynolds Number. NACA Rep. 586, 1937.
- Johnson, R. T.; Lu, P.; Tinoco, E. N.; and Epton, M. A. (1980): An Improved Panel Method for the Solution of Three-Dimensional Leading-Edge Vortex Flows. Volume I. - Theory Document. NASA CR-3278, July 1980.
- Jones, B. Melvill (1933): An Experimental Study of the Stalling of Wings. R&M No. 1588, British A.R.C., 1933.
- Jones, B. Melvill (1934): Stalling. Jour. Royal Aero. Soc., vol. 38, no. 285, Sept. 1934, pp. 753-770. (22d Wilbur Wright Memorial Lecture.)
- Jones, George W., Jr. (1952): Investigation of the Effects of Variations in Characteristics of Three Low-Aspect-Ratio Symmetrical Wings with Rectangular Planforms. NACA RM L52G18, September 1952.
- Jones, R. T. (1946): Wing Plan Forms for High-Speed Flight. NASA TN NO. 1033, 1946.
- Knight, Montgomery and Loeser, Oscar, Jr.: Pressure Distribution Over a Rectangular Monoplane Wing Model up to 90° Angle of Attack. NACA Report No. 288, 1927.
- Kolbe, Carl D.; and Boltz, Frederick W. (1951): The Forces and Pressure Distribution at Subsonic Speeds on a Plane Wing Having 45° of Sweepback, an Aspect Ratio of 3, and a Taper Ratio of 0.5. NACA RM A51G31, October 1951.
- Kuchemann, D. (1953): Types of Flow on Swept Wings - With Special Reference to Free Boundaries and Vortex Sheets. RAE TN Aero 2234, March 1953.
- Kuchemann, D. (1978): The Aerodynamic Design of Aircraft. Pergamon Press, 1978.
- Kulfan, R. M. (1979): Wing Airfoil Shape Effects on the Development of Leading Edge Vortices. AIAA Paper No. 79-1675, 1979.
- Ladson, Charles L. (1988): Effects of Independent Variation of Mach and Reynolds Numbers on the Low-Speed Aerodynamic Characteristics of the NACA 0012 Airfoil Section, NASA TM 4074, 1988.
- Lamar, John E. (1968): A Modified Multhopp Approach for Predicting Lifting Pressures and Camber Shape for Composite Planforms in Subsonic Speeds. NASA TN D-4427, 1968.
- Lamar, John E. (1974): Extension of Leading-Edge-Suction Analogy to Wings with Separated Flow Around the Side Edges at Subsonic Speeds. NASA TR R-428, October 1974.

- Lamar, J. E.; and Luckring, J. M. (1979): Recent Theoretical Developments and Experimental Studies Pertinent to vortex Flow Aerodynamics - With a View Towards Design. High Angle of Attack Aerodynamics, AGARD CP-247, Paper No. 24, Jan. 1979.
- Lan, Edward C.; and Lamar, John E. (1977): On the Logarithmic-Singularity Correction in the Kernel Function Method of Subsonic Lifting-Surface Theory. NASA TN D-8513, Nov. 1977.
- Lancaster, F. W. (1907): Aerodynamics: Constituting the First Volume of a Complete Work on Aerial Flight. Constable & Co. Ltd. London, 1907.
- Lange/Wacke (1948): Test Report on Three- and Six-Component Measurements on a Series of Tapered Wings of Small Aspect Ratio. (Partial Report: Triangular Wing). TM 1176, may 1948.
- Lawrence, H. R. (1951): The Lift Distribution on Low Aspect Ratio Wings at Subsonic Speeds. Jour. Aero. Sci., vol. 18, no. 10, Oct. 1951, pp. 683-695.
- Legendre, R. (1981): Rolling up of Vortex Sheets From the Edges of Lifting Surfaces. Reckerke Aerospace, (1981-2).
- Lemaire, D. A. (1965): Some Observations of the Low-Speed Flow Over a Sharp-Edged Delta Wing of Unit Aspect Ratio. ARL Aerodynamics Report 126, Melbourne, Australia, Jan. 1965.
- Loftin, Laurence K. (1947): Theoretical and Experimental Data for a Number of NACA 6A-Series Airfoil Sections. NACA TR 903, 1947.
- Loftin, Laurence K.; and Bursnall, William J. (1948): The Effects of Variation in Reynolds Number Between  $3.0 \times 10^6$  and  $25.0 \times 10^6$  Upon the Aerodynamic Characteristics of a Number of NACA 6-Series Airfoil Sections. NACA TR 964, 1948.
- Loftin, Laurence K., Jr.; and Smith, Hamilton A. (1949): Aerodynamic Characteristics of 15 NACA Airfoil Sections at Seven Reynolds Numbers from  $0.7 \times 10^6$  to  $9.0 \times 10^6$ . NACA TN 1945, 1949.
- Lomax, Harvard; and Sluder, Loma (1952): Chordwise and Compressibility Corrections to Slender-Wing Theory. NACA Rep. 1105, 1952. (Supersedes NACA TN 2295.)
- Luckring, J. M.; Schoonover, W. E., Jr.; and Frink, N. T. (1982): Recent Advances in Applying Free Vortex Sheet Theory for the Estimation of Vortex Flow Aerodynamics. AIAA Paper No. 82-0095, 1982.
- Luckring, James Michael (1985a): A Method for Computing the Core Flow in Three-

- Dimensional Leading-Edge Vortices. PhD dissertation, Department of Mechanical and Aerospace Engineering. North Carolina State University, Raleigh, North Carolina, May 1985.
- Luckring, James M. (1985b): A Theory for the Core of a Three-Dimensional Leading-Edge Vortex. AIAA Paper No. 85-0108, 1985.
- Luckring, J. M.; Hoffler, K. D.; and Grantz, A. C. (1986): Recent Extensions to the Free Vortex Sheet Theory for Expanded Convergence Capability. NASA CP-2416, 1986.
- Manie, F.; Rehbach, C.; and Schmitt, V. (1978): Etude D'une Aile a Fleche Variable en Ecoulement sub ou Transsonique. ICAS, Lisbonne, 1978.
- McCullough, George B.; and Gault, Donald E. (1948): An Experimental Investigation of the NACA 63-012 Airfoil Section with Leading-Edge Suction Slots. NACA TN 1683, 1948.
- McCullough, George B.; and Gault, Donald E. (1949): Boundary-Layer and Stalling Characteristics of the NACA 64A006 Airfoil Section. NACA TN 1923, 1949.
- McCullough, George B.; and Gault, Donald E. (1951): Examples of Three Representative Types of Airfoil-Section Stall at Low Speed. NACA TN 2502, 1951.
- McCullough, George B.: The Effect of Reynolds number on the stalling characteristics and pressure distributions of four moderately thin airfoil sections. NACA TN 3524, 1955.
- Millikan, C. B.; and Klein, A. L. (1933): The Effect of Turbulence. Aircraft Engineering, vol. 5, no. 8, August 1933, pp. 169-174.
- Multhopp, H. (1950): Methods for Calculating the Lift Distribution of Wings (Subsonic Lifting-Surface Theory). R&M No. 2884. British A.R.C., Jan. 1950.
- Munk, Max M. (1923): Note on the Relative Effect of the Dihedral and the Sweep Back of Airplane Wings. NACA TN 177, 1923.
- Muse, Thomas C. (1943): Some Effects of Reynolds and Mach Numbers on the Lift of an NACA 0012 Rectangular Wing in the NACA 19-Foot Pressure Tunnel. NACA Wartime Report L-406 (originally published as Confidential Bulletin 3E29, May 1943).
- Owen, P. R. and L. Klanfer (1953): On the laminar boundary layer separation from the leading edge of a thin aerofoil. RAE Rep. Aero. 2508 (Oct. 1953); reissued as A.R.C. CP 220 (1955).
- Peckham, D. H. (1961): Low-Speed Wind-Tunnel Tests on a Series of Uncambered Slender Pointed Wings with Sharp Edges. ARC R&M No. 3186, 1961.

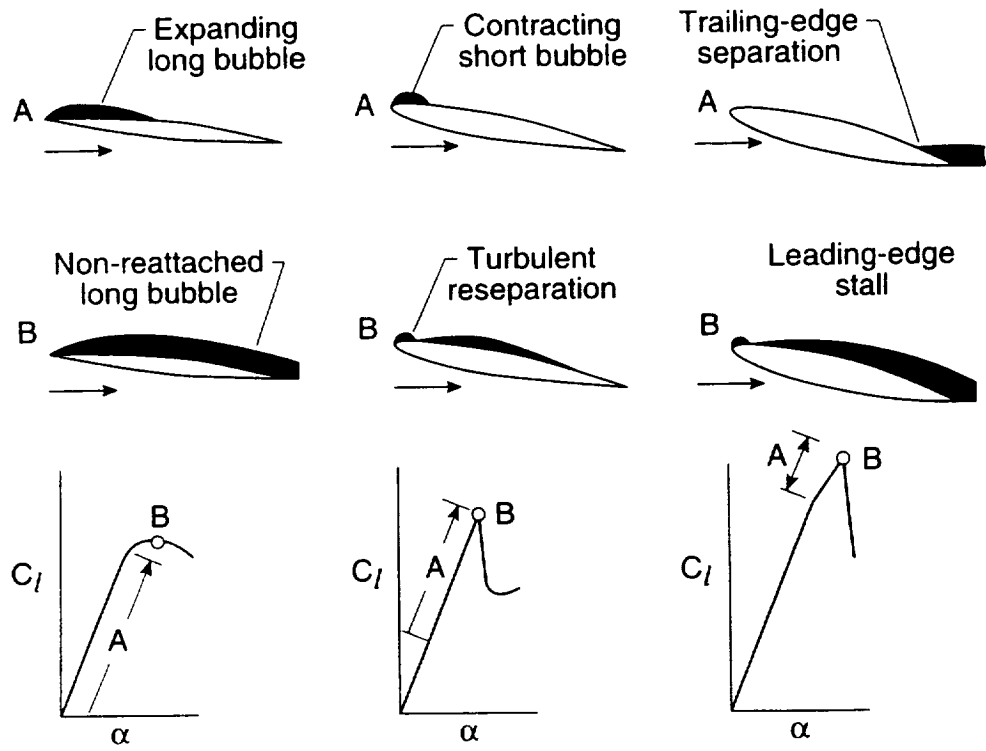
- Polhamus, Edward C. (1955): A note on the drag due to lift of rectangular wings of low aspect ratio. NACA TN 3324, January 1955.
- Polhamus, E. C. (1966): A Concept of the Vortex Lift of Sharp-Edge Delta Wings Based on a Leading-Edge-Suction Analogy. NASA TN D-3767, 1966.
- Polhamus, E. C. (1969): Predictions of Vortex-Lift Characteristics by a Leading-Edge Suction Analogy. AIAA Paper 59-1133, Oct. 1969.
- Polhamus, Edward C. (1986): Vortex Lift Research: Early Contributions and Some Current Challenges. NASA CP-2416, 1986.
- Poll, D. I. A. (1983): On the Generation and Subsequent Development of Spiral Vortex Flow Over a Swept-Back Wing. In AGARD-CP-342, July 1983.
- Poll, D. I. A. (1986): Spiral Vortex Flow Over a Swept-Back Wing. Aeronautical Journal, May 1986.
- Rose, Leonard M.; and Altman, John M. (1950): Low-Speed Investigation of the Stalling of a Thin, Faired, Double-Wedge Airfoil with Nose Flap. NACA TN 2171, 1950.
- Tani, I (1964): Low-Speed Flow Involving Bubble Separations, Progress in Aeronautical Science, vol. 5, Pergamon Press, New York, pp. 70-103, 1964.
- Thwaites, B. (Editor) (1960): Incompressible Aerodynamics. Oxford University Press, 1960.
- von Doenhoff, Albert E. (1938): A Preliminary Investigation of Boundary-Layer Transition Along a Flat Plate with Adverse Pressure Gradient. NACA TN 639, 1938.
- Wallis, R. A. (1954): Experiments with Air Jets to Control the Nose Stall on a 3 ft. Chord NACA 64A006 Aerofoil, Aeronautical Research Laboratories, Australia, Aero Note 139, 1954.
- Weber, J. (1955): Some Effects of Flow Separation on Slender Delta Wings. RAE Tech Note AERO 2425, 1955.
- Wentz, W. H., Jr. (1968): Wind Tunnel Investigations of Vortex Breakdown on Slender Sharp-Edge Wings. NASA CR-98737, 1968.
- Wieghardt, K. (1939): Über die Auftriebsverteilung des einfachen Rechtecksflugels über die Tiefe. Zeitschr. f. angew. Math. U. Mech. vol. 19, p. 257, 1939 (English translation available as NACA TM 963).
- Wilson, H. A.; and Lovell, J. C. (1946): Full-Scale Investigation of the Maximum Lift Flow Characteristics of an Airplane Having Approximately Triangular Planform. NACA RM L6K20, Nov. 1946.

Winter, H. (1936): Flow Phenomena on Plates and Airfoils of Short Span. NACA TM-798, 1936.

Zimmerman, C. H. (1932): Characteristics of Clark Y Airfoils of Small Aspect Ratios. NACA Report 431, 1932.

## 9. ACKNOWLEDGEMENT

The author gratefully acknowledges the many helpful suggestions of James M. Luckring, Head of Langley's Transonic Supersonic Aerodynamics Branch, who also provided the appendix and performed the final technical review.



(a) Thin-airfoil stall      (b) Leading-edge stall      (c) Trailing edge/Leading-edge stall

Figure 1.1 Types of stall associated with leading-edge separation as classified by Gault (1957).

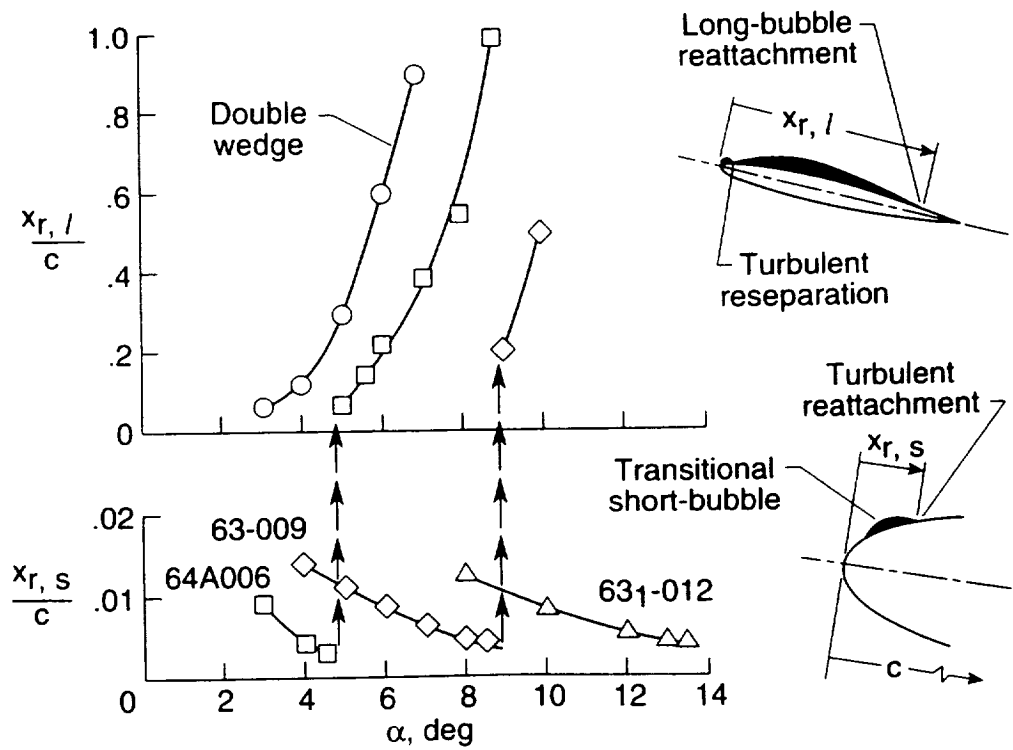


Figure 1.2 Effect of angle-of-attack on turbulent reattachment location. See text for data sources.  $R_c = 5.8 \times 10^6$

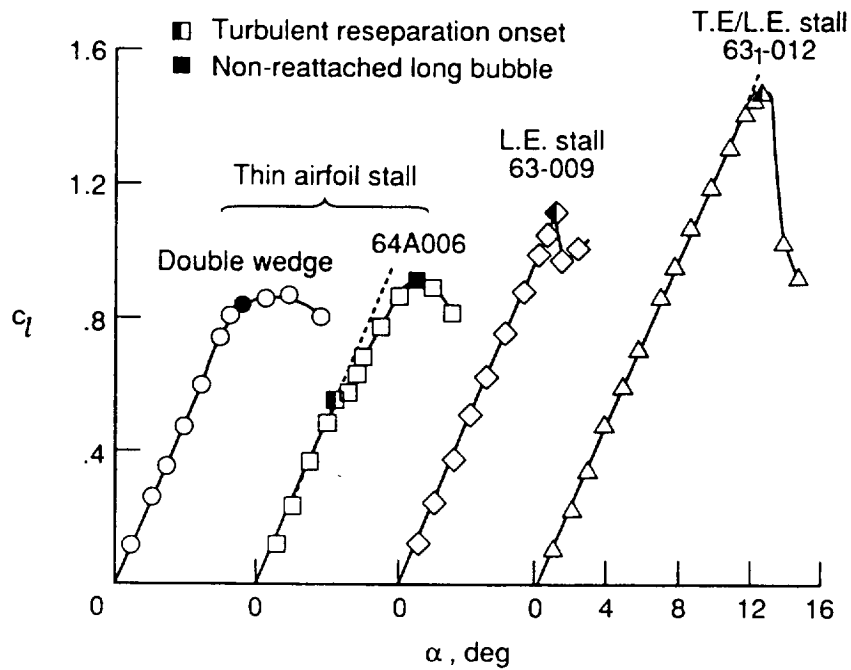
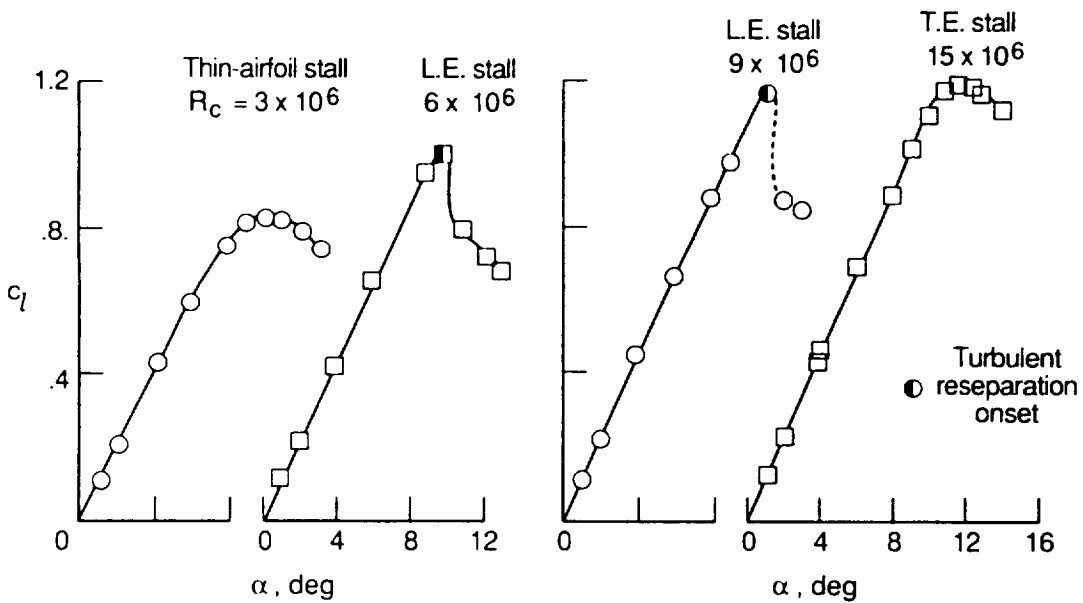


Figure 1.3 Lift characteristics for airfoils of figure 1.2. Data from McCullough and Gault (1951).  $R_c = 5.8 \times 10^6$



(a) NACA 66-009

(b) NACA 64-009

Figure 1.4 Effect of  $R_c$  on stall. See text for data sources.

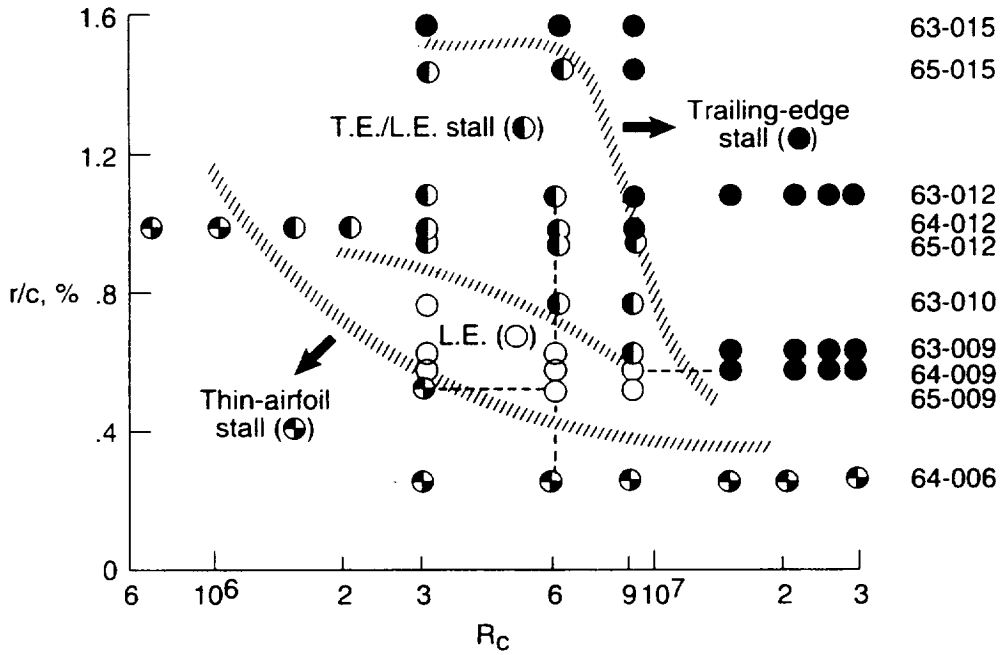


Figure 1.5 Stall boundaries as a function of leading-edge radius and  $Re$  based on NACA 6-series symmetrical airfoils. See text for data sources.

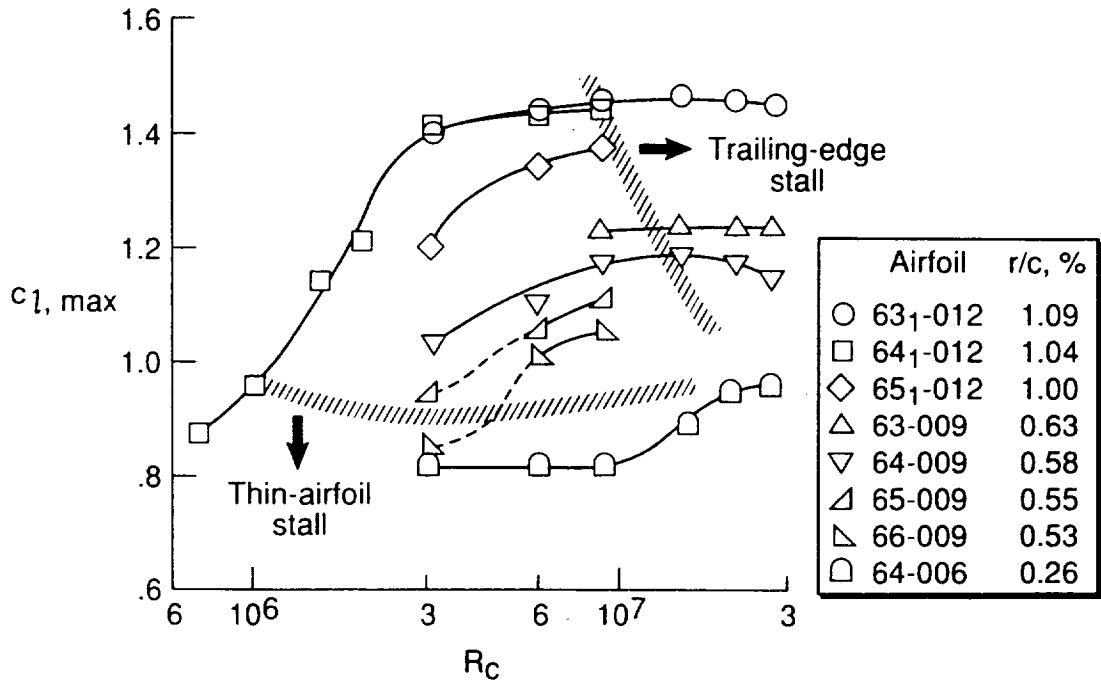


Figure 1.6 Some examples of the effects of  $Re$  and leading-edge radius on  $c_{l,max}$ . See text for data sources.

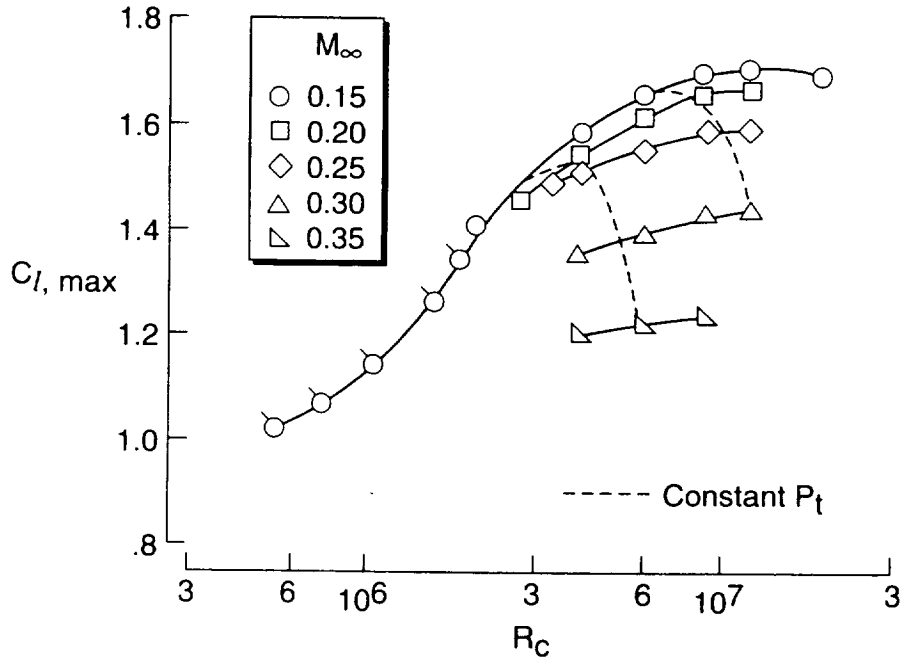


Figure 1.7 Effect of Mach number and Reynolds number on  $c_{l, \max}$  for NACA 0012 airfoil.

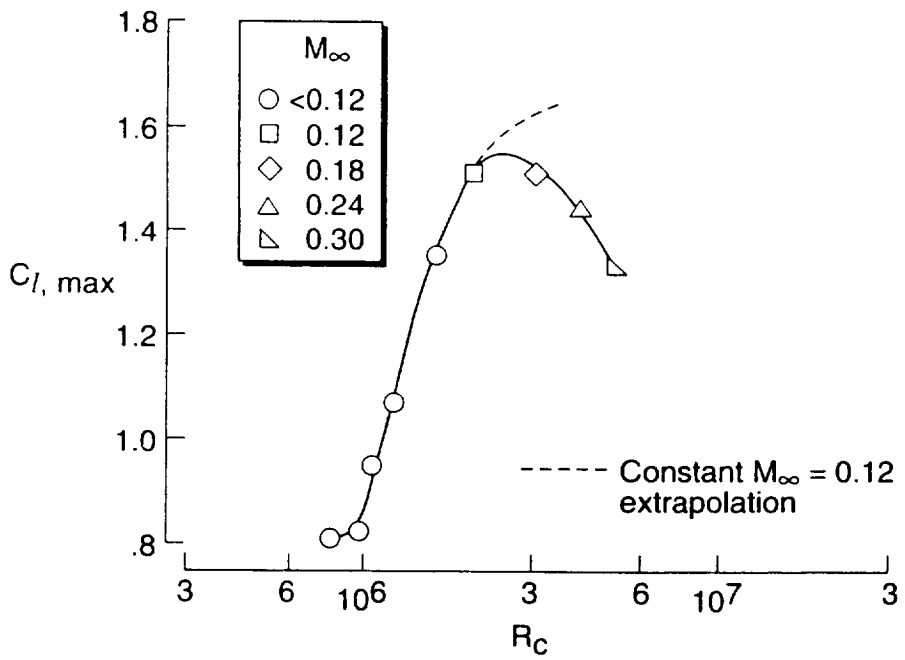


Figure 1.8 Effect of Mach number and Reynolds number on  $c_{l, \max}$  for ONERA "D" airfoil.

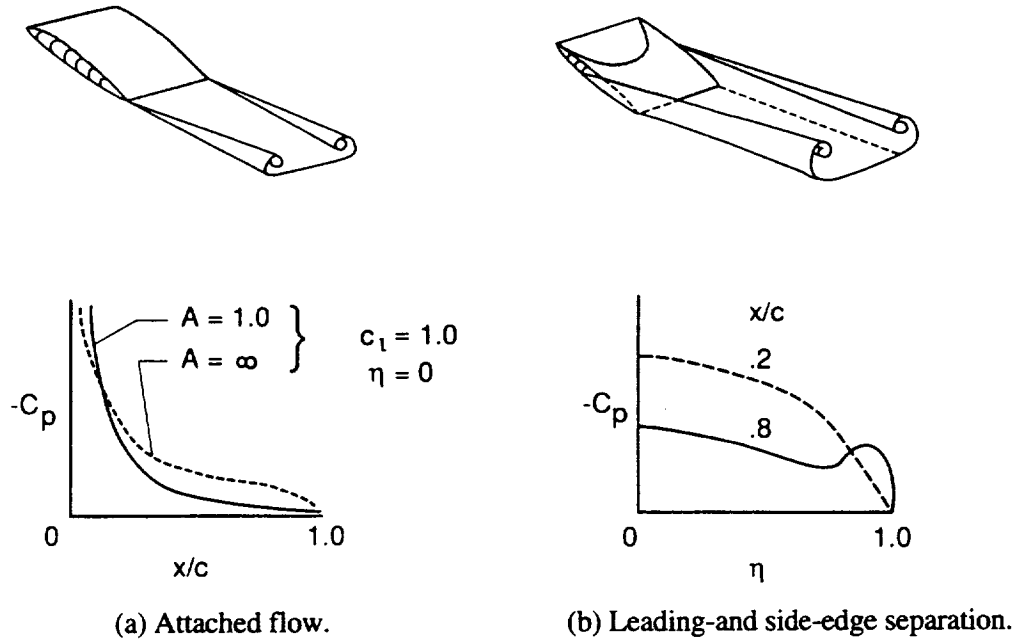


Figure 2.1 Some types of flow to be discussed in relation to the stall of rectangular wings.

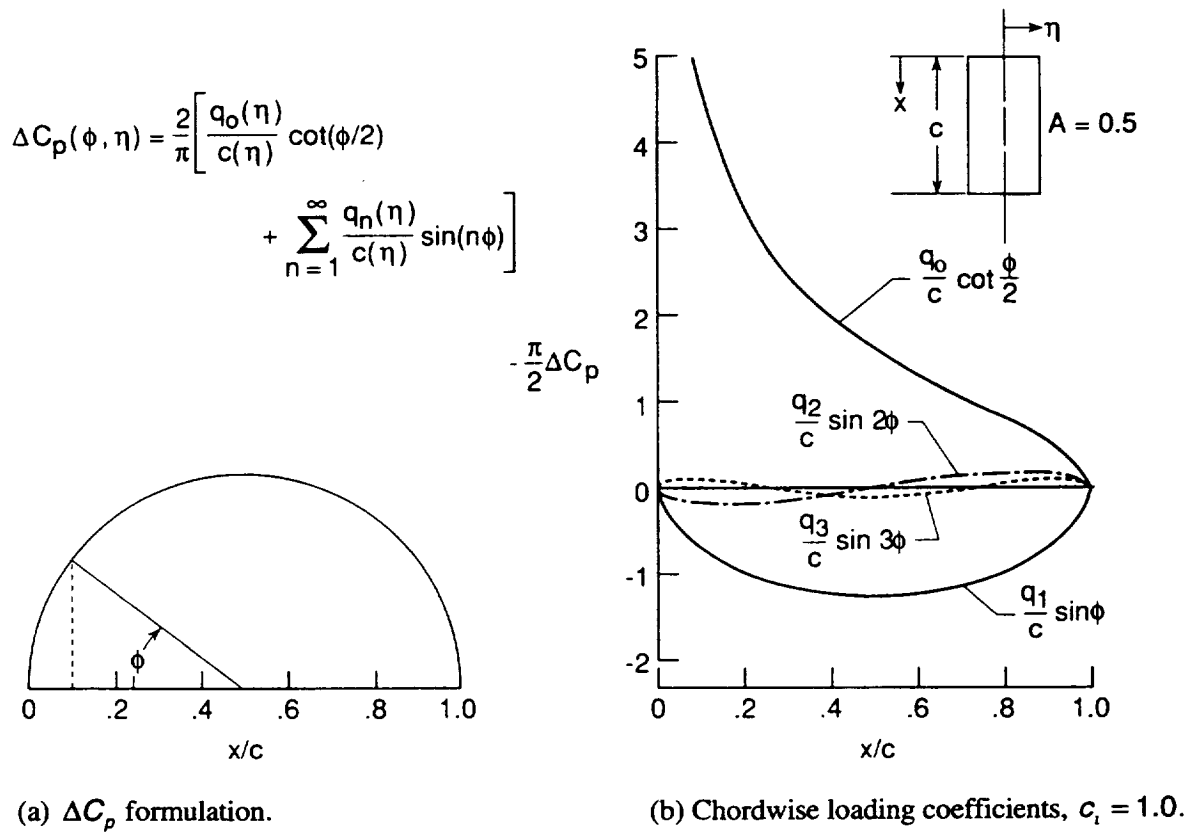


Figure 2.2 The chordwise loading functions used in determining  $\Delta C_p$ .

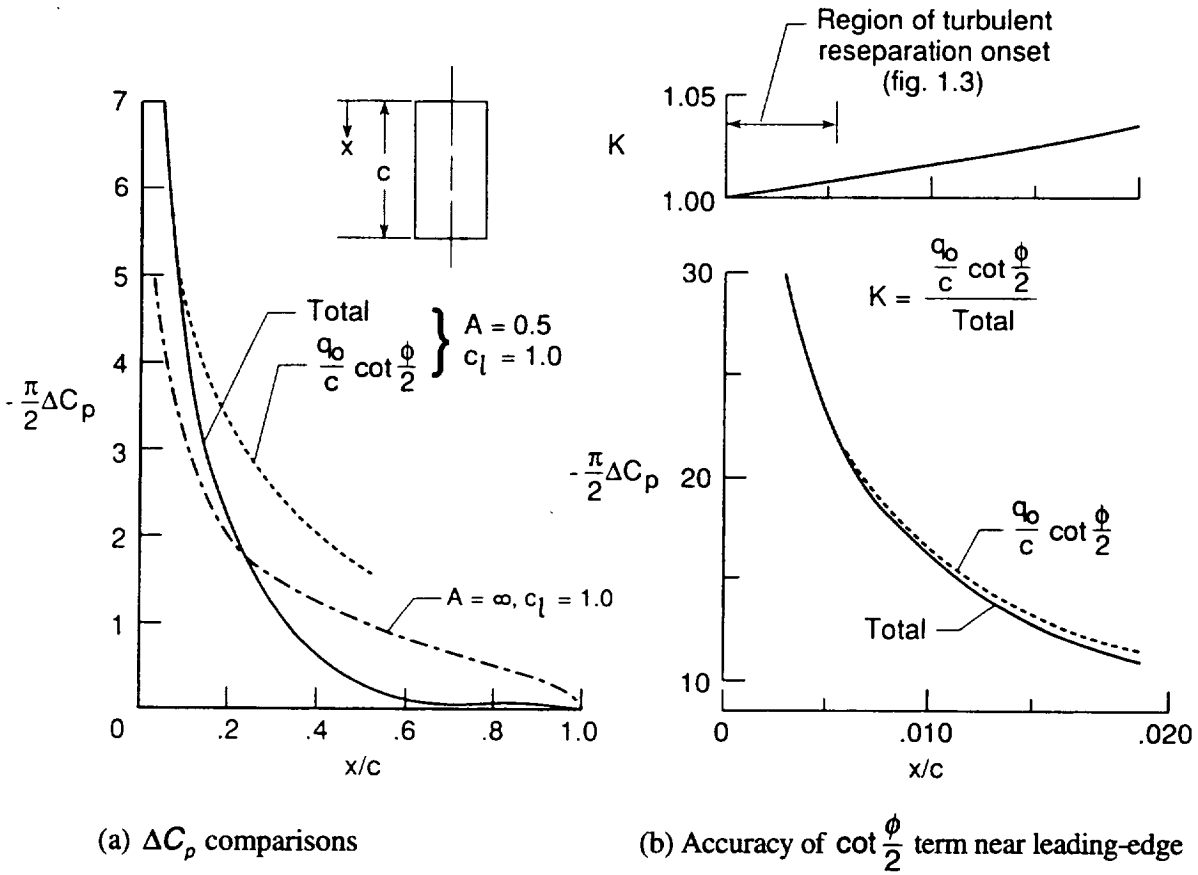


Figure 2.3 Calculated influence of induced camber on the  $\Delta C_p$  distribution at the root of an aspect ratio 0.5 rectangular wing.

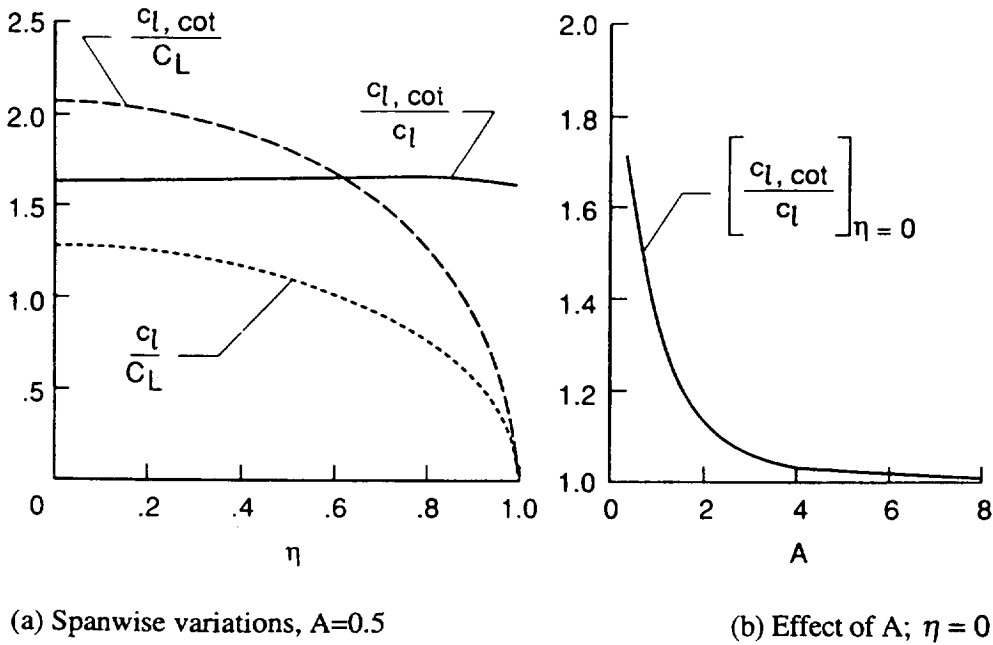


Figure 2.4 Some calculated variations of  $c_{l,cot}$  parameters.

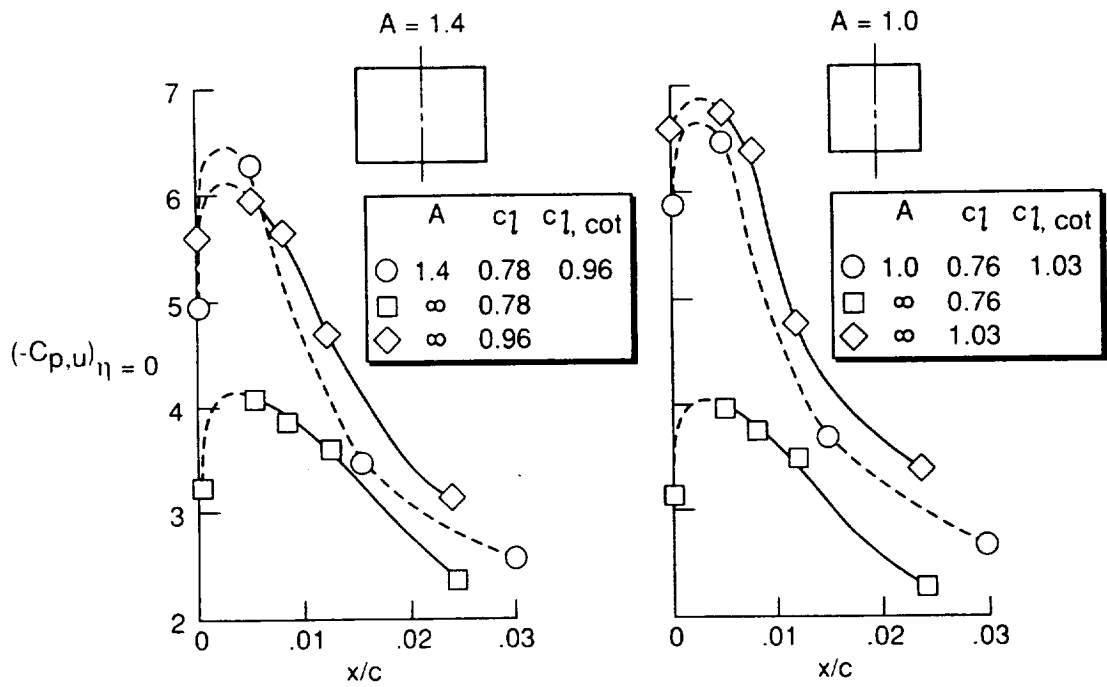


Figure 2.5 Effect of induced camber on pressure distribution near leading edge at root section for rectangular wings.

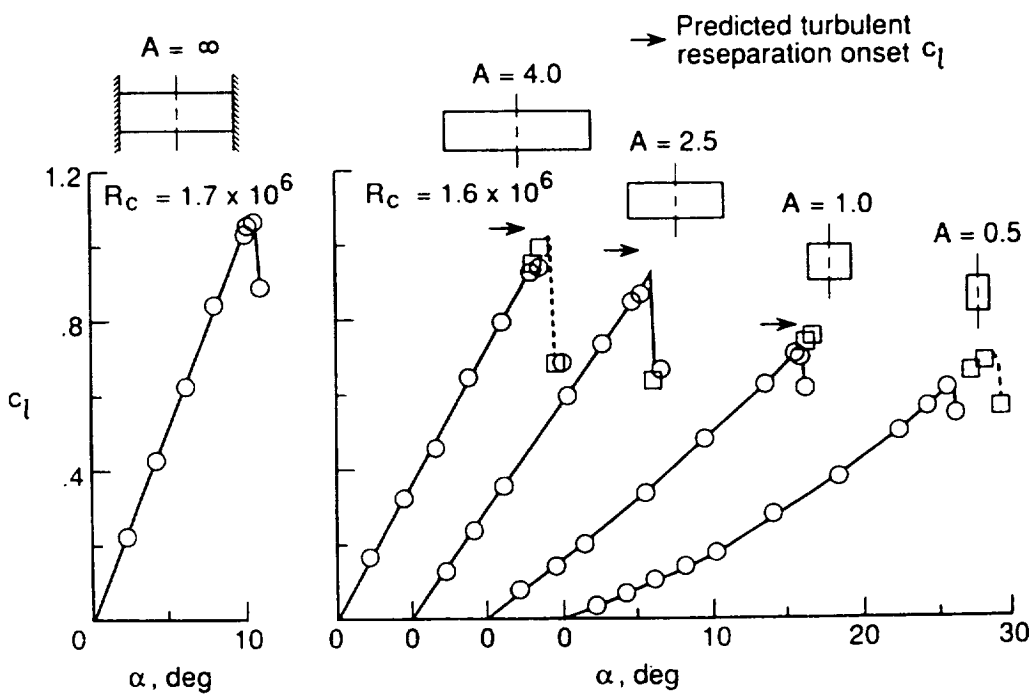
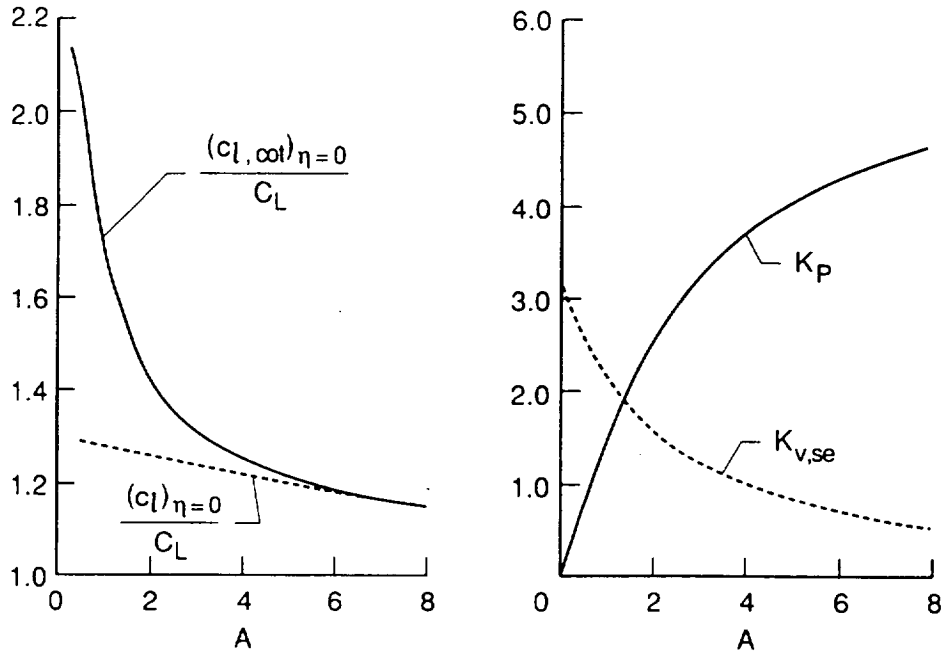


Figure 2.6 Effect of aspect ratio on lift coefficient at root section. Square symbols represent inverted model results.



(a) Root section lift terms

(b) Attached flow and vortex lift terms

Figure 2.7 variation with aspect ratio of various theoretical lift terms for rectangular wings.

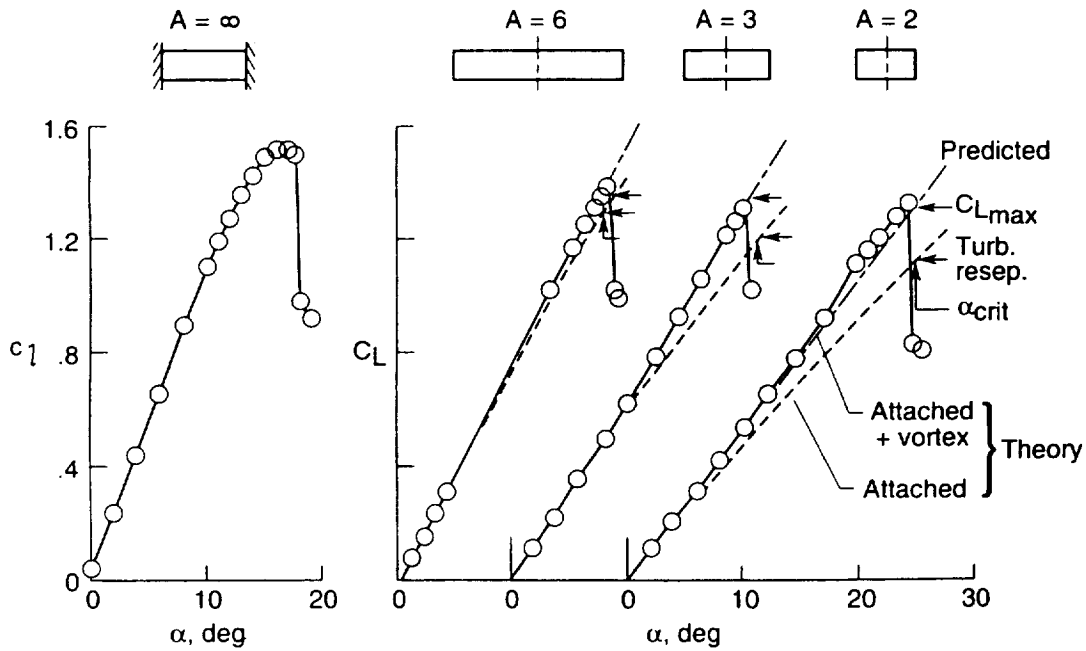


Figure 2.8 Effect of aspect ratio on the total lift of rectangular wings  $R_c = 3 \times 10^6$ , NACA 0012 airfoil sections.

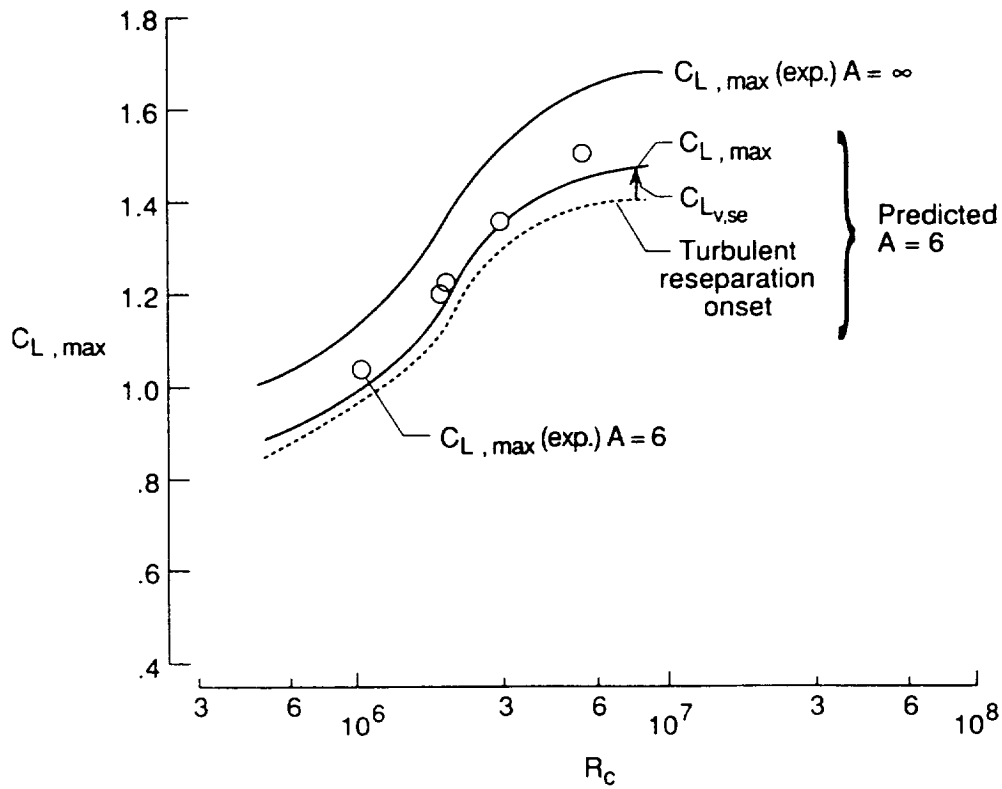


Figure 2.9 Comparison of predicted and measured  $C_{L,max}$  as a function of  $R_c$  for an aspect ratio 6 rectangular wing of NACA 0012 section. Data from Muse (1943).

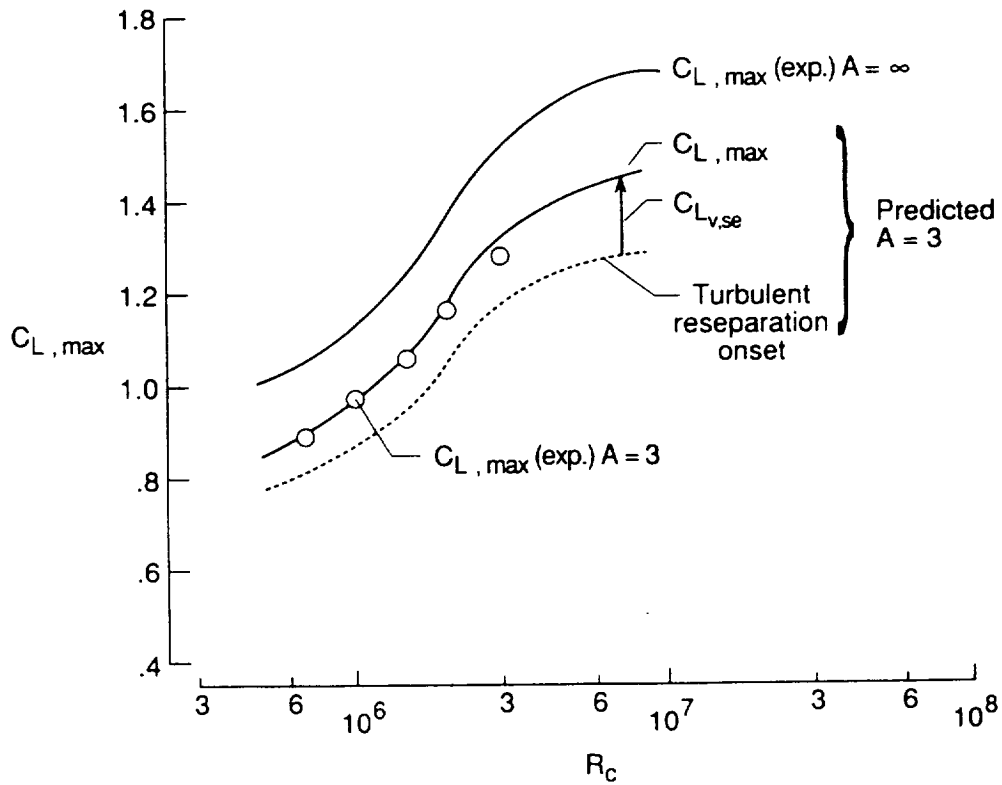


Figure 2.10 Comparison of predicted and measured  $C_{L,max}$  as a function of  $R_c$  for an aspect ratio 3 rectangular wing of NACA 0012 section. Data from Jones (1952).

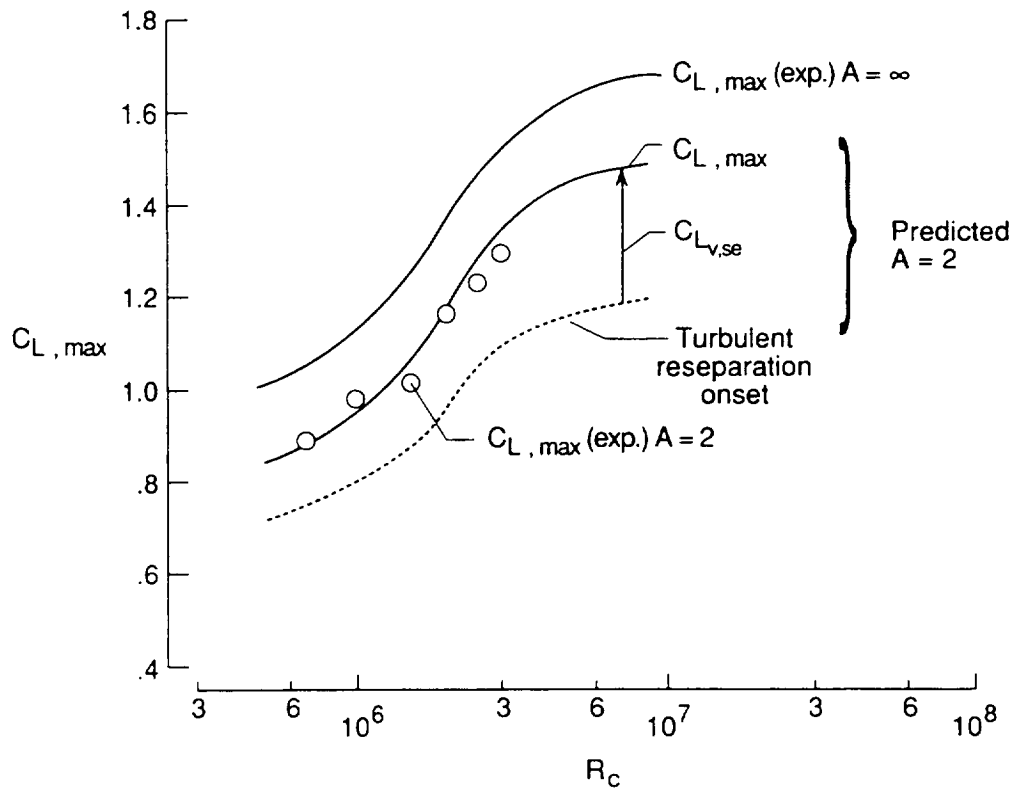


Figure 2.11 Comparison of predicted and measured  $C_{L,max}$  as a function of  $R_c$  for an aspect of ratio 2 rectangular wing of NACA 0012 section. Data from Jones (1952).

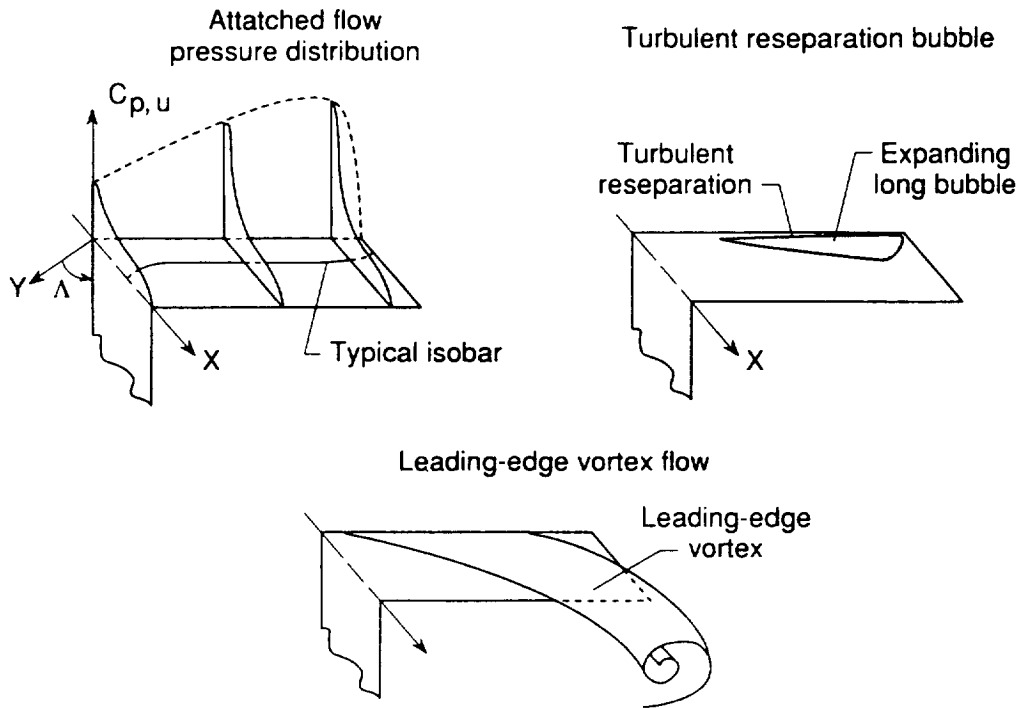


Figure 3.1 Some sweptback wing flow phenomena to be discussed.

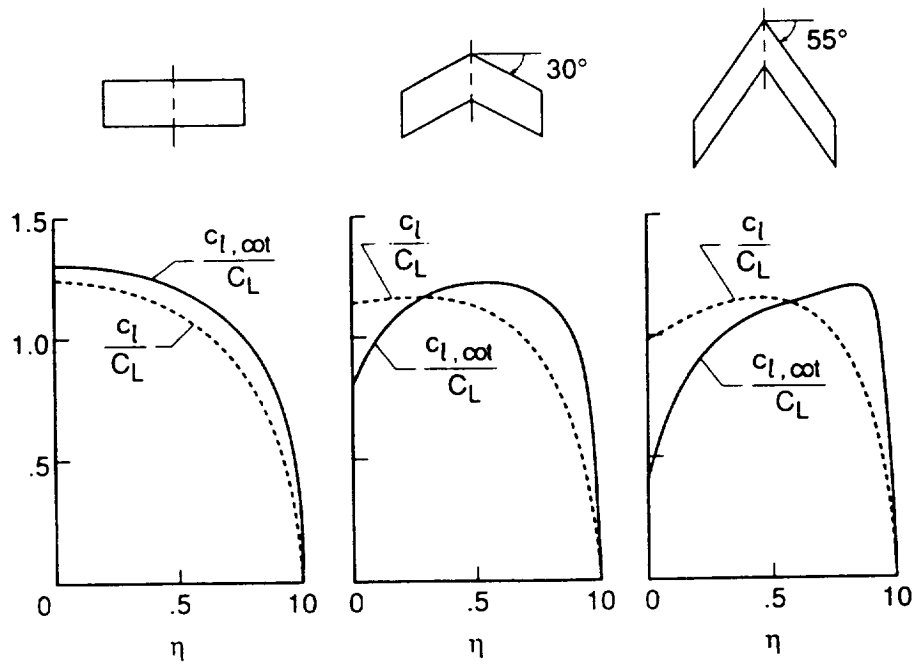


Figure 3.2 Theoretical effect of sweep on the spanwise variation of the section cotangent loading parameter.

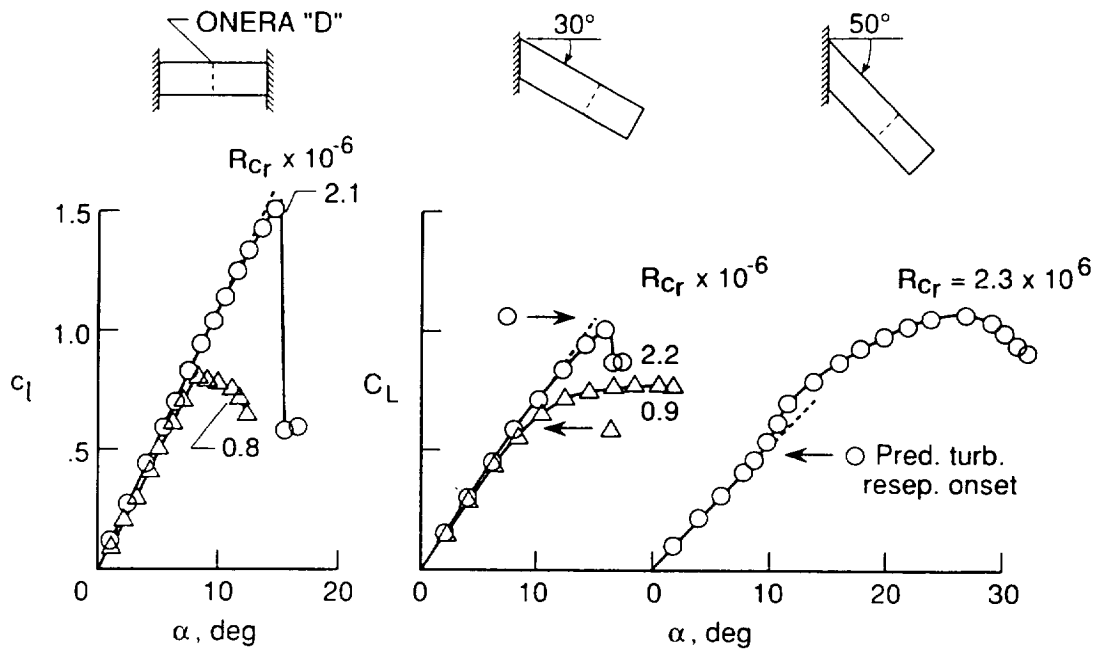


Figure 3.3 Effect of sweep and Reynolds number on the onset of turbulent reattachment and stalling. See text for experimental data sources.

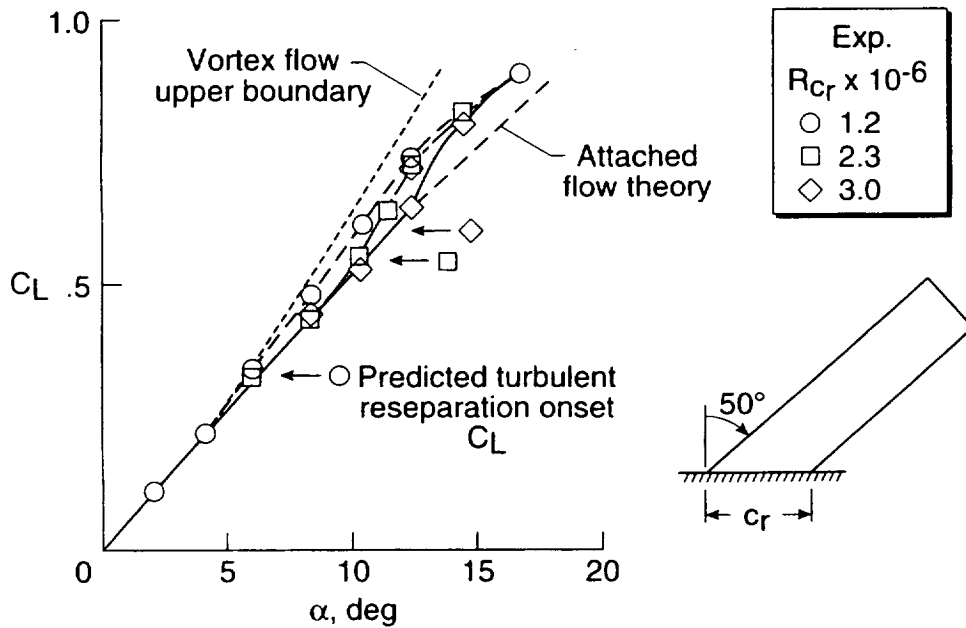


Figure 3.4 Some effects of Reynolds number on the vortex flow of the 50° wing of figure 3.3.

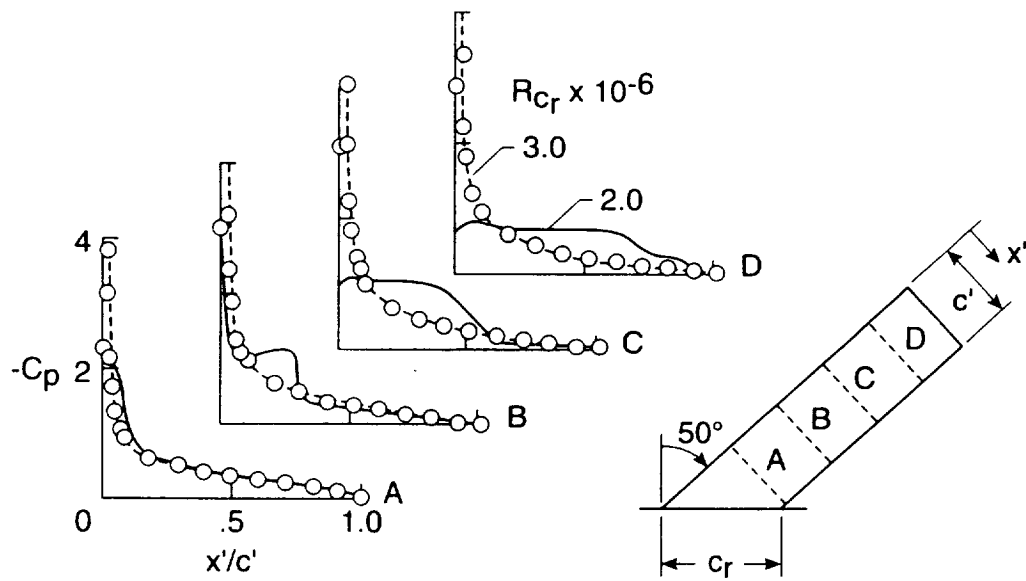


Figure 3.5 Effect of Reynolds number on the chordwise pressure distributions for the wing of figure 3.4

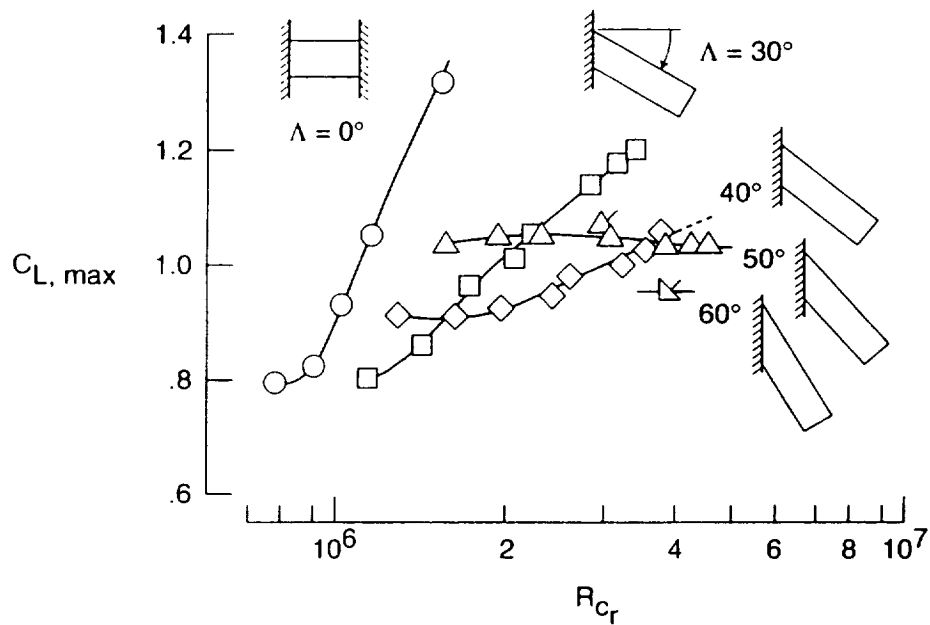


Figure 3.6 Effect of sweep and Reynolds number on  $C_{L,max}$ . Data from Carrara and Masson (1980).

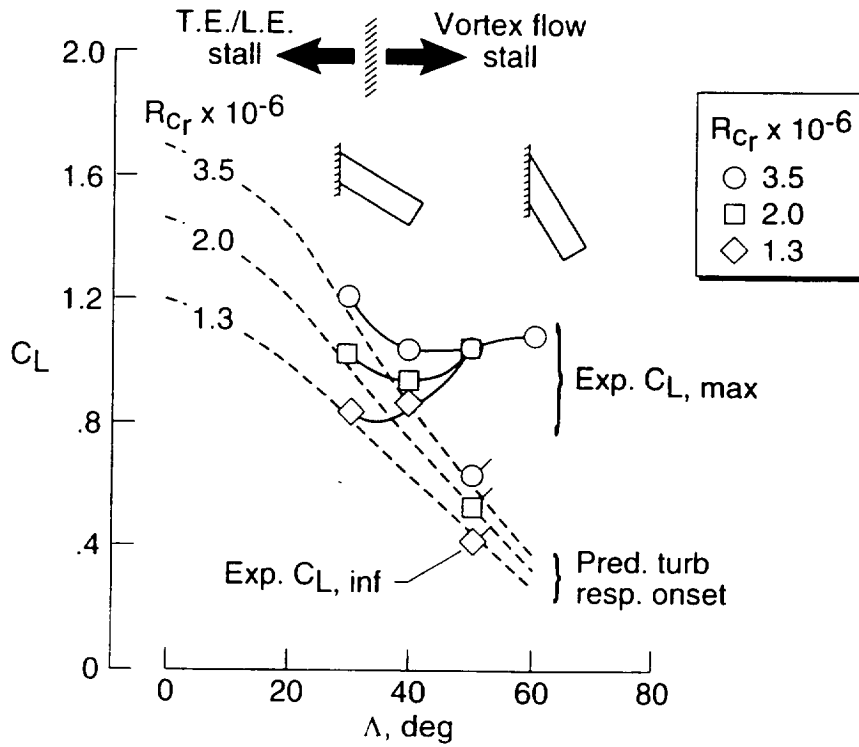


Figure 3.7 An illustration of the transition from leading-edge stall to vortex-flow stall. Experimental data from Carrara and Masson (1980).

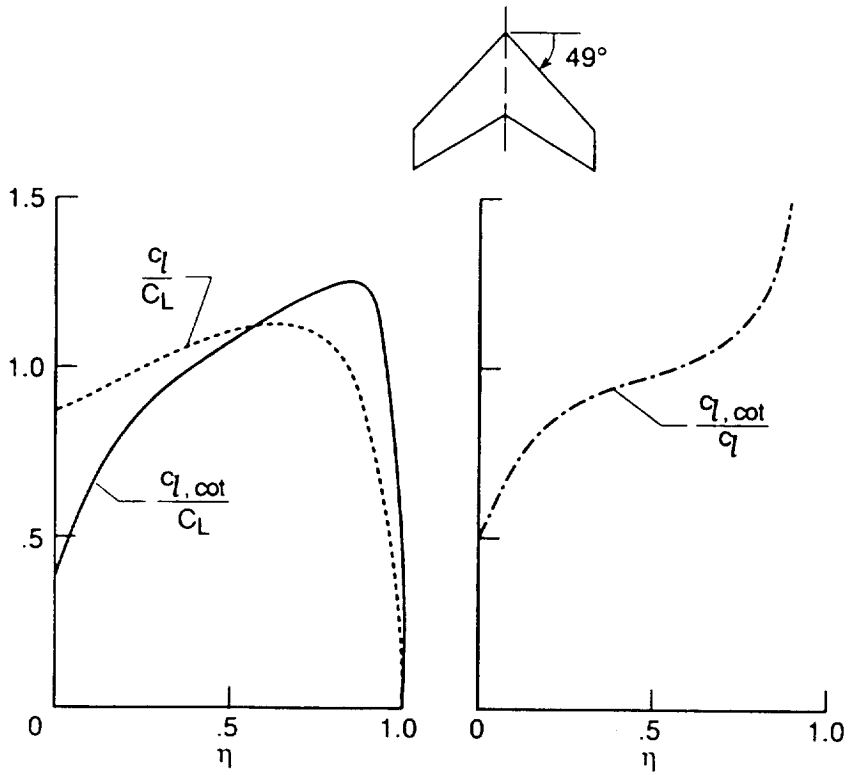


Figure 3.8 Spanwise variation of the theoretical section cotangent loading parameters for the planform to be studied in figures 3.9 and 3.10.

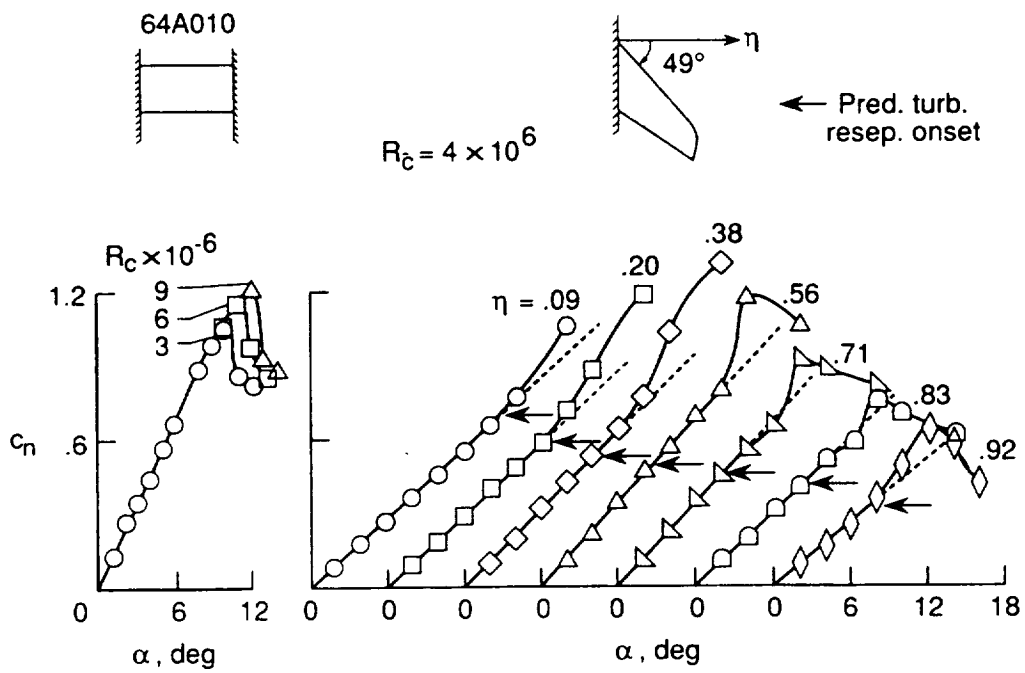


Figure 3.9 Spanwise variation of section normal force coefficient for the wing of Kalbe and Boltz (1951).

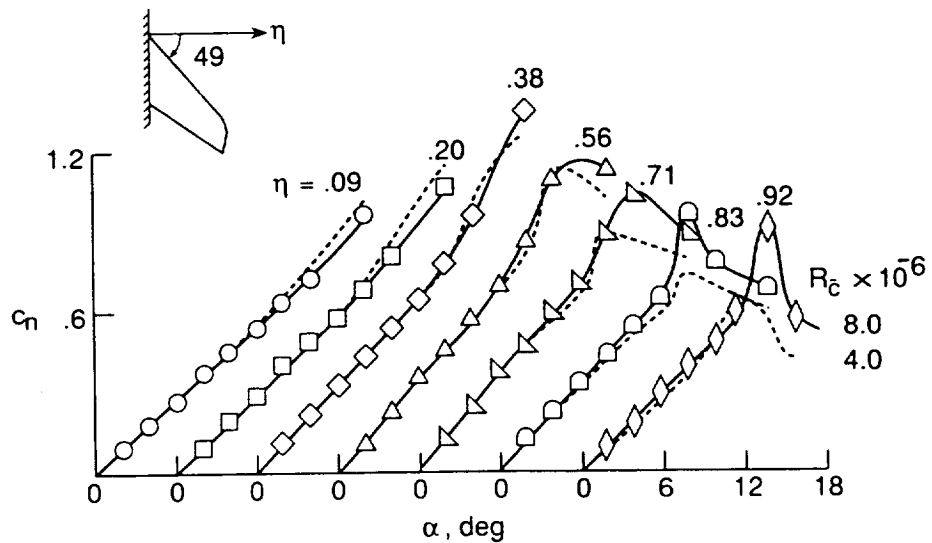


Figure 3.10 Effect of Reynolds number on the section normal force characteristics for the wing of Kalbe and Boltz (1951).

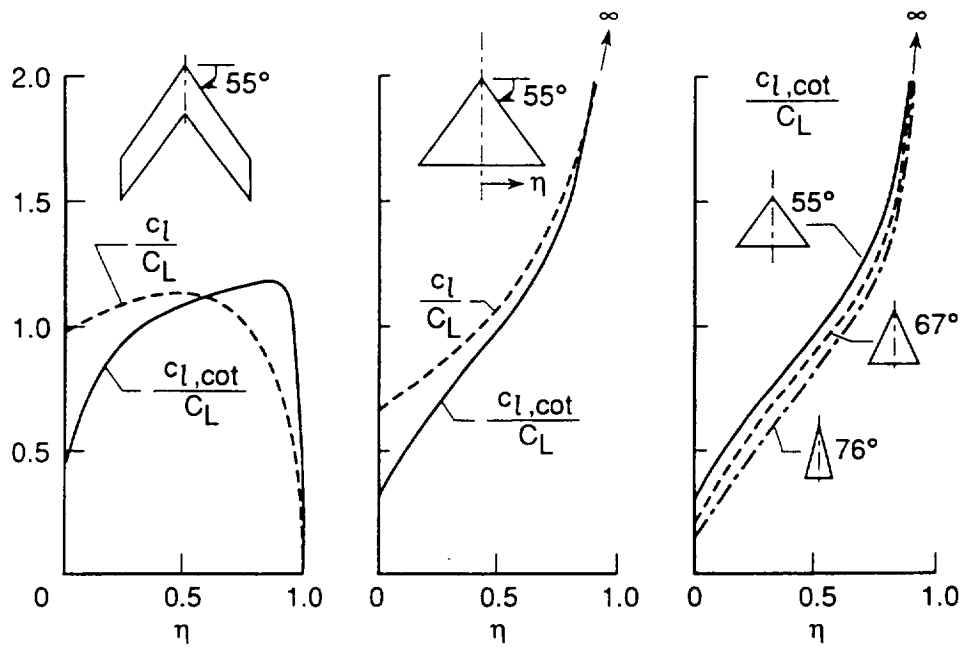
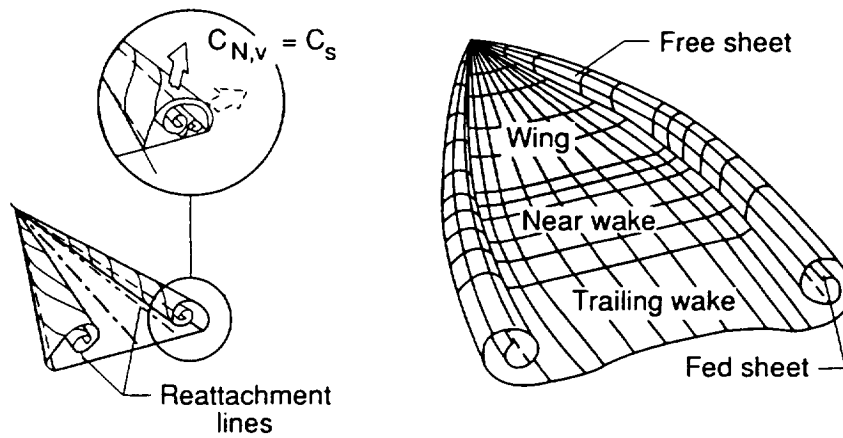


Figure 4.1 Calculated spanwise variation of the cotangent loading parameter for delta wings including a sweptback untapered wing for comparison.



(a) Leading-edge-suction analogy

(b) Free-vortex sheet theory (FVS)

Figure 4.2 Two theoretical methods used for vortex flow calculations.

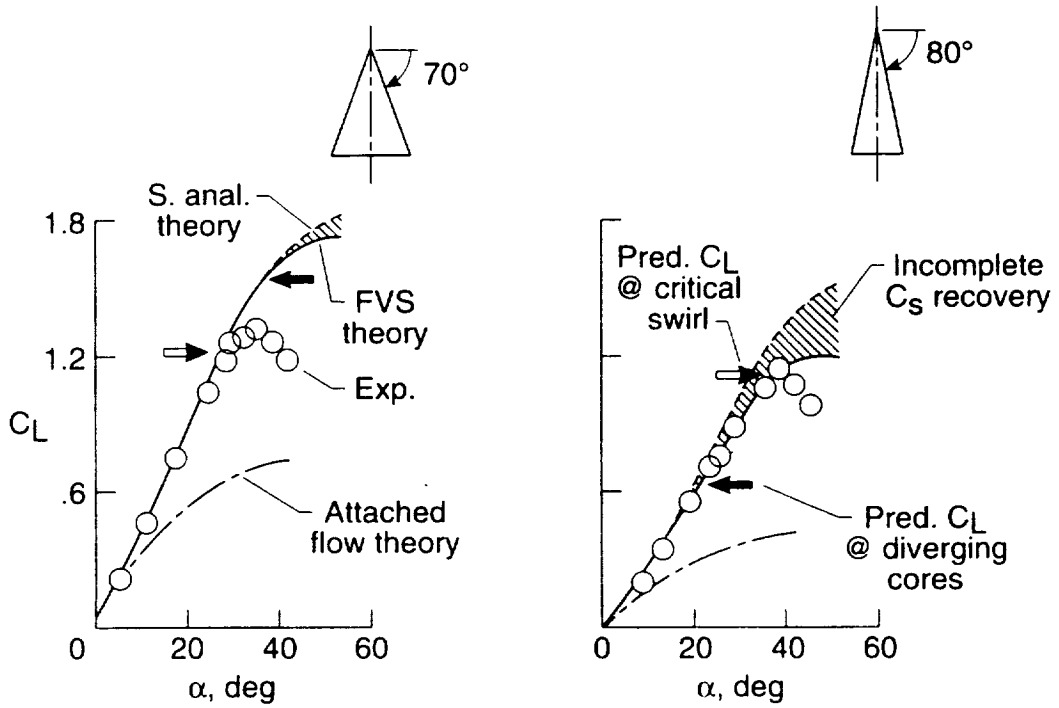


Figure 4.3 Lift characteristics of two delta wings. Experimental data from Wentz and Kohlman (1971). Sharp leading-edges.

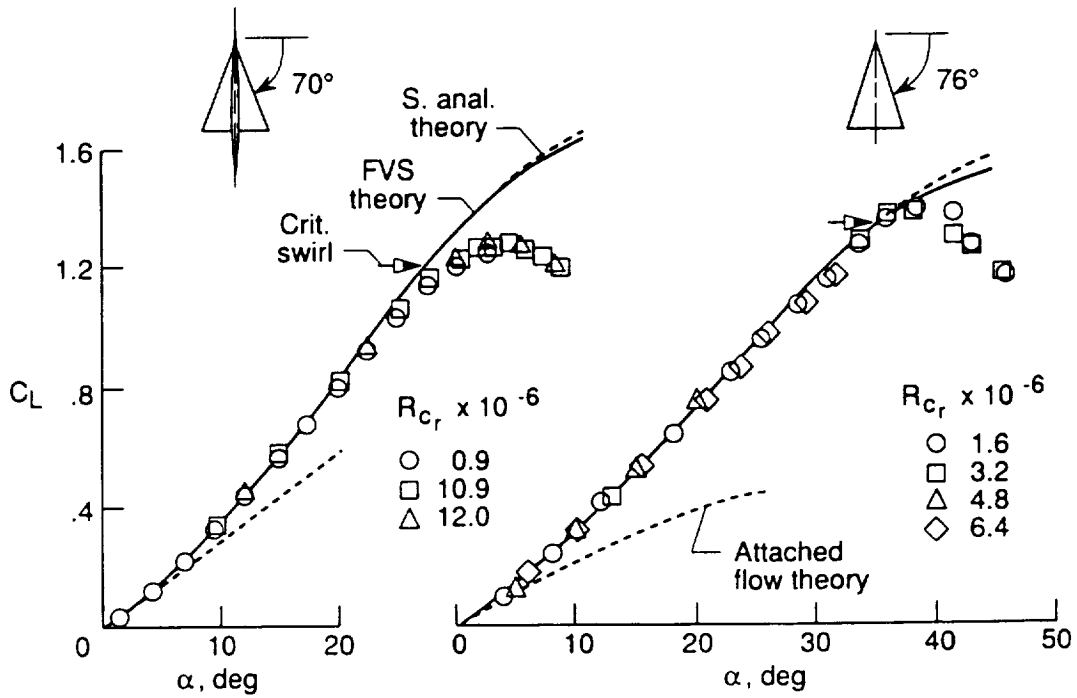


Figure 4.4 Effect of Reynolds number on the lift characteristics of two sharp-edge delta wings. Experimental data from Gould and Cowdrey (1958) and Lemaire (1965).

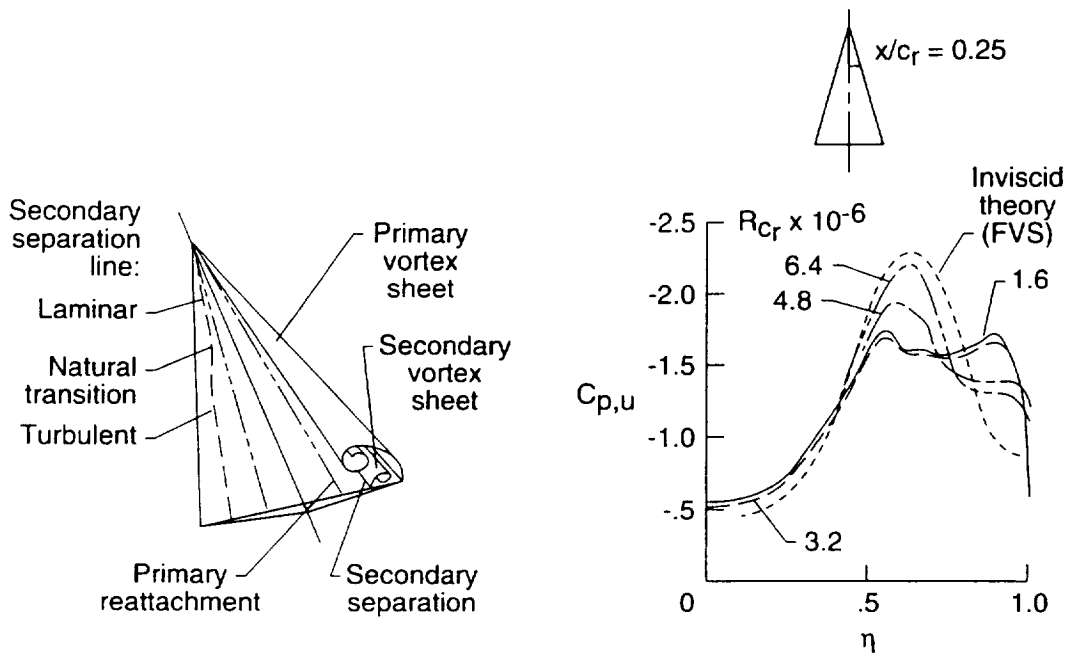


Figure 4.5 Vortex flow phenomena and upper surface pressure distribution for a slender, sharp-edge delta wing.

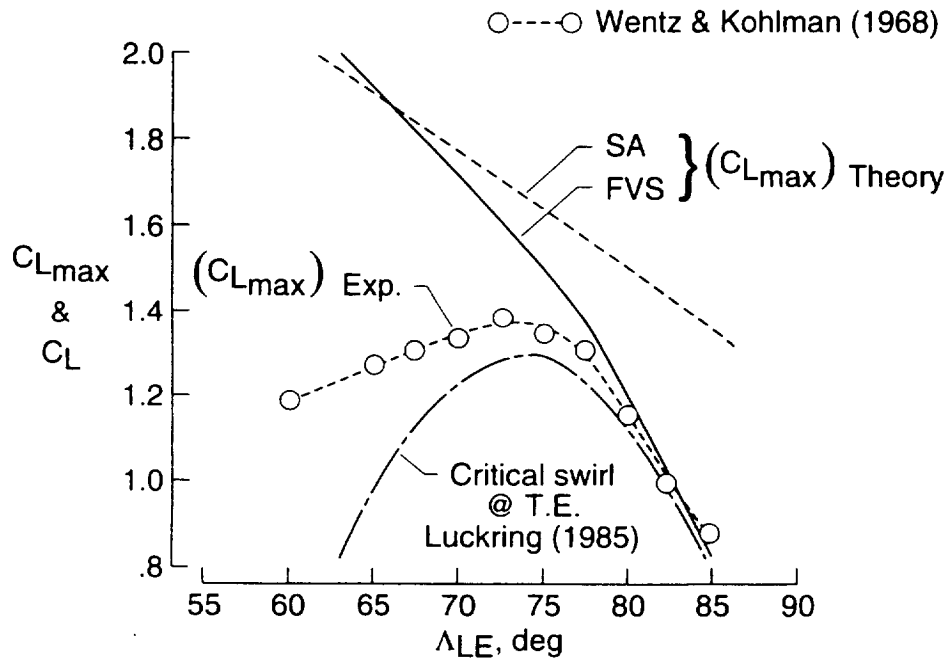


Figure 4.6 Comparison of  $c_{L_{max}}$  variation with leading-edge sweep with various theoretical solutions. Sharp-edge delta wings. Experimental data from Wentz and Kohlman (1968).

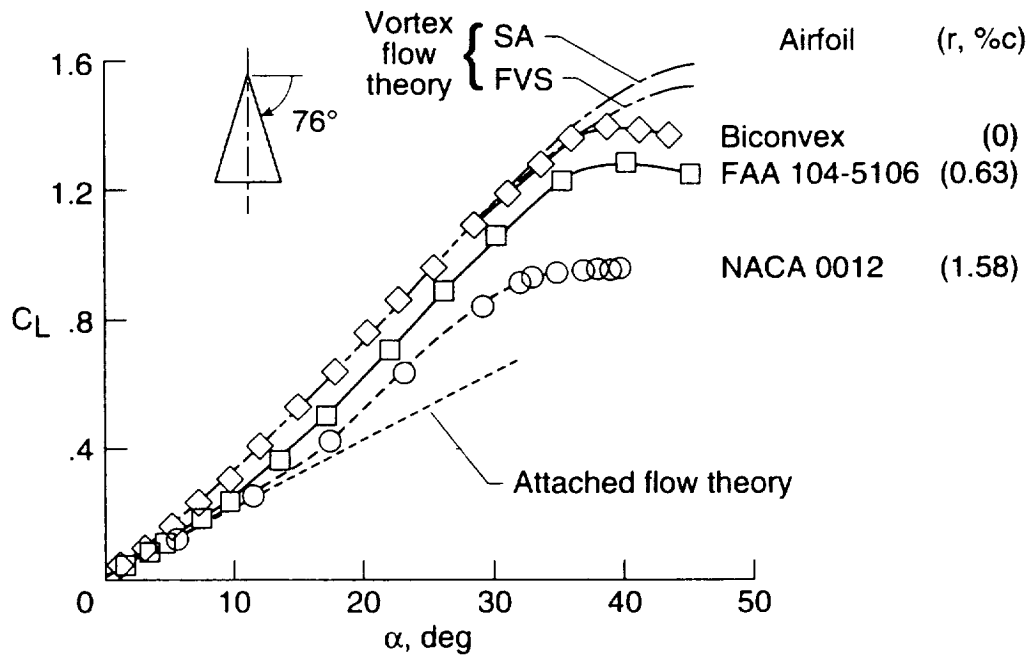


Figure 4.7 Effect of leading-edge radius on the lift of 76° delta wings. See text for data sources.



# REPORT DOCUMENTATION PAGE

*Form Approved*  
OMB No. 0704-0188

Public reporting burden for this collection of information is estimated to average 1 hour per response, including the time for reviewing instructions, searching existing data sources, gathering and maintaining the data needed, and completing and reviewing the collection of information. Send comments regarding this burden estimate or any other aspect of this collection of information, including suggestions for reducing this burden, to Washington Headquarters Services, Directorate for Information Operations and Reports, 1215 Jefferson Davis Highway, Suite 1204, Arlington, VA 22202-4302, and to the Office of Management and Budget, Paperwork Reduction Project (0704-0188), Washington, DC 20503.

<b>1. AGENCY USE ONLY (Leave blank)</b>		<b>2. REPORT DATE</b> June 1996	<b>3. REPORT TYPE AND DATES COVERED</b> Contractor Report	
<b>4. TITLE AND SUBTITLE</b> A Survey of Reynolds Number and Wing Geometry Effects on Lift Characteristics in the Low Speed Stall Region			<b>5. FUNDING NUMBERS</b> PO L21824C WU 505-59-10-43	
<b>6. AUTHOR(S)</b> Edward C. Polhamus				
<b>7. PERFORMING ORGANIZATION NAME(S) AND ADDRESS(ES)</b> Edward C. Polhamus Consultant Newport News, VA 23606			<b>8. PERFORMING ORGANIZATION REPORT NUMBER</b>	
<b>9. SPONSORING / MONITORING AGENCY NAME(S) AND ADDRESS(ES)</b> National Aeronautics and Space Administration Langley Research Center Hampton, VA 23681-0001			<b>10. SPONSORING / MONITORING AGENCY REPORT NUMBER</b> NASA CR-4745	
<b>11. SUPPLEMENTARY NOTES</b> Langley Technical Monitor: James M. Luckring				
<b>12a. DISTRIBUTION / AVAILABILITY STATEMENT</b> Unclassified - Unlimited  Subject Category 02			<b>12b. DISTRIBUTION CODE</b>	
<b>13. ABSTRACT (Maximum 200 words)</b> <p>This paper presents a survey of the effects of Reynolds number on the low-speed lift characteristics of wings encountering separated flows at their leading and side edges, with emphasis on the region near the stall. The influence of leading-edge profile and Reynolds number on the stall characteristics of two-dimensional airfoils are reviewed first to provide a basis for evaluating three-dimensional effects associated with various wing planforms. This is followed by examples of the effects of Reynolds number and geometry on the lift characteristics near the stall for a series of three-dimensional wings typical of those suitable for high-speed aircraft and missiles. Included are examples of the effects of wing geometry on the onset and spanwise progression of turbulent reattachment near the leading edge and illustrations of the degree to which simplified theoretical approaches can be useful in defining the influence of the various geometric parameters. Particular emphasis is placed on the strong influence of "induced camber" on the development of turbulent reattachment.</p> <p>It is believed that the examples selected for this report may be useful in evaluating viscous flow solutions from computational methods based on the Navier-Stokes equations as well as defining fruitful research areas for high-Reynolds-number wind tunnels.</p>				
<b>14. SUBJECT TERMS</b> Reynolds number effects; Wing geometry effects; Lift characteristics; Low speed stall			<b>15. NUMBER OF PAGES</b> 95	
			<b>16. PRICE CODE</b> A05	
<b>17. SECURITY CLASSIFICATION OF REPORT</b> Unclassified	<b>18. SECURITY CLASSIFICATION OF THIS PAGE</b> Unclassified	<b>19. SECURITY CLASSIFICATION OF ABSTRACT</b> Unclassified	<b>20. LIMITATION OF ABSTRACT</b>	